Defining water quality seascapes in the KJCAP, their relationship to hydrographic modeling connectivity, the 2023 coral bleaching, and SCTLD.

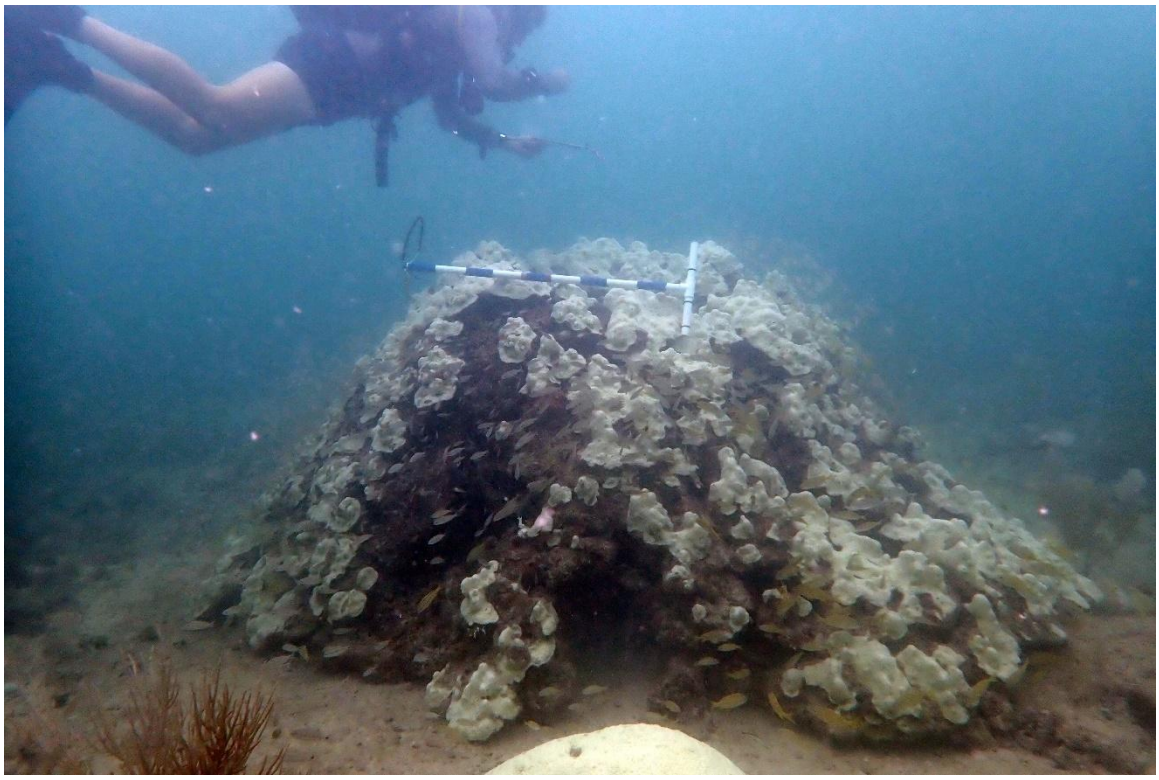

Defining water quality seascapes in the KJCAP, their relationship to hydrographic modeling connectivity, the 2023 coral bleaching, and SCTLD.

Final Report

Prepared By:

Brian K. Walker[1], Gareth J. Williams[2], Emmanuel Hanert[3], Thomas Dobbelaere[3], David Whitall[4], Jeffrey A. Maynard[5], and Greta S. Aeby

[1]Halmos College of Arts and Science, Nova Southeastern University, 8000 N. Ocean Drive, Dania Beach, FL 33004; walkerb@nova.edu; [2]School of Ocean Sciences, Bangor University, LL59 5AB, UK; [3]UCLouvain, Earth and Life Institute, Louvain-la-Neuve, Belgium; [4]NOAA NCCOS, Monitoring & Assessment Branch, Stressor Detection and Impacts Division, 1305 East-West Hwy, Silver Spring, MD 20910; [5]SymbioSeas, 1114 Merchant Lane, Carolina Beach, NC, 28428.

June 30, 2025

Completed in Fulfillment of C3D88F for

Florida Department of Environmental Protection
Coral Protection and Restoration Program
8000 N Ocean Dr.
Dania Beach, FL 33004

This report should be cited as follows:
Walker BK, Williams GJ, Hanert E, Dobbelaere T, Whitall D, Maynard JA, and Aeby GS. 2025. Defining water quality seascapes in the KJCAP, their relationship to hydrographic modeling connectivity, the 2023 coral bleaching, and SCTLD. Final Report. Florida DEP. Miami, FL., 68 p.

This report was funded through a contract agreement from the Florida Department of Environmental Protection's (DEP) Coral Protection and Restoration Program. The views, statements, findings, conclusions, and recommendations expressed herein are those of the author(s) and do not necessarily reflect the views of the State of Florida or any of its subagencies.

Management Summary (300 words or less)

This study identified hydrographic connections between inland water sources in southeast Florida (Government Cut, Baker's Haulover, Port Everglades, and Hillsboro) and coral reefs and investigated the environmental drivers and nutrients associated with bleaching and disease between 2018 and 2024. The most significant outcomes were: 1) analyte concentrations on the reef are increasing, 2) reefs northward of their adjacent inlet are most exposed to the water from that inlet, 3) Government Cut is a major transition between water quality seascapes, 4) increased exposure to terrestrial waters increases SCTLD lesions, 5) turbidity from high winds may help reduce bleaching, 6) mitigative actions in the Biscayne Bay system would have the most beneficial effect to water quality on the reefs, 7) nutrient differences in Biscayne may be affected by oceanside seagrass beds, and 8) the rate of increase in orthophosphates has slowed since the 2021 Miami-Dade County fertilizer restrictions.

This study provides crucial insights into the hydrographic dynamics affecting coral reefs in Southeast Florida. By identifying key nutrient sources and their relationship to bleaching and disease, it lays the groundwork for effective management actions to mitigate coral disease and promote reef resilience. These findings highlight the importance of managing inland water quality to protect coral reefs. The model provides a detailed understanding of how nutrients from inland sources are transported to reefs, offering valuable insights for targeted intervention strategies. We recommend extending the model's spatial footprint to capture the hydrodynamics of the entire FCR in the same way (currently funded by DEP). Then using subsequent modeled nutrient data, compiled environmental data, and reef monitoring data to conduct machine learning models of the relationships between factors relating to reef health for both corals and fishes (phase 2). This would provide a deeper understanding of the factors affecting reef health and the ability to target high impact mitigative actions and restoration strategies.

Executive Summary

Reduced water quality on Florida's Coral Reef (FCR) from anthropogenic sources has long been implicated in the decline of the reef system. Florida's Coral Reef is experiencing significant coral declines due to thermal stress and disease, which is exacerbated by environmental factors such as nutrient pollution. This study identified hydrographic connections between inland water sources in southeast Florida (Government Cut, Baker's Haulover, Port Everglades, and Hillsboro) and coral reefs and investigated the environmental drivers associated with bleaching and disease between 2018 and 2024.

Our machine-learning models explained 41.5 – 78.9% of the variation in the water quality concentrations on the reef with many contributing factors in various analytes including inlet outflow, rainfall, and high winds, however year had a high influence in almost every test. In almost every case, while holding all other predictors at their mean, the model showed nutrient increasing over time. Orthophosphate showed a lower annual increase after 2021, supporting that the Miami-Dade county fertilizer restrictions may be helping to reduce the rate of annual increase.

Hydrographic models showed that the reefs northward of their adjacent inlet are most exposed to the water from that inlet and from inlets further south, but there is also a seasonal non-negligible southern footprint extending tens of kilometers. Government Cut and Baker's Haulover discharge the largest nutrient loads and reducing pollutant loads in the Biscayne Bay system would significantly reduce excess nutrients in the KJCAP.

The machine-learning models explained 93% of the variation of partial bleaching of 5% or greater mostly driven by colony, landward winds, and temperature, which supports that some colonies are more sensitive than others and turbidity from high winds may help reduce bleaching. The SCTLD models explained 46% of the variation in lesions driven by colony, modeled silicate, and hot snaps, supporting some colonies are more disease resistant and that increased exposure to terrestrial waters increases SCTLD lesions.

The highest SCTLD prevalence in five years on the monitored *O. faveolata* colonies was recorded in July 2023. In August, the colonies south of Government Cut had the highest recorded bleaching, which took about five months to recover (no mortality from bleaching was observed), whereas no colonies further north visibly bleached. Unbleached colonies continued to acquire SCTLD lesions in the north, whilst SCLTD quiesced on bleached colonies. Thus, it appears that high temperatures in early and mid-summer exacerbated SCTLD, but the higher temperatures south of Government Cut caused those corals to bleach, which quiesced SCTLD in those colonies

Government Cut has been identified as a major transition between ecoregions in SE FL where significant *Thalassia* seagrass beds exist in the oceanside nearshore habitats further south (Biscayne ecoregion), but none further north. Seasonal analysis of the water quality sites indicated that the waters in the Biscayne ecoregion were distinctly different most of the time over five years on average having lower nitrate, nitrite, and TSS and higher silicate and orthophosphate. Sea grasses uptake large amounts of nutrients for seagrass growth and

can cause imbalances in their ratios, which can be exacerbated in warmer temperatures. Since the ratios of C: N: P: Fe determines the effect of nutrients on coral health, it is possible that the ocean side seagrass beds in Biscayne are affecting the water chemistry and increasing the corals susceptibility to thermal stress and bleaching. In 2023, nearshore reef temperatures south of Government Cut were warmer than further north, however there were also regional differences in nutrient concentrations. The water quality monitoring sites between Government Cut and Baker's Haulover had much higher total phosphorus, nitrate, silicate, and nitrite than those south of Government Cut. A lack of phosphorus can inhibit Symbiodiniaceae cell division and metabolism weakening the corals resistance to stress. In the 2023 wet season, the average values of total phosphorus in Biscayne were 4.7 times lower than normal and nitrate was 1.6 times lower.

This study provides crucial insights into the hydrographic dynamics affecting coral reefs in Southeast Florida. By identifying key nutrient sources and their relationship to bleaching and disease, it lays the groundwork for effective management actions to mitigate coral disease and promote reef resilience. These findings highlight the importance of managing inland water quality to protect coral reefs. The model provides a detailed understanding of how nutrients from inland sources are transported to reefs, offering valuable insights for targeted intervention strategies. We recommend extending the model's spatial footprint to capture the hydrodynamics of the entire FCR in the same way, which is currently being funded by DEP. Then using subsequent modeled nutrient data, compiled environmental, and reef monitoring data to conduct machine learning models of the relationships between factors relating to reef health for both corals and fishes (phase 2). This would provide a deeper understanding of the factors affecting reef health and the ability to target high-impact mitigative actions and restoration strategies.

Table of Contents

List of Acronyms

BRT	Boosted Regression Tree
CREMP	Coral Reef Evaluation and Monitoring Project
DEP	Florida Department of Environmental Protection
ECMWF	European Centre for Medium-Range Weather Forecasts
FCR	Florida's Coral Reef
FL	Florida
FWC	Florida Fish and Wildlife Conservation Commission
GMSH	3D finite element mesh generator
HYCOM	Hybrid Coordinate Ocean Model
ICA	Inlet Contributing Area
IEA	Inlet Exposure Area
KJCAP	Kristin Jacobs Coral Aquatic Preserve
MDL	Minimum Detection Limit
NCEI	National Centers for Environmental Information
NOAA	National Oceanic and Atmospheric Administration
NSU	Nova Southeastern University
RRC	SCTLD Resistance Research Consortium
RSME	Root Mean Square Error
SCTLD	stony coral tissue loss disease
SEFCRI LBSP	Southeast Florida Coral Reef Initiative Land-Based Source Pollution
SECREMP	Southeast Florida Coral Reef Evaluation and Monitoring Project
SLIM	Second-generation Louvain-la-Neuve Ice-ocean Model
TSS	Total Suspended Solids

Acknowledgements

This study was made possible through support from the Florida Department of Environmental Protection, awards C3D88F and C1FC2C. Computational resources were provided by the Consortium des Équipements de Calcul Intensif (CÉCI), funded by the F.R.S.-FNRS under Grant No. 2.5020.11. Thomas Dobbelaere is a Postdoctoral Researcher supported by F.R.S.-FNRS.

1. INTRODUCTION

Spatiotemporal patterns of tropical coral bleaching and disease are driven by a complex array of interactive natural, anthropogenic, and host-specific factors, of which combinations can be beneficial or detrimental. The effects of anthropogenic eutrophication of coral reefs are dependent on the nutrient loads, ratios, sources, and background temperatures, where high nutrient concentrations can increase susceptibility to bleaching and disease. However, certain ratios of high nutrients can decrease bleaching susceptibility.

In 2023, an extreme marine heatwave occurred causing many corals to bleach and die throughout the FL Keys. Monthly monitoring of many *Orbicella faveolata* colonies funded by DEP (C20F00, C00BAE, B96800, B7B6F3) showed that stony coral tissue loss disease (SCTLD) prevalence and incidence on the large *O. faveolata* colonies in southeast Florida was the highest ever recorded leading up to the bleaching. In August, all colonies south of Government Cut bleached extensively, whereas no colonies further north visibly bleached even though temperature stress was fairly equivalent. Unbleached colonies continued to acquire SCTLD lesions in the north, while SCLTD quiesced on bleached colonies. The most likely explanations for this differing bleaching response are differences in temperature, nutrient exposure, and the hosted Symbiodiniaceae communities.

Degree heating weeks comparisons from regional NOAA coral reef watch virtual stations showed very little difference north and south of Government Cut (Figure 1), but the southern Biscayne site experienced slightly higher temperature stress. This indicates that regional water quality may have been a more important factor in the varying bleaching response, however a formal analysis of the *in situ* temperature data is needed for confirmation. Ongoing hydrographic modeling of inlet water in the Kristin Jacobs Coral Aquatic Preserve (KJCAP) (DEP C1FC2C) shows that the reefs northward of their adjacent inlet are most exposed to the water from that inlet and from inlets further south (Dobbelaere et al. 2024). Spatial and temporal statistical modeling (DEP B9CAF9) reef water quality sites found that inlet flow, rainfall, and wind predictors explained 79% and 55% of the overall variation in orthophosphate and nitrate concentrations, respectively (Whitall et al, *In revision*). Prior to the 2023 bleaching, Symbiodiniaceae communities in large *Orbicella faveolata* colonies showed spatial patterns associated with inlet exposures (Figure 2). A bootstrap analysis of 2021 symbiodiniaceae communities by Inlet Exposure showed that corals in the Biscayne and Government Cut areas harbored significantly different symbionts than the other northern areas even though they are closest in proximity to each other. The Biscayne colonies had higher densities of *Breviolum* and *Cladacopium* algal symbionts than the unbleached colonies further north that were historically exposed to nutrient-laden inlet waters.

SCTLD persists in the shallow (<10 m) habitats in southeast Florida on intermediately susceptible species (Walker et al, 2025). Disease incidence varies temporally, with total infections highest during warm, wet season, and lowest in the dry season (DEP B9CAF9, C3D4C8). Statistical modeling showed that five predictors explained 60.6% of the model variation in the number of SCTLD lesions over time: mean temperature in the 90 days prior (36.7%), mean rainfall in the 90 (9%) and 30 (6.9%) days prior, the number of Hot Snap

events in the 60 days prior (5.7%), and flow out of the Inlet Contributing Areas (ICAs) inlets over the previous 7 days (2.3%). The Baker's Haulover inlet exposure area has the highest mean number of new SCTLD incidences and frequency of infections (Figure 3).

Symbiodiniaceae have been implicated as a key component of SCTLD and previous studies show that SCTLD quiesces with bleaching, however no studies have shown how this dynamic relates to varying responses across differing water quality seascapes. The 2023 marine heatwave had the highest amount of SCTLD on these colonies in 4 years. SCTLD persisted and visible bleaching did not occur in the areas most exposed to inlet waters. In contrast, further south, SCTLD abated and bleaching occurred in all of the corals in Biscayne. These patterns exemplify the complex nature of the coral holobiont response to thermal stress and disease in the context of local anthropogenic impacts. We proposed to compile the recent relevant datasets to run statistical models to determine which variables drove the observed bleaching and SCTLD response patterns in 2023.

Project Goals and Priorities:

The goal of this work was to define water quality seascapes in the KJCAP using hydrographic modeling, *in situ* water quality data, and other environmental data (such as *in situ* temperature) to investigate the observed varying spatial coral bleaching responses and SCTLD during the 2023 marine heatwave.

This work addressed the following FCRRP priorities:

- To understand and conduct evidence mapping of the deleterious impacts of different known chronic and acute water quality stressors such as turbidity, sedimentation, and key nutrients (nitrogen and phosphorus) on coral physiological and reproductive processes.
- Advance diagnostics related to coral diseases that are causing significant mortality, relative to other coral diseases, on Florida's Coral Reef.
- Research into the spatiotemporal patterns of coral diseases causing significant mortality on FCR, with an emphasis on SCTLD.
- To identify traits indicative of resistant and resilient corals and understand what parameters (physical, chemical, and biological; individual and synergistic; organismal and environmental) drive these factors.

It also addressed many long-standing SEFCRI LBSP management priorities (projects 18, 28, 29) and Our Florida Reefs recommended management actions (N-71, N-97, S-28, S-104), as well as the 2023 SCTLD Research Priorities 2 and 3, and the Resilience Action Plan for Florida's Coral Reef (2021-2026) goal 1 objectives 1 and 3.

The outcomes herein inform all aspects of future *O. faveolata* restoration planning for the KJCAP. They should be incorporated into an on-going coral disease response effort which seeks to improve understanding about the scale and severity of the coral disease outbreak on Florida's Coral Reef, identify primary and secondary causes, identify management actions to remediate disease impacts, restore affected resources, and ultimately prevent future outbreaks.

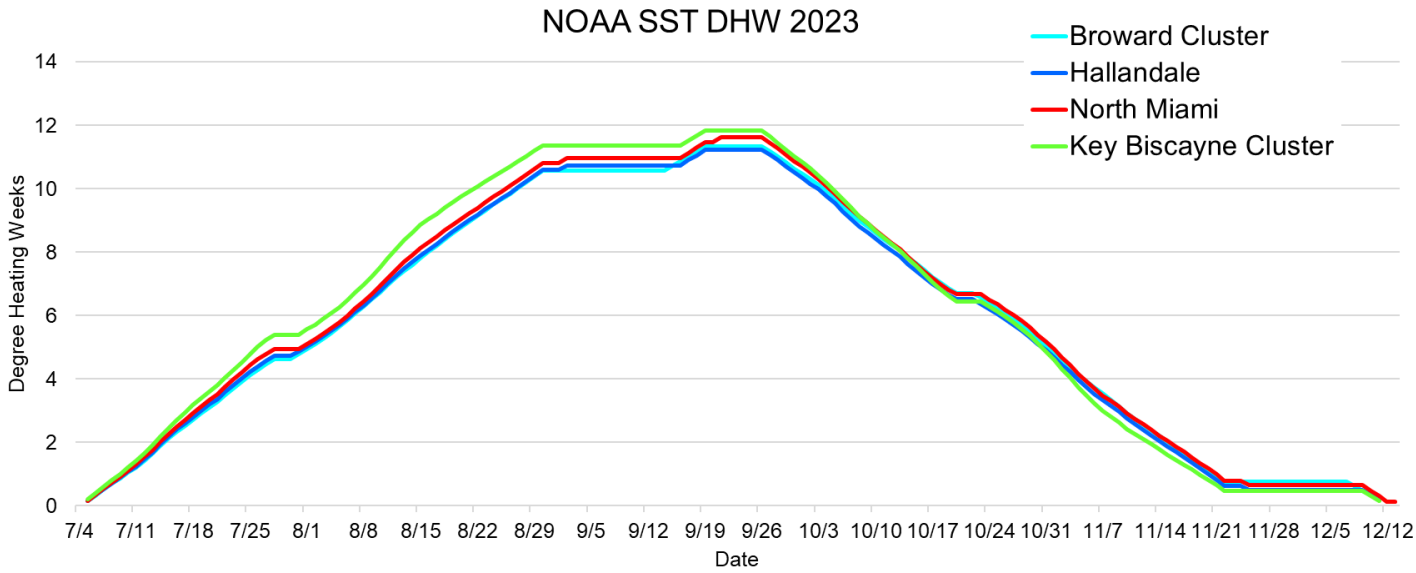

Figure 1. NOAA coral reef watch virtual station degree heating weeks for July – Dec 2023.

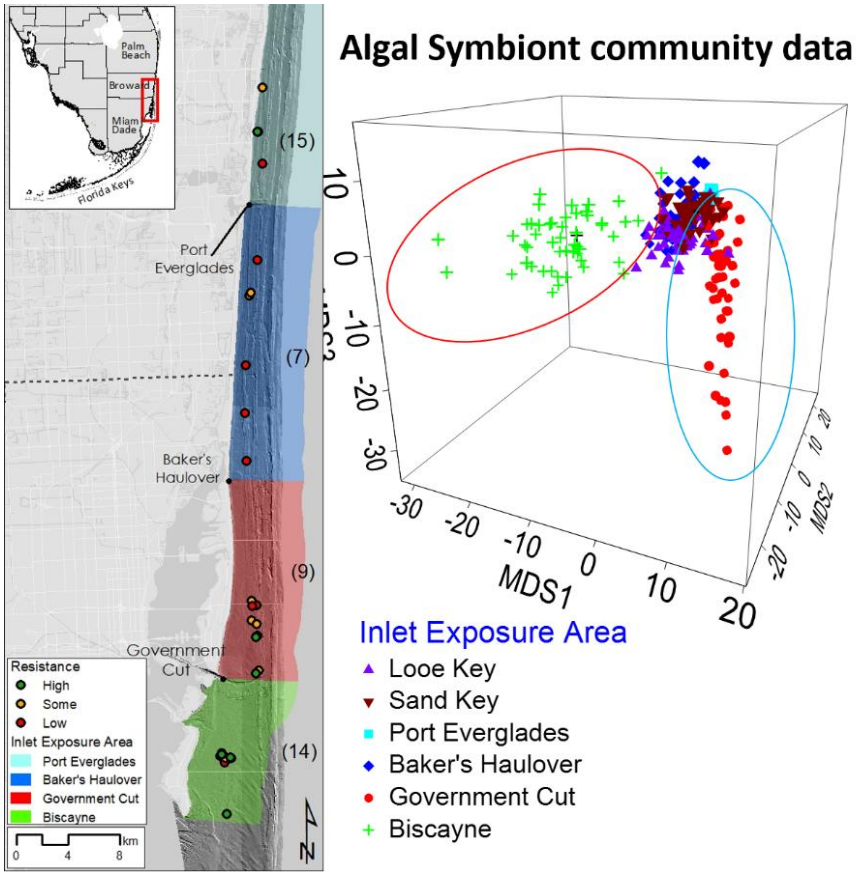

Figure 2. A bootstrap analysis of symbiodiniaceae communities by the nearest Inlet Exposure showing that corals in the Biscayne and Government Cut areas harbor different symbionts than the other areas even though they are closest in proximity to each other.

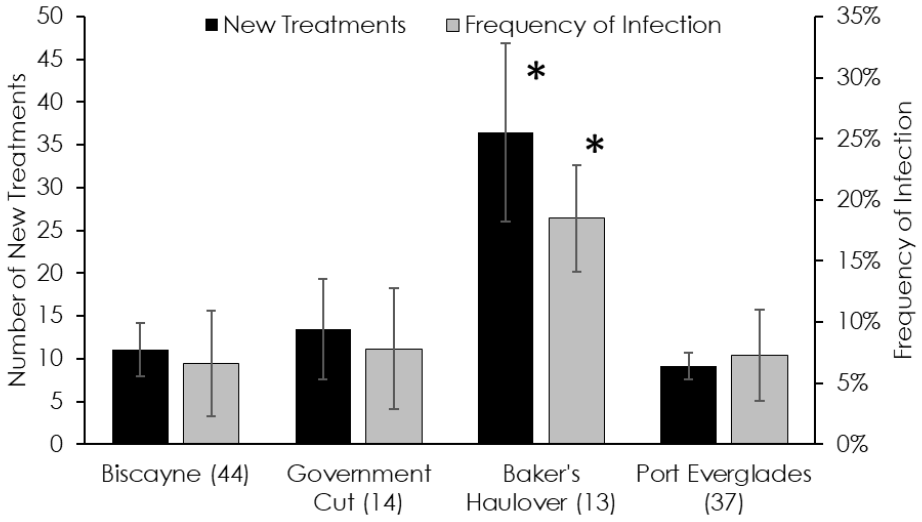

Figure 3. Mean number of new SCTLD treatments and frequency of infection are significantly higher in the Baker's Haulover exposure area.

2. METHODS

2.1. Task 2: Compile relevant regional environmental data (temperature, rainfall, inlet flow, wind) from 2021 – 2023

Based on previous analyses, a suite of environmental predictors were synthesized that were hypothesized to explain variations in coral bleaching and SCTLD affecting monitored large coral colonies in the KJCAP (Figure 4). The predictor datasets included data from January 2021 through to the end of December 2023. When combined with previous data, this generated data spanning from January 2018 to December 2023. This time-series was then trimmed as necessary to align with the monitoring periods for bleaching and SCTLD in the KJCAP – *see below*). The core methods behind generating each of these environmental data sets is described below.

2.1.1. Seawater temperature

In situ temperature stress experienced by the coral colonies was quantified using data from sites BC1, DC1, DC6, and DC8 of the Southeast Coral reef Evaluation and Monitoring Project (SECREMP) (Figure 4). Each coral was spatially joined to the nearest logger. From the temperature time series, we calculated the seasonal mean and standard deviation for each summer period (July 1st – September 31st) and from this calculated the number of anomalously high temperature events using the "Hot Snap" metric, defined as any temperature event that exceeds 1SD of the long-term seasonal mean (Heron et al. 2010). We used a "period of accumulation" of 3, 7, 14, 30, 60 and 90 days, meaning that for each coral survey date we calculated the number of Hot Snaps over these temporal windows prior to the survey date. These summed numbers of Hot Snap events were then multiplied by two to estimate the number of exposure hours over each period (due to the 2-hr sampling resolution of the loggers, i.e., one event equals two hours, two events equal 4 hours and so on).

2.1.2. Seawater nutrient concentrations

The water quality data used for this analysis were from a joint NOAA-Florida Department of Environmental Protection (FDEP) assessment program (Whitall et al. 2019). The central inlet and reef site sample data were used in the analysis (). To analyze water quality data at the reefs themselves, only water collected using Niskin bottles at the depth of the reef (not surface waters) were included in this analysis. The sampling protocol involved starting sample collection as far into the ebb tide as possible and at a minimum of two to three hours after the peak high tide. Sampling equipment was rinsed with deionized water three times between sites and then three times with site water once on site. Field clean equipment blanks were collected (at least one per day and at least one per 20 samples collected). Analytical chemistry was performed via standard methods (Whitall et al. 2019; Whitall and Bricker 2021).

The database captures a suite of common nutrient parameter analytes (e.g., phosphate, nitrate). The number of non-detects (i.e. values falling below the minimum detection limits, MDL) within this database is often quite large (sometimes more than 50% of the water samples for any given analyte). We adjusted the analyte values to account for the MDLs using a modified version of the Flynn methodology (Flynn 2010). The approach maximizes the normality of a distribution of samples, after making a best-guess approach for values below a detection limit, setting the starting value for iterative calculations to half the reported detection limit for each analyte. Here, if an analyte had several different detection limits, the mean detection limit was used to approximate the best guess starting point for all values below the detection limit. Calculations were made using a R routine previously developed by this project team that combines four existing R functions (*optim*, *readxl*, *dplyr*, *signal*) with a novel function (named "*shapiro_weights*") to calculate the Shapiro Weights used in Flynn (2010). We adapted the Flynn (2010) methodology to account for the time-series nature of the data set. An important consideration of the Flynn (2010) approach is that it estimates the values for samples of analytes below the MDL along the x-axis of a normal distribution built from those values above the MDL for that analyte (moving from left to right, i.e. from low to increasingly higher values) in the order in which the data are received. As such, if the data are inputted in time order, then estimated values later in the time series will be higher than those earlier in the time series. This results in a slow systematic 'creep' in analyte concentrations that becomes apparent when temporal trends in the nutrient data are then visualized. To overcome this, we permuted the order of the data set stratified by sampling station. This ensured that time was randomized when predicting values below the MDL within each sampling station but more importantly ensured that any underlying spatial gradients in nutrient concentrations across the KJCAP (and their relation to changes in concurrent flow, rainfall and wind) were maintained. These synthesized *in situ* nutrient data were used to parameterize the temporal extension of the hydrographic nutrient loading model (using a subset of the sampling stations clustered around the inlets: GOC002, BAK020, PEV040 and HIL050, Task 3) and examine temporal trends in water quality across the KJCAP (Task 5).

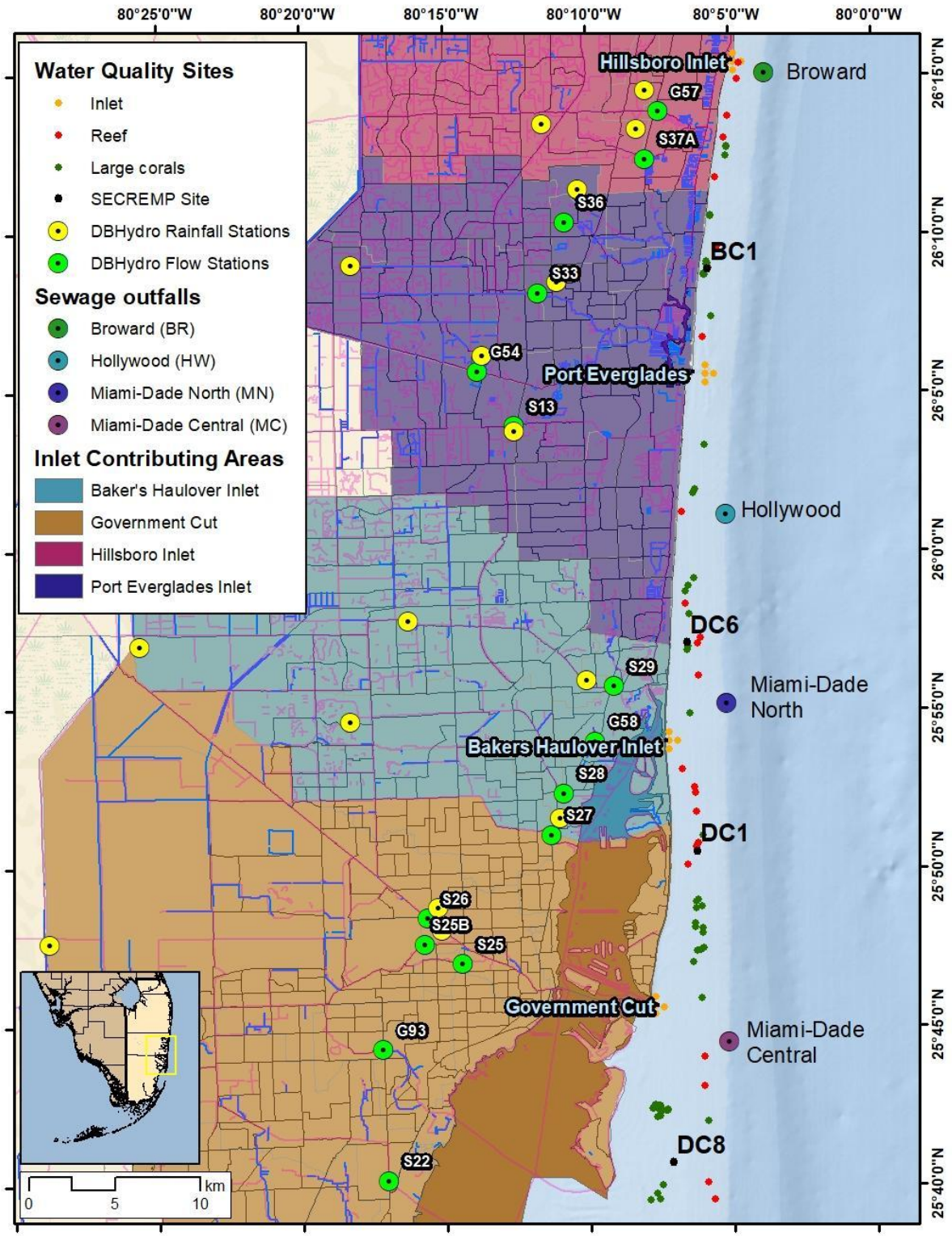

Figure 4. Map of the project area depicting the Inlet Contributing Areas, DBHydro flow stations, the inlet mouths, large corals, sewage outfalls, and water quality monitoring stations and reef temperature logger locations.

Table 1. Water quality monitoring sites used in this analysis from the NOAA-Florida Department of Environmental Protection (FDEP) assessment program.

Site ID	*Latitude*	*Longitude*	*Type*	*Inlet Contributing Area*	*Inlet Exposure Area*
GOC002	25.76100000	-80.12842500	Inlet	Government Cut	Government Cut
GOC005	25.84455000	-80.10415000	Reef	Government Cut	Government Cut
GOC006	25.73414210	-80.10023920	Reef	Government Cut	Biscayne
GOC007	25.84636670	-80.10323330	Reef	Government Cut	Government Cut
GOC008	25.83518330	-80.10928330	Reef	Government Cut	Government Cut
GOC009	25.66821730	-80.09874200	Reef	Government Cut	Biscayne
GOC010	25.65916350	-80.09482490	Reef	Government Cut	Biscayne
GOC011	25.71883000	-80.10008000	Reef	Government Cut	Biscayne
BAK020	25.90000000	-80.11971400	Inlet	Baker's Haulover	Baker's Haulover
BAK024	25.87298300	-80.10450000	Reef	Baker's Haulover	Government Cut
BAK025	25.88526000	-80.11218000	Reef	Baker's Haulover	Government Cut
BAK026	25.87570000	-80.10496670	Reef	Baker's Haulover	Government Cut
BAK027	25.86261000	-80.10401000	Reef	Baker's Haulover	Government Cut
BAK028	25.95145000	-80.10286700	Reef	Baker's Haulover	Baker's Haulover
BAK029	25.93450000	-80.10250000	Reef	Baker's Haulover	Baker's Haulover
PEV040	26.09300600	-80.09733300	Inlet	Port Everglades	Port Everglades
PEV044	26.15998300	-80.09028300	Reef	Port Everglades	Port Everglades
PEV045	26.11206700	-80.09883300	Reef	Port Everglades	Port Everglades
PEV046	26.02060000	-80.11190000	Reef	Port Everglades	Baker's Haulover
PEV047	26.14840000	-80.09520000	Reef	Port Everglades	Port Everglades
PEV048	25.97240000	-80.10980000	Reef	Port Everglades	Baker's Haulover
PEV049	25.95423000	-80.10117000	Reef	Port Everglades	Baker's Haulover
HIL050	26.25659200	-80.08019700	Inlet	Hillsboro	Hillsboro Inlet
HIL054	26.28915000	-80.07511670	Reef	Hillsboro	Port Everglades
HIL055	26.21693000	-80.08620000	Reef	Hillsboro	Port Everglades
HIL056	26.22868330	-80.08381670	Reef	Hillsboro	Port Everglades
HIL057	26.24786670	-80.07821670	Reef	Hillsboro	Port Everglades
HIL058	26.19612000	-80.09100000	Reef	Hillsboro	Port Everglades
HIL059	26.25616670	-80.07691670	Reef	Hillsboro	Port Everglades

2.1.3. Inlet flow

The South Florida Water Management District's DBHydro database (https://www.sfwmd.gov/science-data/dbhydro) stores hydrologic, meteorologic, and water quality data, and is the source of historical and up-to-date environmental data for the 16-county region covered by the District. Using this database, we generated estimates of water flow from ICAs to our monitored corals in the KJCAP as a proxy for exposure to land-based sources of nutrients and pollutants. A subset of the DBHydro monitoring stations that independently captured the full extent of the flow within each Inlet

Contributing Area (ICA) were identified. Stations that were upstream or downstream from each other, and therefore were artificially inflating summed flow values, were identified using a map of the flow channel paths throughout the ICAs and one of each pair removed (Walker et al. 2022). Through this iterative pairwise process, 20 stations were identified for inclusion in the analyses and used to generate flow data for each ICA across the entire project period. Each large coral and *in situ* water quality monitoring site was then spatially joined to its nearest ICA directly south of its position owing to our previous hydrographic modeling work showing a predominantly northern flow out of the coastal inlets (Dobbelaere et al. 2024). The flow patterns for each coral/water quality site were then pulled from the ICA summary across a series of pre-defined temporal windows (1, 3, 7, 14, 30, 60 and 90 days) prior to each survey date. This was then repeated for one-month increment windows over a full year prior to each coral/water quality site survey date.

2.1.4. Rainfall

Episodes of heavy rainfall can lead to land-based runoff to nearby coastal areas and contribute to the establishment and persistence of coral diseases. Furthermore, extreme events in shallow water can stir up deposited sediment and introduce new sediment sources from the land into suspension that can also exacerbate coral disease (Pollock et al. 2014). Here we used the South Florida Water Management District's Daily Historical Rainfall database (www.sfwmd.gov/weather-radar/rainfall-historical/daily) to quantify the amount of rainfall experienced by each monitored coral and *in situ* water quality sample site over the same temporal windows as for inlet flow. Here, unlike inlet flow, each coral and water quality site were spatially attributed to the nearest ICA running directly to land from their position, as there was no prior expectation that land-based runoff (rather than inlet outflow) would be coming from a predominant spatial direction.

2.1.5. Wind speed and direction

High wind events can cause the resuspension of sediment on reefs (Priestas 2022) resulting in changes in water quality. Previous analyses within the KJCAP showed wind speed and direction (landward versus seaward) to explain a reasonable proportion of the spatiotemporal variation in some of the water quality analytes. We used NOAA's tides and currents database (https://tidesandcurrents.noaa.gov/met.html) to quantify wind speed (mean and SD) and direction (0-179°, blowing towards land; 180-359°, blowing towards sea) for the KJCAP, as well as the number of high wind events (> 5 m sec^{-1}). These metrics were computed using the 6-minute resolution wind data, averaged to daily values to estimate patterns over time for each ICA. Like for rainfall, each coral and water quality site were spatially attributed to the nearest ICA running directly to land from their position and rainfall values quantified over the same temporal windows prior to the survey dates as for flow and rainfall.

2.2. Task 3: Update hydrographic modeling through 2024

2.2.1. Task 3a: Simulating ocean dynamics from Sep. 2021 to Aug. 2024

We simulated the ocean circulation along East Florida's coastline with the multiscale ocean model, which has already been extensively applied and validated in Florida's coastal waters (Frys et al., 2020; Dobbelaere et al., 2020; Dobbelaere et al., 2022). Here, we considered

an area of interest situated between Florida and the Bahamian Banks, and between 25.2°N and 27.5°N (Figure 5). The Government Cut, Baker's Haulover, Port Everglades, and Hillsboro inlets were included in the area of interest as open boundaries through which water flow and analytes could enter in the model domain. SLIM uses an unstructured mesh whose resolution can be locally increased to accurately represent fine-scale flow features, such as those produced near the inlets and over the nearshore and offshore coral reefs. The mesh was generated with GMSH (Geuzaine & Remacle, 2009) using the Python package seamsh. The model resolution reached 25 m around the inlets, 50 m along the coastlines, 100 m over the coral reefs, and a few km further offshore, in the Florida Straits. The model bathymetry was obtained by combining data from NCEI Coastal Relief Model (3 arcseconds) and NCEI Continuously Updated Digital Elevation Model (1/9 arcseconds). Reef polygons were extracted from FWC's unified reef map. The model was forced with winds from ECMWF-ERA5, large-scale currents (including tides) from HYCOM-GoM and processed DBHydro flow rates at the inlet boundaries. The model was run between September 1, 2021, and September 1, 2024, with hourly exports of the simulated sea surface elevation and currents.

2.2.2. Task 3b: Simulating plumes from the 4 main inlets

We used the modeled currents to simulate the dispersal of inland plumes from the four primary inland water inlets—Government Cut, Baker's Haulover, Port Everglades, and Hillsboro. Our inland water dispersal model employs a Eulerian approach, solving an advection-diffusion equation for each of the seven analyte concentrations released from each of the four inlets, resulting in a total of 28 equations. The seven analytes for which concentration measurements (in g/m^3) were available at each inlet include nitrite, nitrate, total nitrogen, orthophosphate, total phosphorus, silicate, and total suspended solids (TSS). The model assumed that each analyte behaves as a passive, non-reactive tracer that does not decay in the water column due to biological consumption (in the case of nutrients) or sedimentation (for TSS). Additionally, the model considered the initial concentration of each analyte within the domain is zero, with the only sources being the four inlets. We computed the temporal average of the 28 simulated concentrations for the wet (May to October) and dry (November to April) seasons at all mesh nodes. These averages were then compared to highlight seasonal differences for each inlet

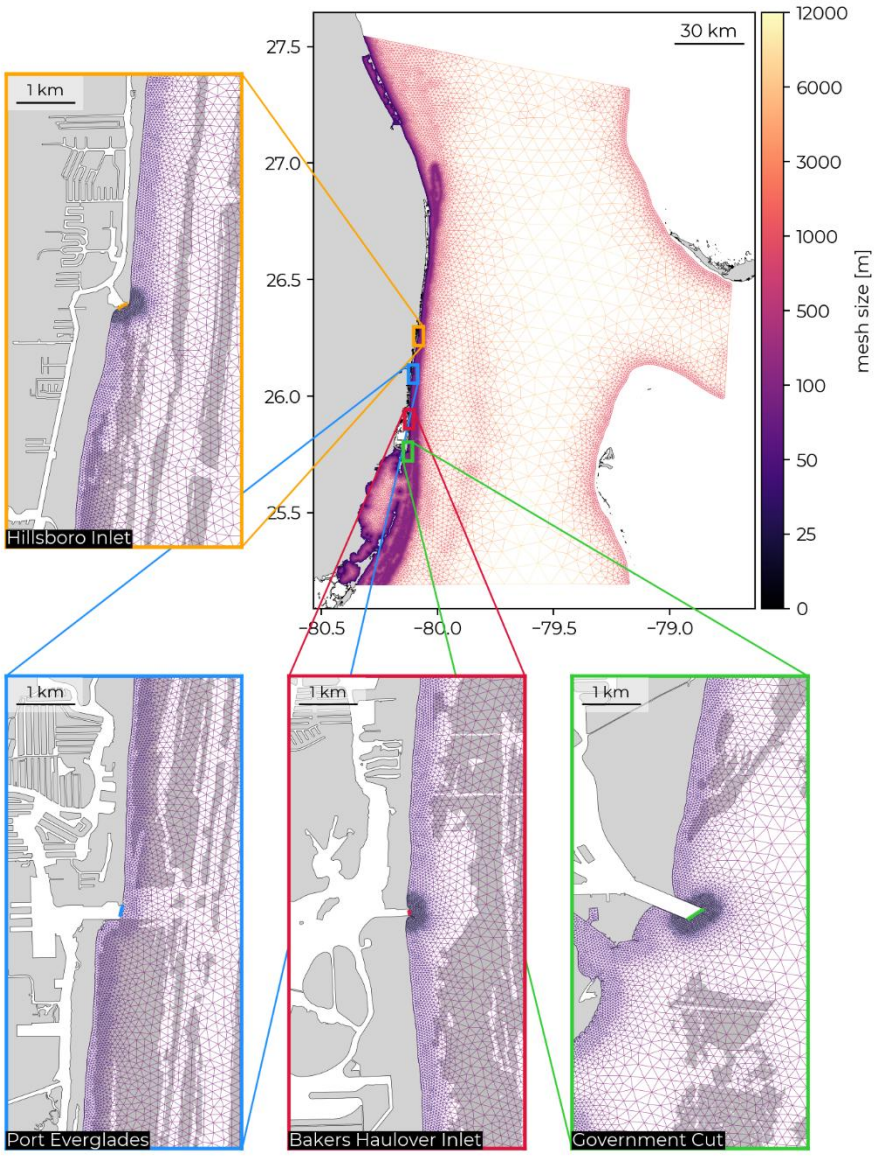

Figure 5. Model mesh and close-up views near the four ICA inlets, where the model resolution reaches 25 m. The inlet open boundaries where flow rates and analyte loads were imposed are highlighted with thick colored lines. The land is shown in light grey and reef polygons in dark grey.

The simulated concentrations were validated against monthly water quality measurements from the reef water quality monitoring sites. Due to the disparity in temporal resolution (hourly vs monthly) and the water quality measurement uncertainty, this validation was performed by comparing the distributions of the observed and simulated concentrations at the monitoring sites. We computed the first and third quartiles of the distributions of the observed and daily resampled simulated concentrations. We then defined three concentration levels: low below the first quartile, high above the third quartile, medium otherwise. We then defined an accuracy score by computing the proportion of simulated concentration levels matching the observed concentration levels. This score was first

computed using the predicted concentration level at the date of the observation. We then used a tolerance of at most 2.5 days between the observed and simulated concentration levels. Simulated concentration peaks occurring within 2.5 days before or after the date of the observed peaks were then considered correct.

2.2.3. Task 3c: Estimating nearshore coral reef inlet exposure

The 28 simulated concentrations (for the seven analytes originating from four different inlets) were also computed over reef polygons to estimate coral reef exposure to the analytes released at each of the inlets. Reef polygons were extracted from the coral and hardbottom layer of the Unified Reef Map (FWC-FWRI, 2017) and intersected with a 500 m × 500 m grid. The resulting heat maps highlight reefs most exposed to inland water plumes and indicate the seasonal variability of this exposure .

2.2.4. Task 3d: Identifying the analyte(s) and inland source responsible for disease occurrence

Finally, we computed time series of the 28 analyte concentrations at reef sites monitored and treated for SCTLD (Whitall et al. 2019). To identify the most important source of analyte to each site and its potential impact on the occurrence of disease lesions, we computed the total accumulated analyte concentration at the sites during the ten days preceding the observation of new lesions. This period was chosen as it matches the disease incubation time obtained in laboratory experiments (Dobbelaere et al., 2020; Aeby et al., 2021; Meiling et al., 2021). The contribution of each inlet was then obtained by computing the fraction of the total accumulated concentration coming from this inlet.

2.3. Task 4: Quantify *in situ* temperature stress differences between Biscayne and further

In situ temperature data was compiled for 2022 and 2023 at four nearshore SECREMP monitoring stations, BC1, DC6, DC1, and DC8 (Figure 4). These stations differed latitudinally along the coast. Raw temperature data between April and October each year were plotted and compared across sites and years to evaluate differences in temperature regimes between Broward and Miami-Dade counties and how temperature related to the 2023 disease and thermal stress observations in the large *Orbicella* colonies. Non-parametric analyses of variance with Kruskal-Wallace post hoc tests between pairs were used to determine significance between sites and years.

2.4. Task 5: Quantify seasonal patterns in water quality by inlet exposures of each analyte through 2023

Water quality data from the NOAA-Florida Department of Environmental Protection (FDEP) assessment program were used in a multivariate analysis to investigate spatial differences between inlet exposure areas. Due to temporal variation, data were analyzed for each wet and dry season individually. Because dry seasons spanned multiple years, they were assigned the latest year. For example, samples collected between November 1, 2020 and May 1, 2021 were labeled Dry 2021.

Corrected values for nitrate, nitrite, orthophosphate, total phosphorous, total suspended solids, and silicate for each sample period and location were input into Primer 7. Data were

4th root transformed and then normalized to account for differences in ranges between analytes. A Euclidean distance similarity matrix was produced which was used to test significance in a permutational multivariate analysis of variance (PERMANOVA) and create bootstrap averages plots of significant factors (Year, Season, IEA) with 100 iterations. Similarity percentages on transformed data were calculated for IEAs for each season and compiled into a database. A Euclidean distance similarity matrix of the SIMPER results by season was produced which was used to test significance in PERMANOVAs and create a multidimensional scaling to evaluate the similarity between each IEA each season. Similarity percentages were calculated by IEA to determine the overall factors affecting differences between IEAs.

2.5. Task 6: Build statistical models to investigate the possible links between water quality seascapes, SCTLD occurrence, and patterns of coral bleaching

The analyses here aimed to test whether correlative links existed between water quality seascapes, patterns of SCTLD, and coral colony bleaching response during the 2023 marine heatwave. To do this, we built a series of statistical models that connected the various parts of this puzzle in different combinations in an iterative manner: 1) relationship between changes in water quality and changes in flow, rainfall, and wind (i.e. how local environmental factors drive water quality changes), 2) relationship between changes in water quality and spatiotemporal patterns of SCTLD (i.e. what specific changes in water quality result in increased or decreased SCTLD occurrence), and 3) relationship between water quality seascapes and thermal stress with patterns of coral bleaching during the 2023 marine heatwave (i.e. what specific combinations of historical nutrient exposure and thermal stress result in either higher or lower bleaching). These analyses utilized all the various data layers generated through Tasks 2 – 5 as necessary to synthesize across them to advance our understanding of how local land-sea connections affect disease and bleaching dynamics on nearshore coral reefs, a critical area of ongoing research in coral reef ecology.

All statistical models were built using a boosted regression tree (BRT) framework. Unlike many modeling techniques that aim to fit a single parsimonious model, BRT incorporates machine learning decision tree methods (Breiman et al. 1984) and boosting, a method to reduce predictive error (Elith et al. 2008), to build an additive regression model in which individual terms are regression trees, fitted in a forward stage-wise manner (i.e., sequentially fitting each new tree to the residuals from the previous ones). In summary, BRT gives two crucial pieces of information, namely the underlying relationship between the response and each predictor, and the strongest statistical predictors (among the simultaneously tested predictors) of the response variable in question.

BRTs were constructed using the *gbm.step* routine (Elith et al. 2008) in the *dismo* package (Hijmans et al. 2017) for R (www.r-project.org) and all model outputs were visualized in *ggplot2* using *ggBRT* (Jouffray et al. 2019). For the *in situ* water quality and coral bleaching models, the data were modeled using a Gaussian distribution. For the SCTLD models, the data were modeled using a Poisson distribution. We used a 10-fold cross-validation approach to test the model against withheld portions of the data (iterated thousands of times) and the cross-validated percentage deviance explained, calculated as (1 – (cross-

validated deviance/mean total deviance)), as our measure of model performance (Jouffray et al. 2019). To optimize model predictive performance, we varied three core parameters of the BRT algorithm: the *bag-fraction* (bf, proportion of training data to be selected at each step), the *learning rate* (lr), used to shrink the contribution of each tree as it is added to the model), and the *tree complexity* (tc), the number of terminal nodes in a tree). Using a customized loop routine (Richards et al. 2012), we identified the combination of these three parameters that resulted in the lowest cross-validation deviance (CVD) over bf-values 0.5, 0.7, and 0.8, lr-values 0.001, 0.0001, and 0.00001, and tc-values 1–5, while maintaining a minimum of ≥ 1000 fitted trees and a maximum of 50,000 trees. To ensure the optimal bag fraction for each analyte did not result in high model performance because of overtraining (i.e. a high proportion of training data relative to test data), we also recalculated and report the overall model performance values with a bag fraction of 0.5 (50% training data) in each case. For each final BRT model, the relative importance of each predictor was calculated based on the number of times a variable was selected for splitting, weighted by the squared improvement to the model, as a result of each split, and averaged over all trees (Friedman and Meulman 2003; Elith et al. 2008).

Prior to model-fitting, the predictor variables were investigated for collinearity. We calculated pairwise Pearson's correlations across the various temporal windows for inlet outflow, rainfall, and wind (landward and seaward) and excluded one of each pair where r >0.8. During this, we strived to retain either short (3, 7 days prior) or medium (30 days prior) over very short (1 day prior) or long (90 days prior) periods. We also included 'depth' as a predictor to account for any effect variations in depth across the water samples and coral locations might have and 'Year' (2019-2023) to account for any temporal effects not captured by temporal changes in our other predictors. Finally, we included three different spatial terms to capture any effects not captured by spatial changes in our other predictors: 1) the inlet contributing area (ICA) directly to shore from the water quality sampling station or monitored coral location (Hillsboro, Port Everglades, Baker's Haulover, Government Cut), 2) the ICA directly south of their location (because of the predominantly northern flow out of the inlets (Dobbelaere et al. 2024) (Port Everglades Baker's Haulover, Government Cut, south of the ICA inlets), and 3) the inlet exposure area (IEA), which were assigned based on previous modeling efforts (Port Everglades, Baker's Haulover, Government Cut, Biscayne).

For the *in situ* water models, this resulted in the following 17 predictors included in the model fitting process: depth (m), Year (categorical: 5 levels), ICA (categorical: 4 levels), ICA south (categorical: 4 levels), IEA (categorical: 4 levels), summed inlet flow (calculated using IEA) (7, and 30 days prior), summed rainfall (calculated using ICA) (1, 3, 7, 30 days prior), number of landward wind events >5 m sec^{-1} (7, 30 days prior) and number of seaward wind events >5 m sec^{-1} (1, 3, 7, 30 days prior).

For the SCTLD and coral bleaching models, several other predictors were also included, namely 'Colony' as a categorical variable (to capture any colony-specific effects not captured by our colony-level estimates of the other predictor variables), the number of septic tanks within the radius of each coral location as a proxy for nearshore urbanization (Walker et al. 2022), mean seawater temperature, and the modeled summed nutrient

loading estimates for the six analytes generated from the hydrographic model in Task 3. After removing one of each pair where r >0.8, this resulted in the following 36 predictors included in the model fitting process: depth (m), Colony (42 levels), number of septic tanks within a 8, 13 and 21 km radius, Year (categorical: 5 levels), ICA (categorical: 4 levels), ICA south (categorical: 4 levels), IEA (categorical: 4 levels), mean seawater temperature (7 and 90 days prior), Hot Snap exposure (7, 30 and 90 days prior), summed inlet flow (calculated using IEA) (7, and 90 days prior), summed rainfall (calculated using ICA) (7, 30, 90 days prior), number of landward wind events >5 m sec^{-1} (7, 30, 90 days prior), number of seaward wind events >5 m sec^{-1} (7, 30, 90 days prior), summed nitrate loading (7 and 30 days prior), summed nitrite loading (7 and 90 days), summed orthophosphate loading (30 and 90 days prior), summed phosphorus loading (7 and 90 days), summed silicate loading (7 and 90 days), and summed total suspended solids (7 and 90 days).

For the SCTLD models, we modeled both the number of new treatments and number of new lesions over time. Unfortunately, the lack of nutrient input boundaries precluded our ability to use the hydrographic modeled nutrient data off Biscayne. Although shown to have lower nutrient values at the water quality monitoring sites, the hydrographic model didn't have any inputs from lower or mid-Biscayne Bay. Therefore, we first modeled the entire geographic extent of the data set (across all four inlets) but with the modeled nutrient loading estimates excluded (because of high uncertainty in the nutrient loading estimates in the Biscayne IEA) (No Nutrients – NN). We then modeled a second scenario, where the Biscayne corals (n=17) were removed from the data set and the nutrient loading estimates for the remaining IEA included as predictors (No Biscayne – NB). The results were then compared. For coral bleaching, the focus here was on modeling the entire geographic extent because of our hypothesis that temperature stress in the southern regions was, in part, driving bleaching patterns. As such, the modeled nutrient loading estimates were once again excluded as predictors. We then modeled two bleaching response variables: one with all bleaching values less than 5% removed, and one with all bleaching values less than 10% removed.

2.6. Task 7: Integrate the inlet exposures into the RRC data analyses

A key part of using statistical inference to identify possible causal relationships in ecology is the correct design, application, and (perhaps most importantly) correct interpretation of statistical models. Here our team continued to provide key statistical oversight and targeted assistance to help those researchers from the RRC identify and execute appropriate statistical tests for their questions and hypotheses. This helped to ensure continuity in data analysis approaches across the RRC and ensure statistical rigor when it comes to data interpretation and peer-reviewed publication of the results. We provided this assistance through a series of online meetings and email exchanges with individual RRC team members.

3. RESULTS

3.1. Task 3: Update hydrographic modeling through 2024

3.1.1. Task 3a: Simulating ocean dynamics from Sep. 2021 to Aug. 2024

The simulated ocean circulation patterns along East Florida's coastline are predominantly northward under the influence of the Florida Current (Figure 6). The primary northward ocean circulation is however influenced by tidal currents, which introduce oscillatory dynamics that can alter the flow direction, occasionally causing it to reverse and move southward. Additionally, this northward circulation is affected by the passage of (sub)mesoscale baroclinic eddies, which induce meandering in the Florida Current and can further influence changes in its direction. In addition to these two physical processes, the ocean currents interact with the coral reefs along the coast. As those reefs are shallower and have a higher rugosity than the sandy seabed, they tend to slow down and deflect the ocean currents. The ocean circulation model outputs have been validated against observations at different stations within the area of interest (see Figure 7 for an illustration in January 2024).

3.1.2. Task 3b: Simulating plumes from the four main inlets

The changes and variability in the ocean circulation patterns in turn affect the dispersal of inlet plumes originating from the four inlets. While they tend to move north, they can also be flushed southward and hence affect reefs not directly downstream of the inlets (Figure 6). The footprint of each inlet can be assessed for each of the analytes present in the inland water. For the sake of illustration, we only show here the results for silicate but the same has been done for the other six analytes for which we had load measurements at each inlet (see Appendix). We computed the mean silicate concentration over both the wet (May to October) and dry (November to April) seasons over the 3-year period that we simulated (Figure 8). While the analyte plumes extend mostly north of each of the source inlets, they also have a non-negligible southern footprint that extends over tens of kilometers. This is particularly the case for Government Cut and Baker's Haulover inlets whose inland water plumes clearly intrude into Biscayne Bay. Government Cut and Baker's Haulover also discharge the largest amounts of pollutants leading to inland water plumes with a higher analyte concentration. As these two inlets are further the southernmost, they have the most detrimental effect on the marine environment. When comparing wet and dry seasons, we observe that inland water plumes generally have a larger analyte concentration during the wet season. However, higher analyte concentrations were observed south of the inlet during the dry season, especially for Government Cut and Baker's Haulover.

3.1.3. Task 3c: Estimating nearshore coral reef inlet exposure

When looking more specifically at the inlet source of analyte concentration over each reef, we see that Government Cut's inlet not only has the largest footprint in terms of surface area but also exhibits the highest concentration of inland water over the reefs across that area (see illustration for silicate in November 2023 in Figure 9). This is due to both its southern location and its highest pollutant load. While Government Cut, Baker's Haulover and Port Everglades inlets predominantly impact reefs north of the inlets, analyte concentrations from Hillsboro's inlet are largest over reefs south of the inlet.

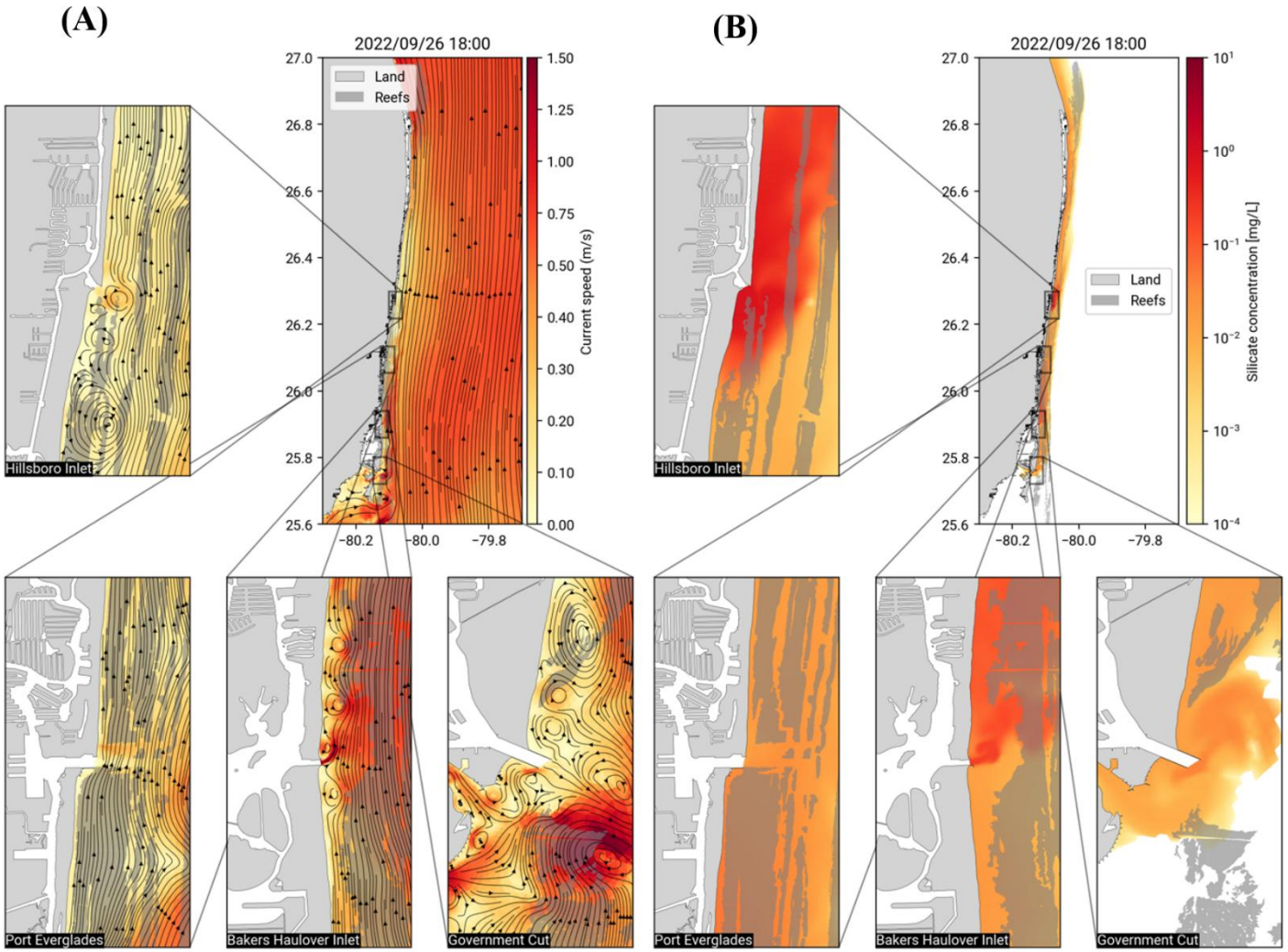

Figure 6. **(A)** Snapshot of the simulated currents near the inlets on September 26, 2022 at 6pm and **(B)** silicate plumes released from the different inlets. The land is shown in light gray and coral reefs in darker gray. This illustrates how the flow rates at the inlets and small-scale eddies are captured by the model.

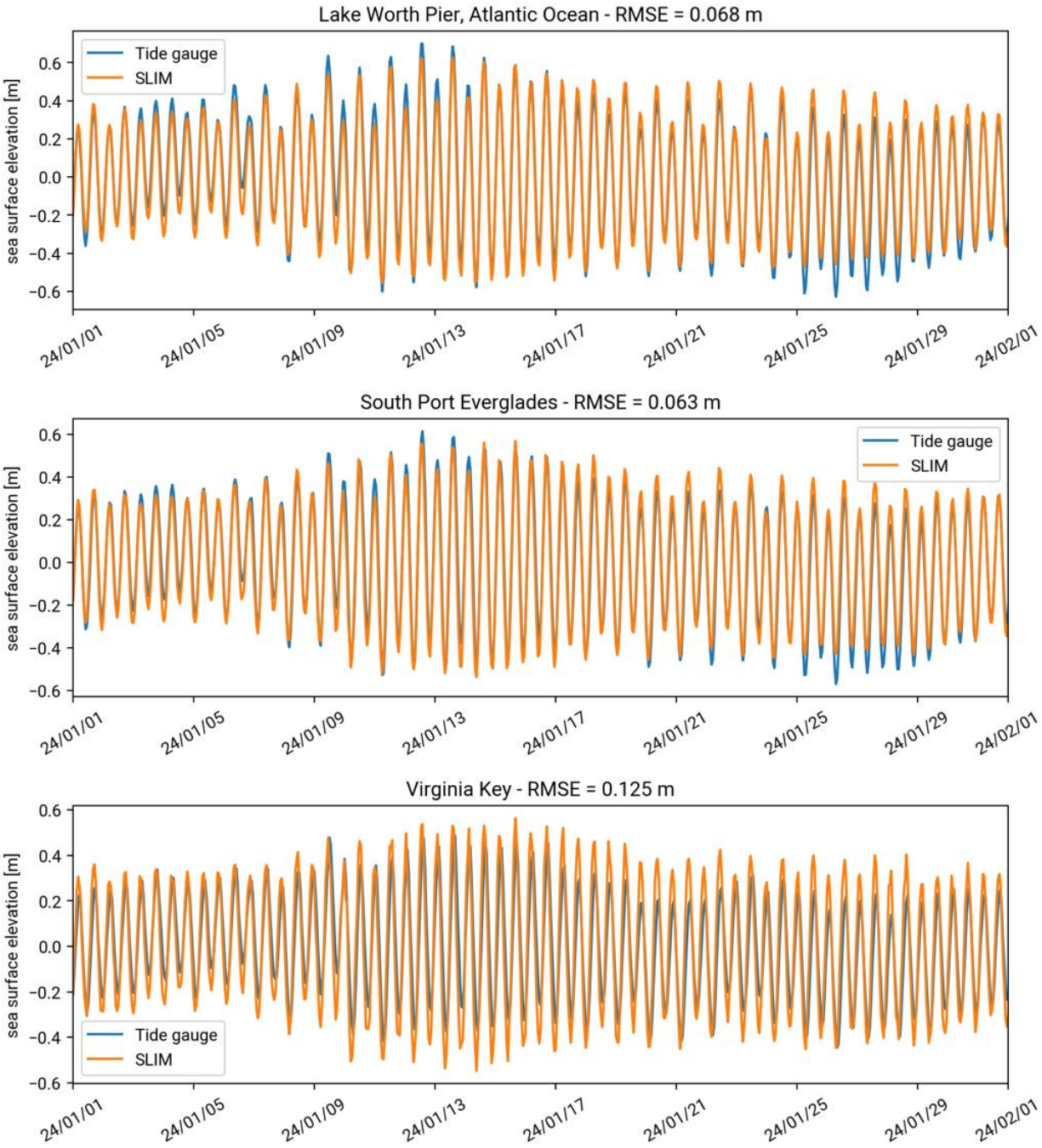

Figure 7. Validation of the simulated sea surface elevation at three stations within the area of interest in January 2024.

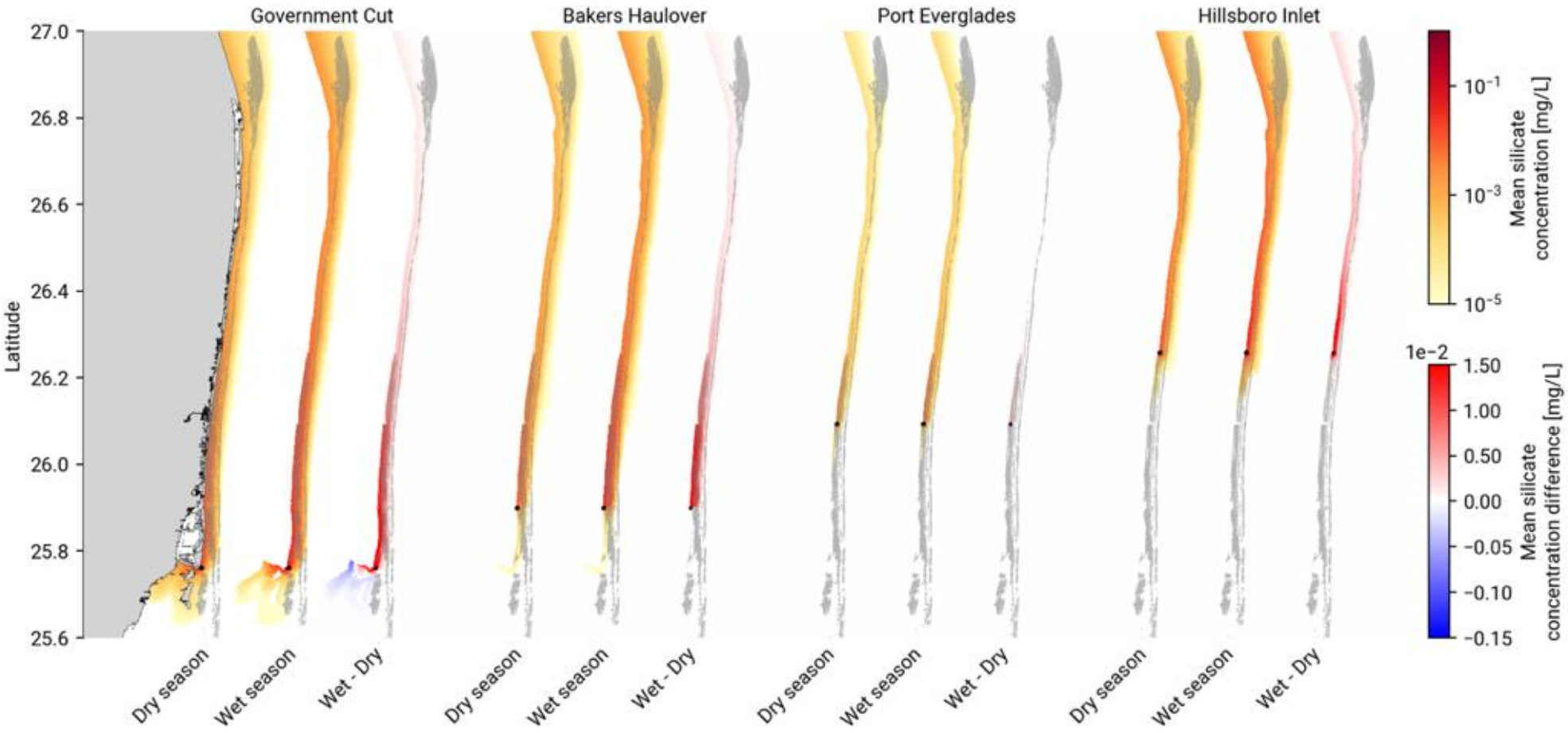

Figure 8. Seasonal mean concentration of silicate originating from the different inlets for the dry (left panels) and wet seasons (middle panels). The difference in concentration between wet and dry seasons is shown in the right panels. Silicate concentrations were higher during the wet season, while the simulated plumes extend further south during the dry season, especially near Government Cut.

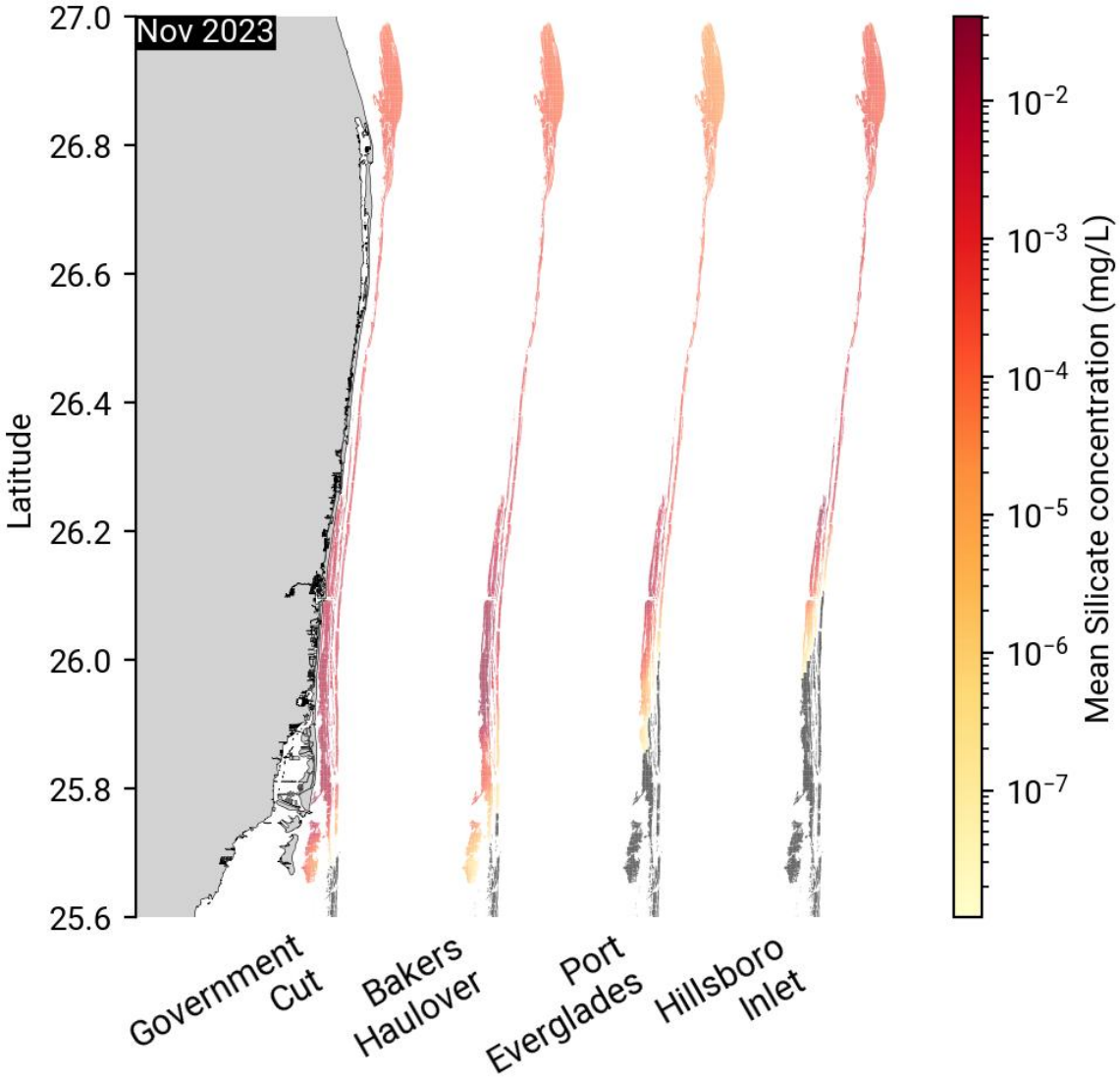

Figure 9. Illustration of coral reefs exposure to silicate in November 2023. Among the four inlets, Government Cut has the largest footprint, impacting most of the reefs in the KJCAP.

We further validated the simulated analyte concentrations against measurements at DBHydro monitoring stations (Figure 10). The model performs best near the inlets, where boundary conditions from DBHydro were imposed. At these sites, accuracy scores of up to 75% were found. The accuracy scores decreased with increasing distance from the inlets. On average, the simulated concentration levels matched 41% of the observed silicate concentration levels when no lag was allowed. The lowest accuracy scores were found at the northernmost and southernmost monitoring sites, in regions probably also impacted by sources of analytes that were not included in the model (*e.g.* Saint Lucie Inlet). Allowing for a lag of at most 2.5 days between the simulated and observed concentrations slightly increased the model performance. It shifted the distribution of the accuracy scores to the right and increased the mean accuracy score from 0.41 to 0.50.

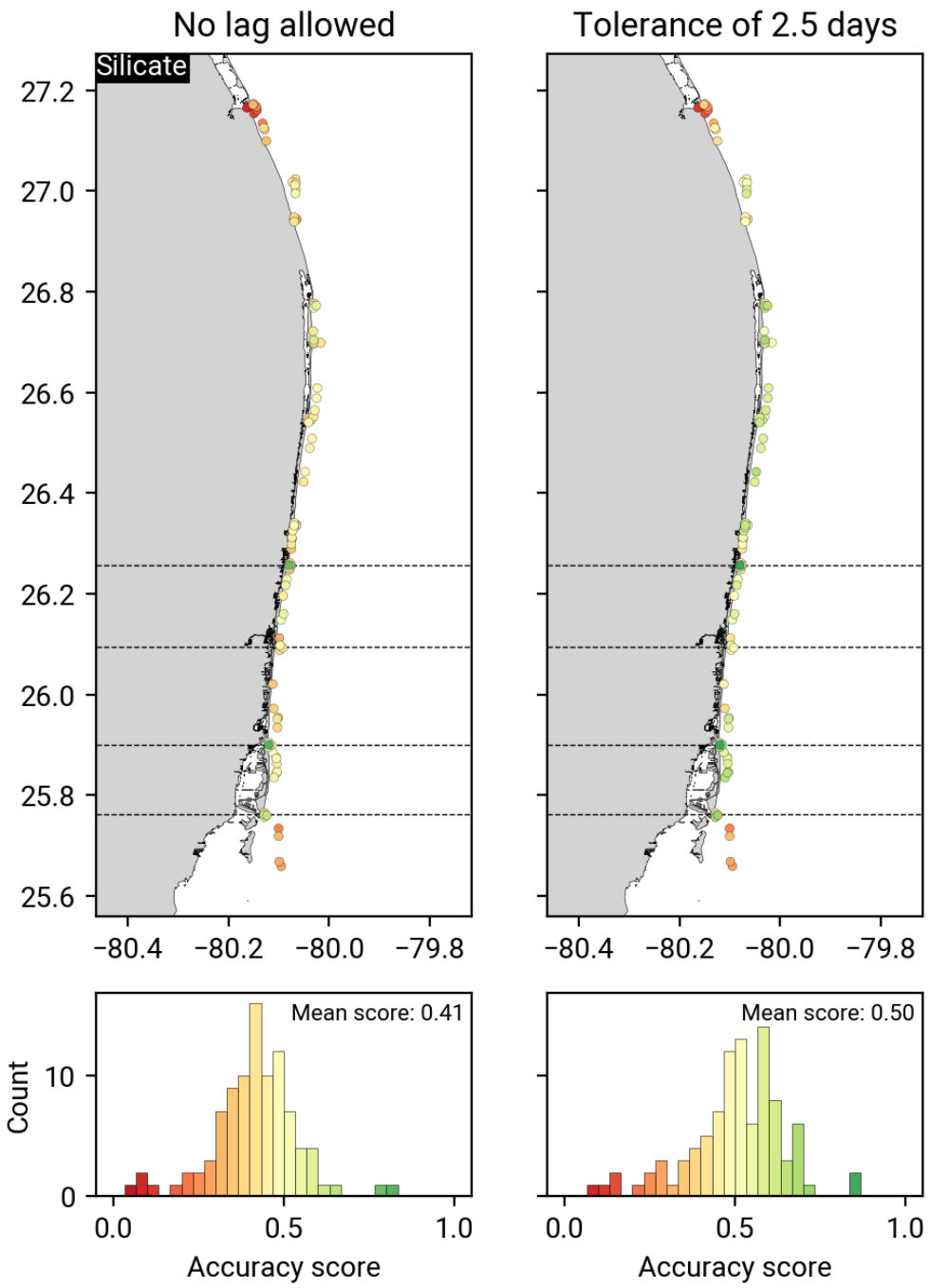

Figure 10. Validation of the simulated silicate concentration against measurements at monitoring stations. Three concentration levels (low, medium, high) were defined based on the first and third quartiles of the distributions of the observed and simulated concentrations. The accuracy score gives the fraction of simulated concentration levels matching the measured levels with no lag allowed (left), or with a tolerance of at most 2.5 days between the simulated and measured concentration peaks (right). The model performance decreases with increasing distance from the inlets. The lowest accuracy scores are observed at the southernmost and northernmost sites. Allowing a lag between the measured and simulated concentrations slightly improves the accuracy score.

3.1.4. Task 3d: Identifying the analyte(s) and inland source responsible for disease occurrence

For all the large corals where disease lesions were observed, we could use our model to identify which inlet contributed the most. These reef sites are ordered from south to north along the y axis in the four panels of Figure 14. Each panel represents an inlet, with its latitude highlighted by a dashed line on the y-axis. As Government Cut is the southernmost inlet, it had an impact on almost all the diseased reef sites. The other inlets, being further north, had a more limited impact, which further decreased with increasing inlet latitude. It is, however, noteworthy that these inlets could impact reefs located south of the inlet, which again shows that the ocean circulation along East Florida's coastline is not a mere conveyor belt transporting disease agents northward. It however remains that Government Cut inlet had the largest detrimental effect, followed by Baker's Haulover and then Port Everglades. On average, 78% of the silicate found at sites with lesions originated from Government Cut, while 17% and 4% came from Baker's Haulover and Port Everglades, respectively. The relative contribution of Government Cut to the analyte concentration over the northern reef sites varies seasonally and was lower during the wet season.

We also derived a complete time series of analyte concentrations on reefs where disease signs were observed. These time series were derived from the analyte dispersal simulations initiated at each inlet and cover the entire 3-year simulated period. They indicated the concentration of all analytes over the reef site for each of the four considered inlets. As an illustration, we show the time series of the concentrations of the 7 considered analytes at reef site LC-005 (Figure 11). This site is located north of Port Everglades and was mostly impacted by Government Cut and Baker's Haulover (see Figure 12), with some punctual peaks of analyte concentrations from Port Everglades.

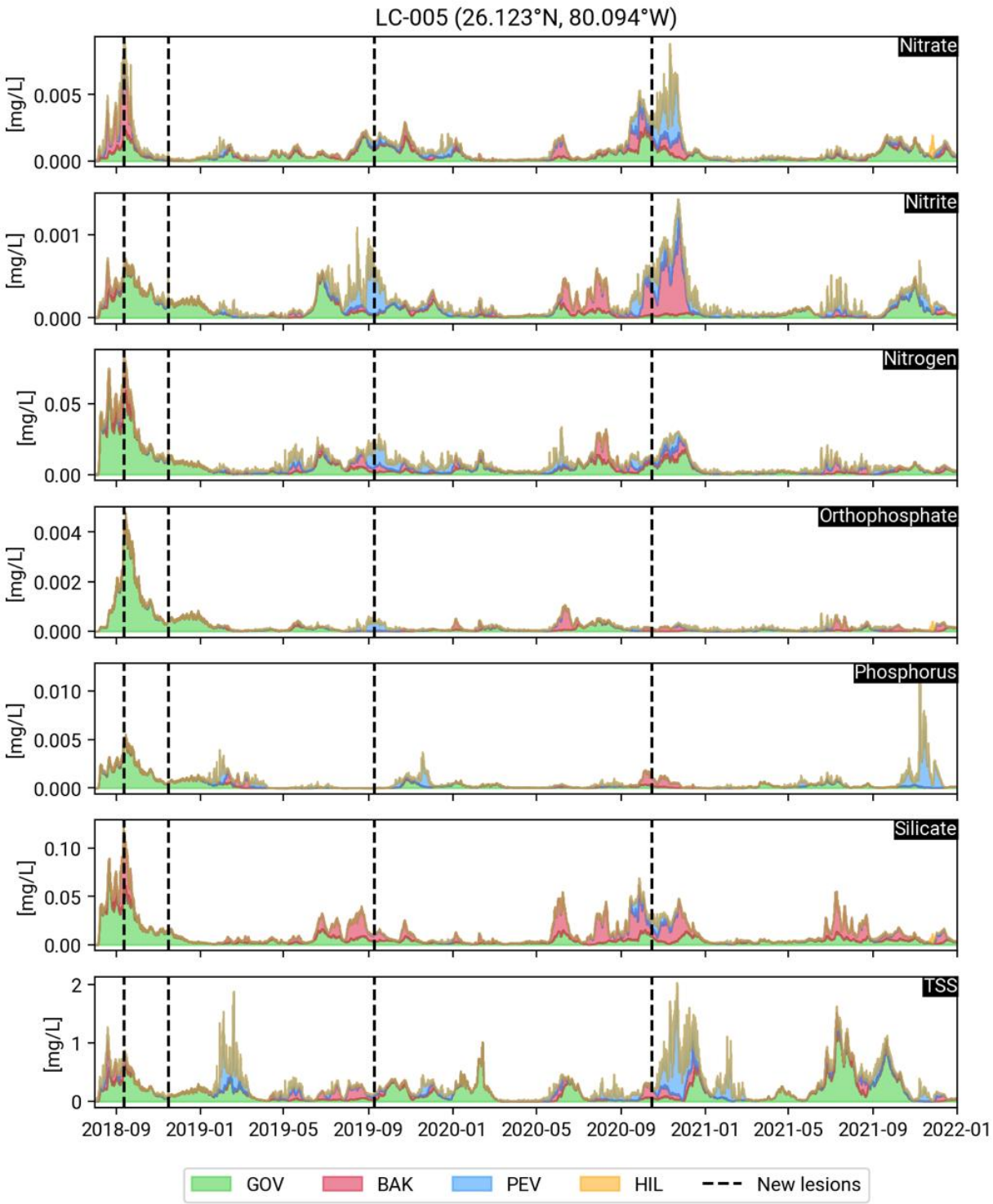

Figure 11. Time series of the contribution of each inlet to the modeled analyte concentrations over reef site LC-005. Dotted lines correspond to the observation dates of new lesions. Government Cut (GOV) and Bakers Haulover (BAK) were the main source of analytes to the reef site. Punctual peaks of analyte concentrations from Port Everglades (PEV) were observed. Hillsboro Inlet (HIL) had a negligible impact on the site.

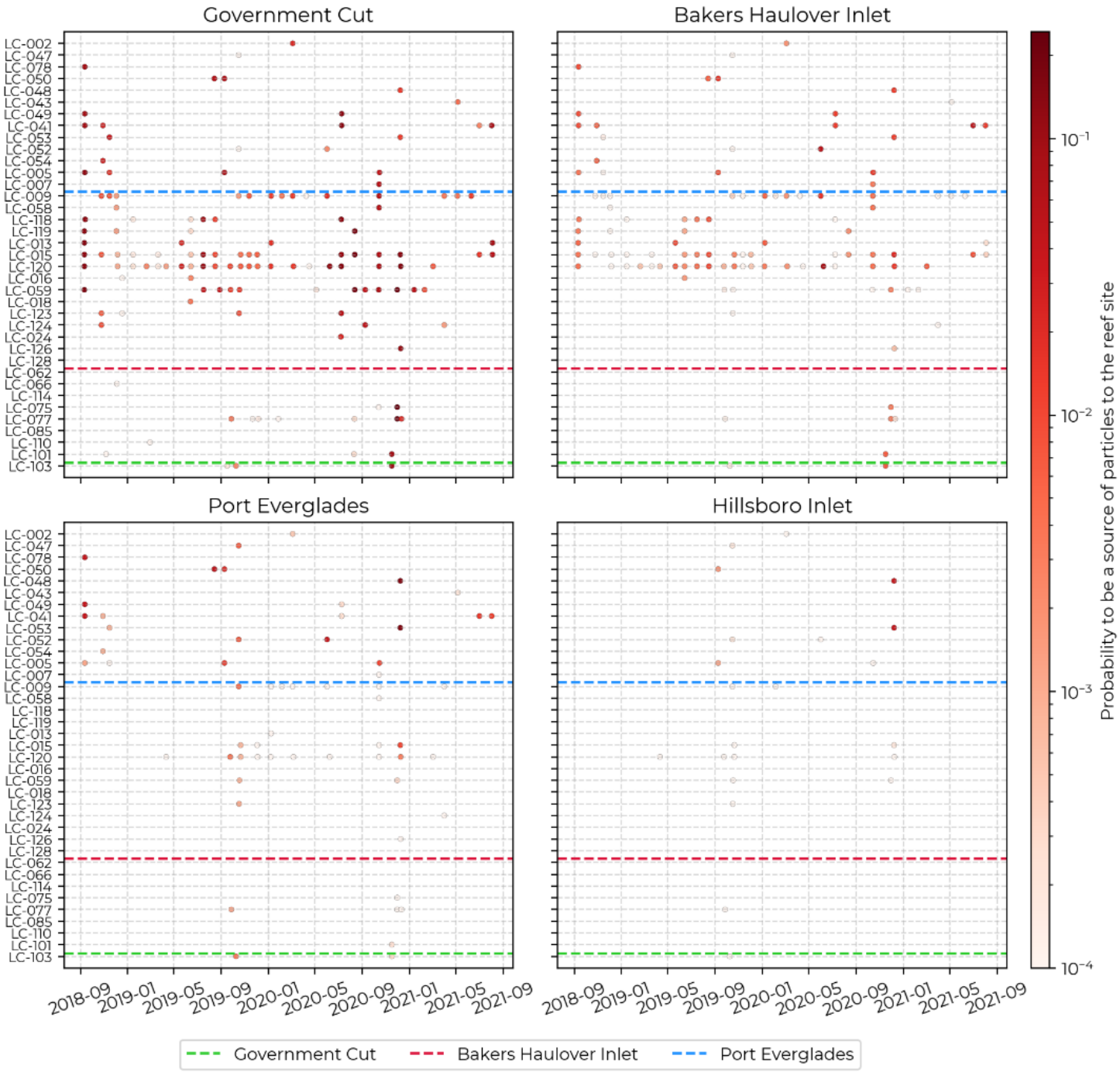

Figure 12. Probability for each inlet to be a source of particles that reached the reef monitoring sites during the 10 days preceding the observation of new SCTLD lesions. The sites on the y-axis are ordered from south to north, the points correspond to the dates and locations of observation of new lesions and their color indicate the probability for particles to originate from the different inlets. The latitudes of the different inlets are indicated by colored dashed lines.

3.2. Task 4: Quantify *in situ* temperature stress differences between Biscayne and further north

Significant differences in mean nearshore reef temperatures were found from April through October between BC1 (Fort Lauderdale) (28.6 ±0.04), DC6 (Haulover) (28.7 ±0.04), and DC8 (Key Biscayne) (28.9 ±0.04) in 2022 and in 2023 (BC1=28.8 ±0.03; DC6=28.9 ±0.03; DC8=29.3 ±0.03). Temperature differences were also significant at each site between years, with 2023 being higher in every case. Key Biscayne mean temperatures were the highest between sites four of seven months in 2022 (Figure 13) and six of seven in 2023 (Figure 14). The highest monthly mean temperatures were at Key Biscayne in July (31.4°C) and August (31.1°C) 2023. The distribution of temperatures in 2022 showed that Key Biscayne was equal to or greater than 31°C 12.1% of the time versus 8.5% in Haulover and 5.6% in Fort Lauderdale (Figure 15). In 2023, Key Biscayne was equal to or greater than 31°C 17.6% of the time (898 hours) versus 7.5 % in Haulover, and 4.7% in Fort Lauderdale (Figure 16). In both years, Key Biscayne reached the 30.5°C bleaching threshold earlier than the more northern sites and reached the maximum temperature of all sites either year on August 9 and 10 2023 of 32.7°C (Figure 17 and 18).

Monthly monitoring data on 59 large *Orbicella faveolata* colonies in the study area from September 2018 to July 2024 showed spatiotemporal patterns in the number of SCTLD treatments and percentage of bleaching per colony (Figure 19). The SCTLD seasonal variation in these corals has been reported many times, however the bleaching has not. Several corals had a high prevalence of low partial bleaching (e.g. LC-123, LC-120, LC-059, LC-157) whereas LC-002 had higher partial bleaching percentages during 38 out of 73 visits (52.6%) (Figure 20). The highest bleaching in the dataset occurred between August and December 2023 on corals south of Government Cut inlet (Figure 19). Figure 18 illustrates the raw temperature values from the four stations with the large *O. faveolata* SCTLD and bleaching prevalence across the study period. SCTLD spiked on these colonies in July and dropped in consecutive months as bleaching prevalence rose. SCTLD prevalence and incidence on the large *O. faveolata* colonies in southeast Florida was the highest ever recorded leading up to the bleaching (Walker et al 2024). In August, all colonies south of Government Cut bleached extensively, whereas no colonies further north visibly bleached. Unbleached colonies continued to acquire SCTLD lesions in the north, whilst SCLTD quiesced on bleached colonies (Figure 21).

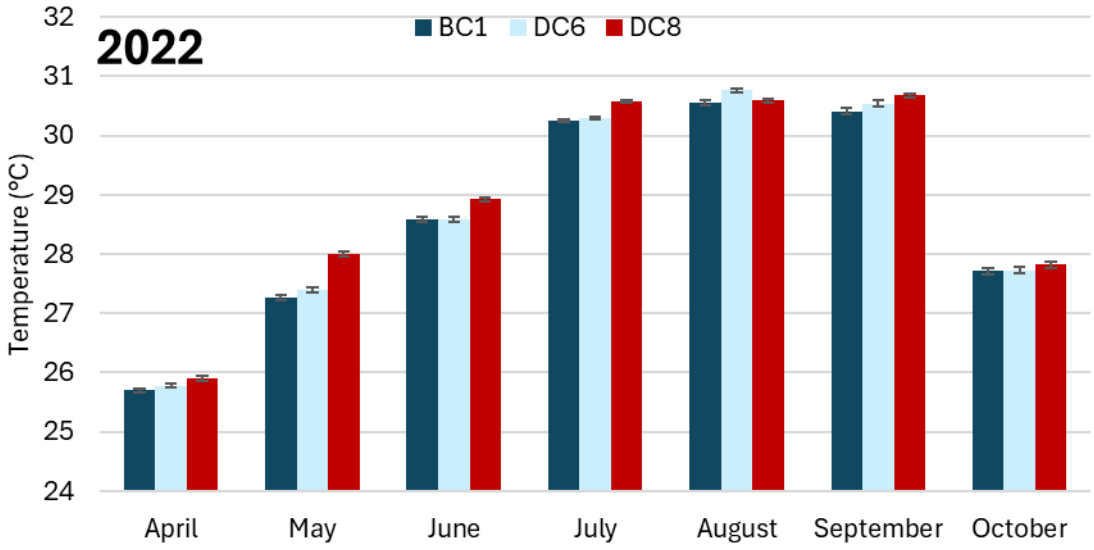

Figure 13. Mean monthly temperature by site between April and October for three nearshore SECREMP stations that differ by latitude in 2022. Error bars indicate standard error.

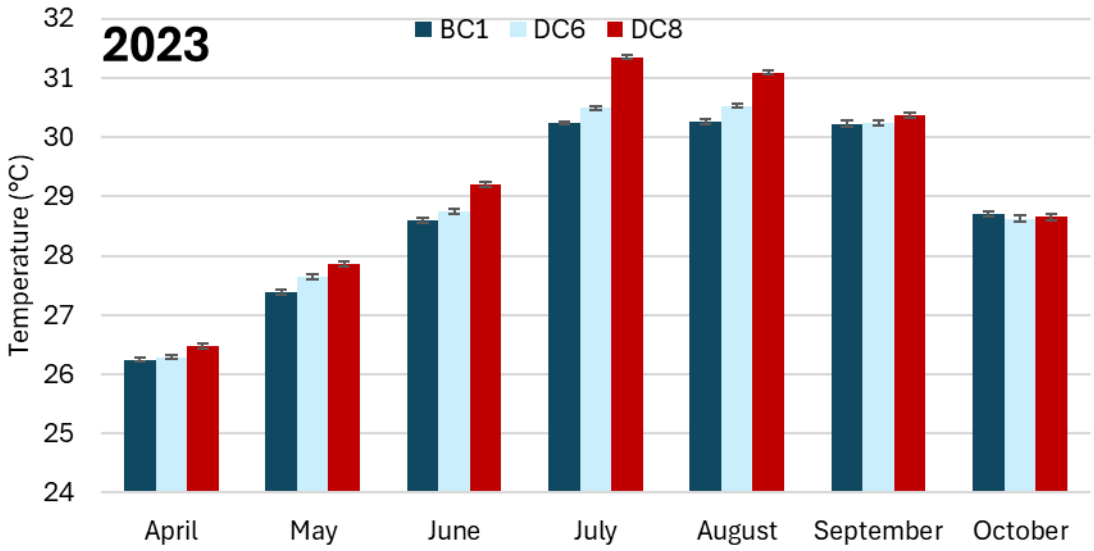

Figure 14. Mean monthly temperature by site between April and October for three nearshore SECREMP stations that differ by latitude in 2023. Error bars indicate standard error.

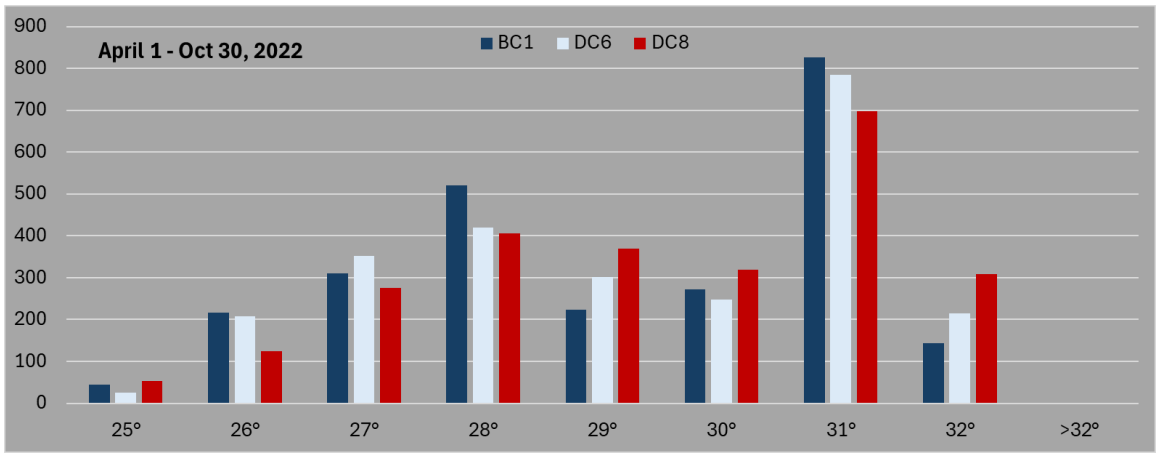

Figure 15. Distribution of temperatures logged by site between April and October for three nearshore SECREMP stations that differ by latitude in 2022.

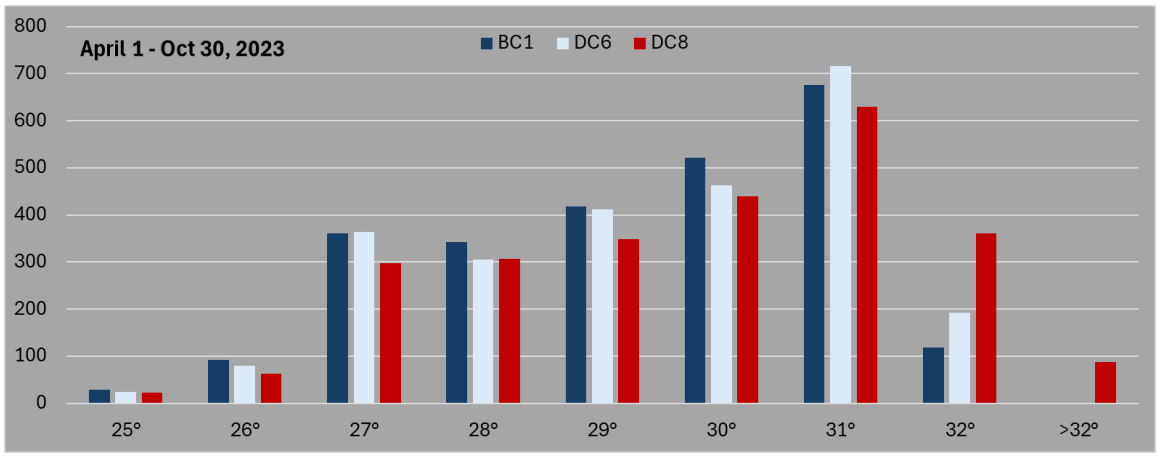

Figure 16. Distribution of temperatures logged by site between April and October for three nearshore SECREMP stations that differ by latitude in 2023.

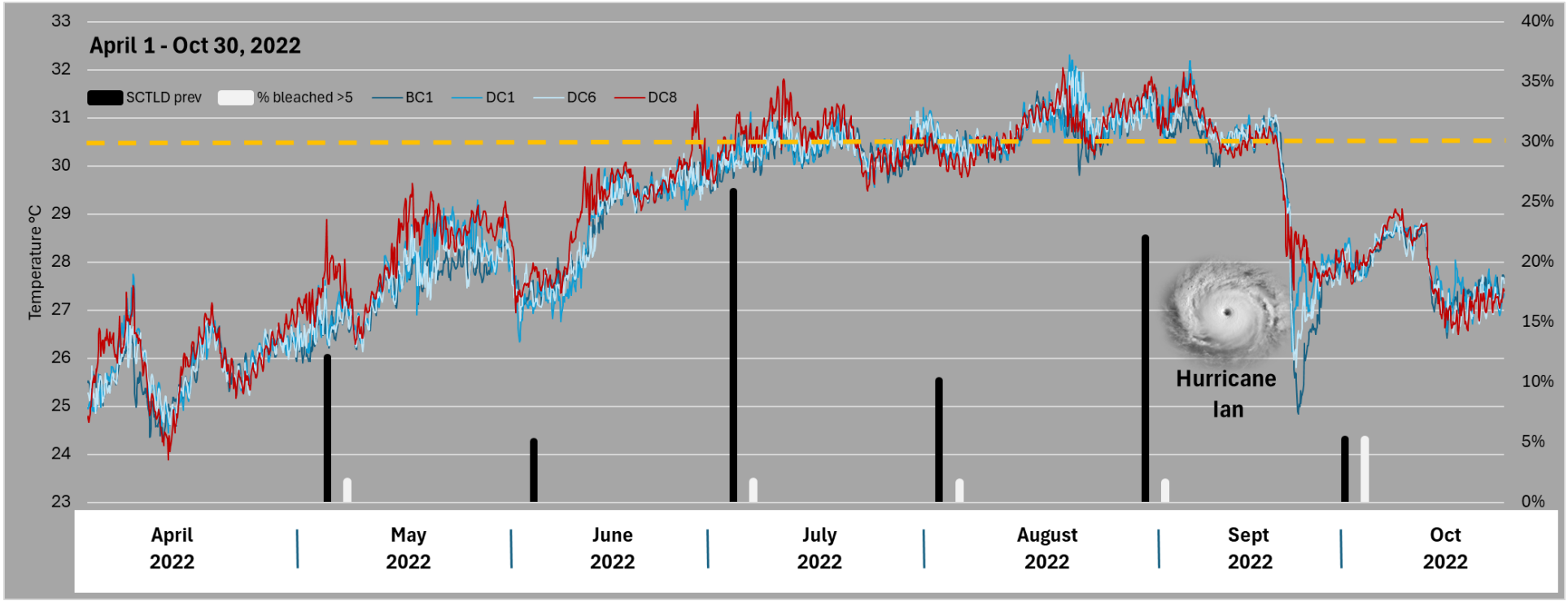

Figure 17. Raw temperature data from four *in situ* loggers at nearshore reef SECREMP stations combined with SCTLD and bleaching prevalence of the large priority monitoring *O. faveolata* colonies between April and October 2022. Left axis indicates temperature and right axis indicates percentage of afflicted colonies. Yellow dotted line indicates coral bleaching threshold. Note the significant dip in temperatures at sites north of Government Cut during Hurricane Ian.

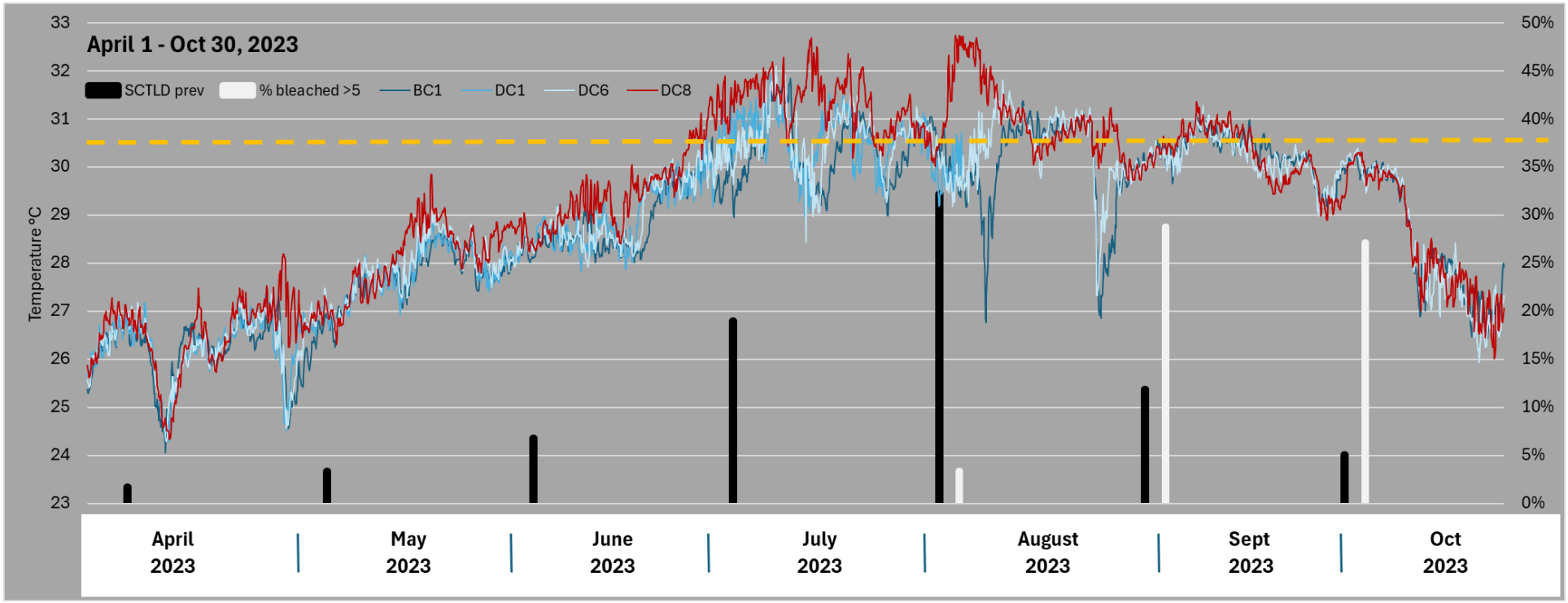

Figure 18. Raw temperature data from four *in situ* loggers at nearshore reef SECREMP stations combined with SCTLD and bleaching prevalence of the large priority monitoring *O. faveolata* colonies between April and October 2023. Left axis indicates temperature and right axis indicates percentage of afflicted colonies. Yellow dotted line indicates coral bleaching threshold. Red line indicates the only site south of Government Cut was substantially higher than more northern sites through much of the timeline.

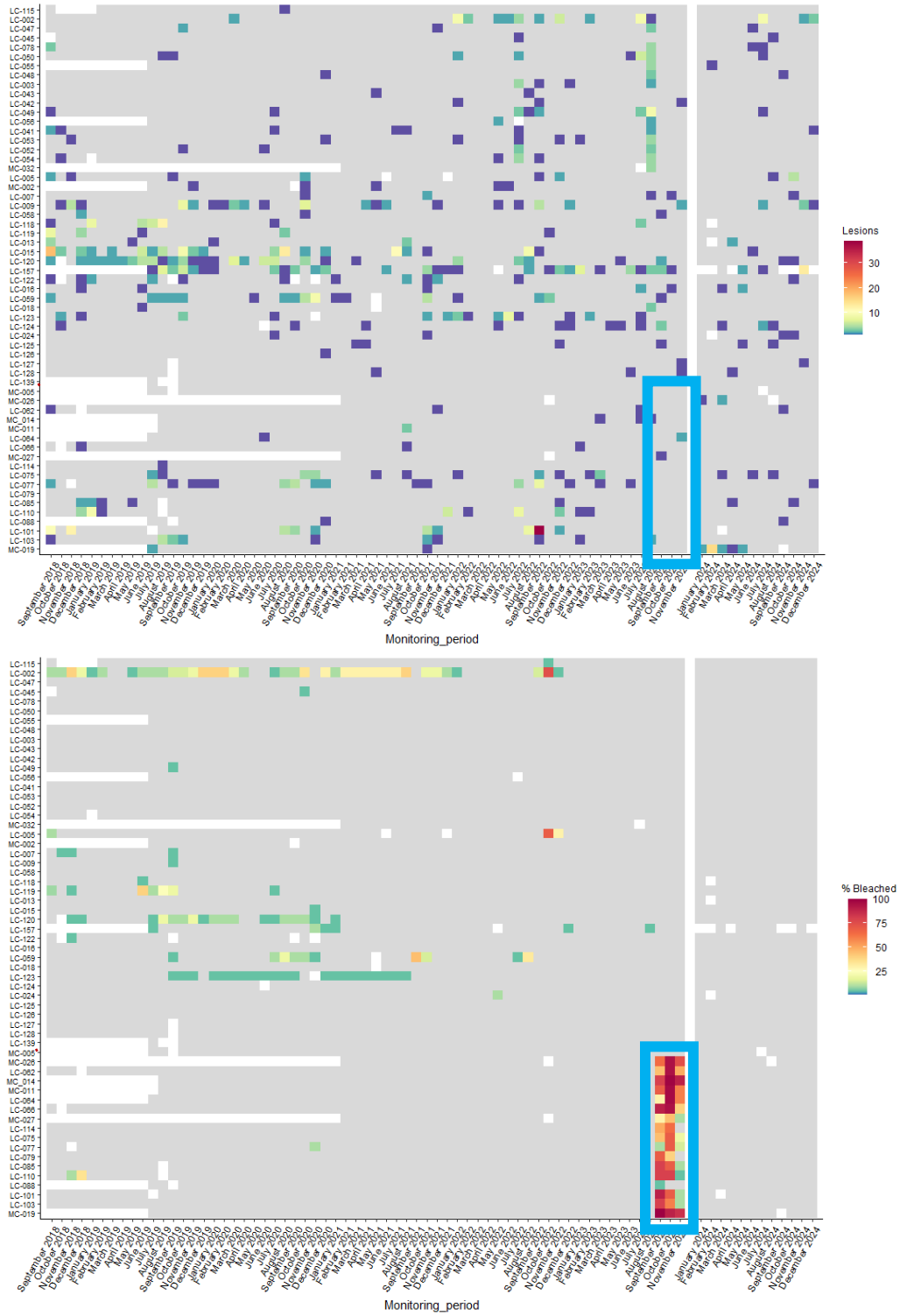

Figure 19. Tile plots showing the number of SCTLD lesions (top) and percent bleached on colonies that bleached at least 5% (bottom) between Sept. 2018 and Dec. 2024. Colonies are sorted by descending latitude. Blue square outlines the 2023 bleaching event in both plots. Red dashed line indicates the corals north (above) and south (below) of Government Cut. Note the near absence of SCTLD in the corals that bleached and their slow recovery.

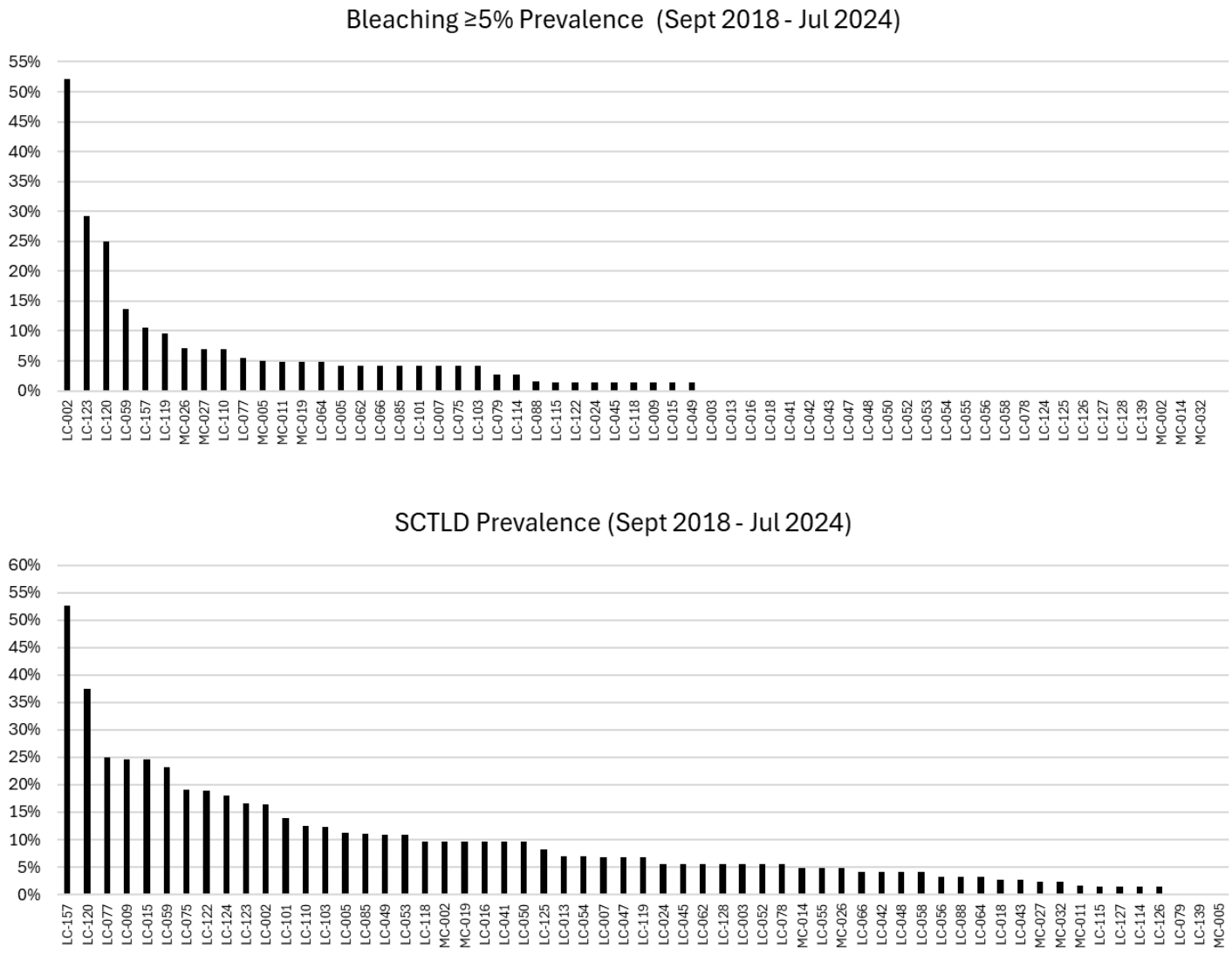

Figure 20. The percentage of visits by colony that had at least 5% partial bleaching (top) and at least one SCTLD lesion (bottom) sorted from high to low between September 2018 and July 2024.

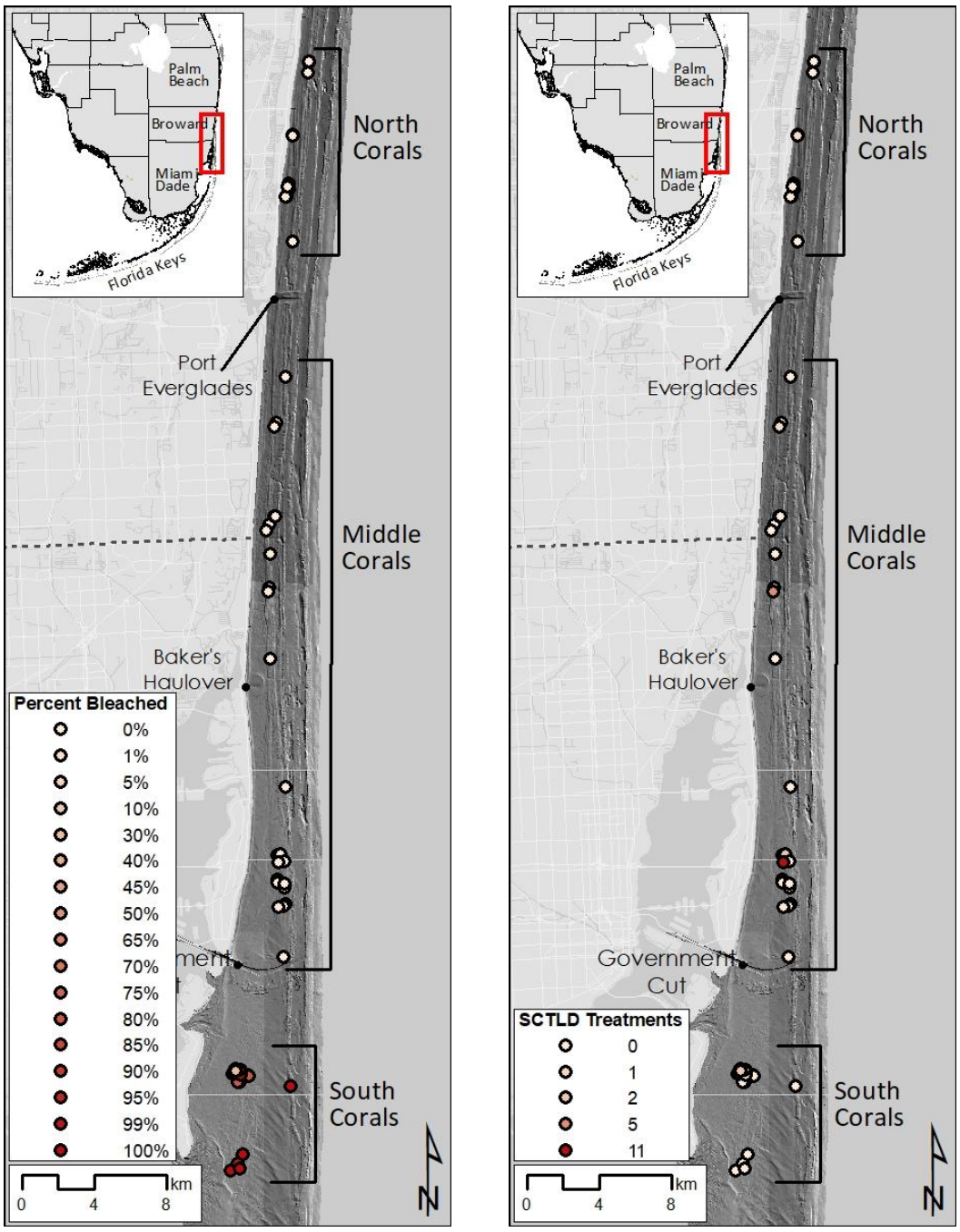

Figure 21. Large *Orbicella faveolata* colonies colored by the percent bleached (left) and the number of SCTLD treatments (right) in September 2023. All bleached colonies were south of Government Cut and SCLTD persisted in unbleached colonies.

3.3. Task 5: Quantify seasonal patterns in water quality by inlet exposures of each analyte through 2023

A permutational multivariate analysis of variance (PERMANOVA) of the transformed and normalized water quality analytes at each site identified a significant combined interaction with three fixed factors: Year, Season, and Inlet Exposure Area (IEA) (p=0.001). When analyzed by individual season per year, Inlet Exposure Area was significant in every test except Dry 2020 (p=0.09) and Dry 2022 (p=0.21). Aside from those seasons, pairwise comparisons between IEAs showed that Biscayne water quality sites were significantly different than other areas in 23 out of 27 comparisons (85%). Conversely, the 27 comparisons between other IEAs yielded nine significant ones (33%). The majority of those were between Port Everglades and Government Cut which were significantly different seven out of eleven seasons (64%). Baker's Haulover and Government Cut were only different one out of eleven seasons.

Seasonal bootstrap averages plots of the analytes by samples based on the Inlet Contributing Areas aid in visualizing the differences (Figure 22 & 23). The plots illustrated the significant PERMANOVA results where in almost every season Biscayne water quality sites differed from locations further north. The plots also showed how the similarity of water quality between the IEAs differed over time. Some seasons (e.g. Dry 2022) were all similar, whereas other seasons (e.g. Wet 2019) they were all different. During the wet season in 2023, Biscayne was significantly different from the other IEAs. A similarity percentages comparison of water quality analytes driving the difference between Government Cut and Biscayne during the 2023 wet season (summer) showed that Government Cut had much higher total phosphorus, nitrate, silicate, and nitrite (Table 3). A multivariate pairwise PERMANOVA of the similarity percentages of the IEA water quality analytes each season between IEAs found that Biscayne was significantly different from Government Cut (p=0.03), driven by higher nitrite, nitrate, and TSS in Government Cut and higher silicate and orthophosphate in Biscayne (Table 4). An MDS plot of IEA seasonal similarity percentages of each analyte showed Biscayne in mostly on the right side indicating it had lower nutrients as compared to those further left (Figure 24). In Dry 2024 and 2021, Biscayne had higher orthophosphates than other IEAs and higher TSS in Wet 2021.

Table 2. PERMANOVA p-values from post-hoc pairwise test across Inlet Exposure Areas by year and season. Bold shaded indicates a significant difference between areas for the season.

Group comparisons	Dry 2019	Wet 2019	Dry 2020	Wet 2020	Dry 2021	Wet 2021	Dry 2022	Wet 2022	Dry 2023	Wet 2023	Dry 2024
Biscayne, Government Cut	**0.005**	**0.03**	0.254	**0.017**	**0.041**	0.076	0.147	**0.005**	0.112	**0.009**	**0.014**
Biscayne, Baker's Haulover	0.359	**0.019**	0.292	**0.011**	**0.036**	**0.001**	0.287	**0.003**	**0.007**	**0.003**	**0.047**
Biscayne, Port Everglades	**0.03**	**0.012**	0.301	**0.008**	**0.006**	**0.001**	0.462	**0.018**	0.467	**0.007**	**0.021**
Government Cut, Baker's Haulover	0.862	**0.001**	0.417	0.426	0.784	0.129	0.498	0.07	0.474	0.751	0.438
Government Cut, Port Everglades	**0.001**	**0.001**	**0.011**	**0.005**	0.291	**0.008**	0.108	**0.007**	**0.016**	0.495	0.175
Baker's Haulover, Port Everglades	0.105	0.271	0.292	**0.025**	0.449	0.06	0.274	0.226	**0.005**	0.383	0.754

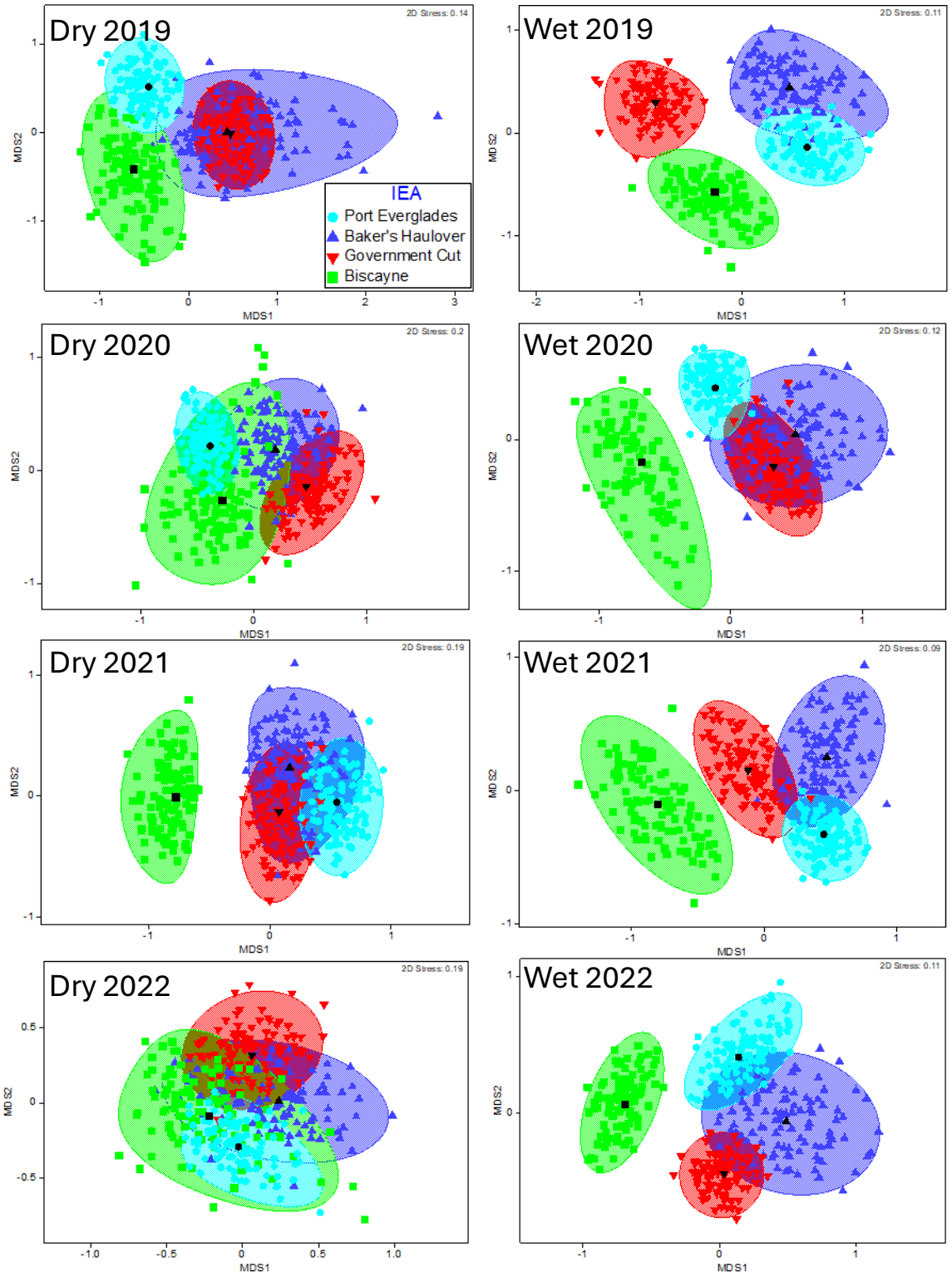

Figure 22. Bootstrap averages plots by season (2019-2022) of the analytes at the reef water quality monitoring sites categorized by inlet exposure area. Note that Biscayne sites had distinct and significantly different water quality from those further north in most seasons.

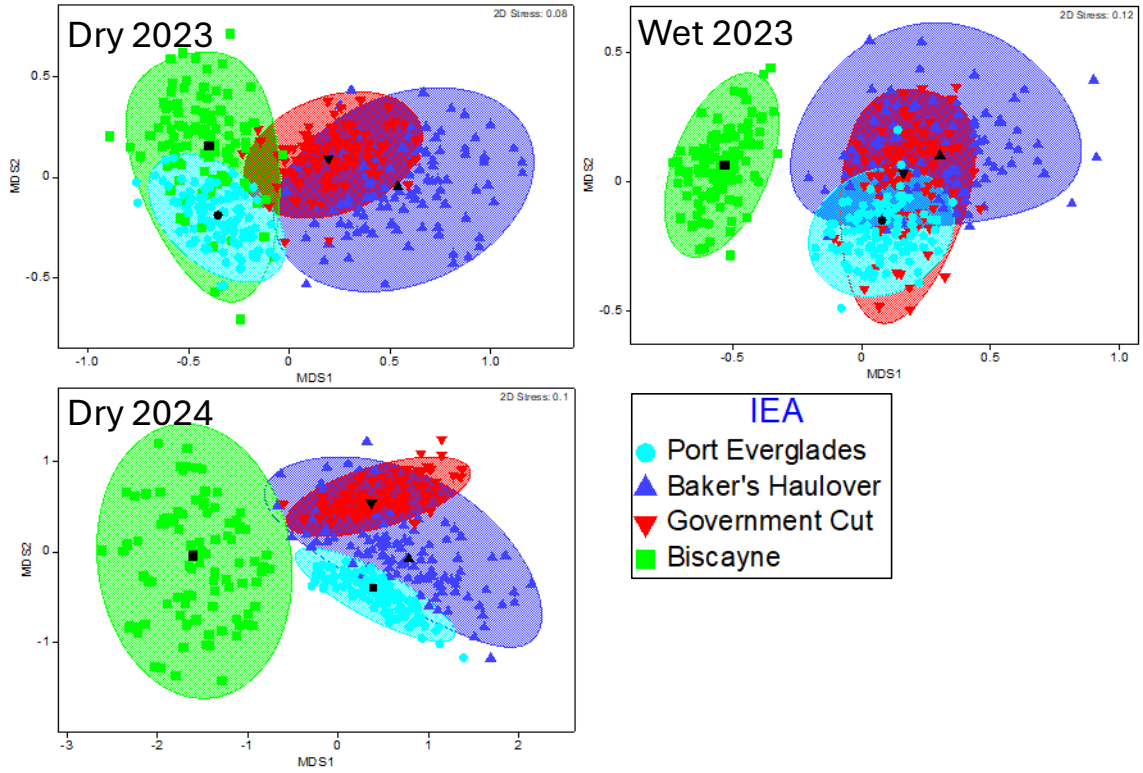

Figure 23. Bootstrap averages plots by season (2023-2024) of the analytes at the reef water quality monitoring sites categorized by inlet exposure area. Note that Biscayne sites had distinct and significantly different water quality from those further north in most seasons.

Table 3. Similarity percentages comparison of water quality analytes driving the difference between Government Cut and Biscayne during the 2023 wet season (summer). Government Cut had much higher Total Phosphorus, Nitrate, Silicate, and Nitrite.

Analyte	Gov Cut Av.Value	Biscayne Av.Value	Av.Sq.Dist	Sq.Dist/SD	Contrib%	Cum.%
Total Phosphorus	0.141	-0.0285	1.33	0.28	38.19	38.19
Nitrate	0.00492	-0.186	0.941	0.76	26.95	65.14
Silicate	0.262	-0.268	0.585	0.81	16.75	81.9
Nitrite	0.316	0.0398	0.428	0.52	12.25	94.15
TSS	-0.413	-0.507	0.179	0.76	5.13	99.29
Orthophosphate	0.0452	0.0328	0.0249	0.59	0.71	100

Table 4. Similarity percentages comparison of IEA analytes by season driving the difference between Government Cut and Biscayne. Government Cut had much higher Nitrite, Nitrate, and TSS and Biscayne had higher Silicate and Orthophosphate.

Analyte	Gov Cut Av.Value	Biscayne Av.Value	Av.Sq.Dist	Sq.Dist/SD	Contrib%	Cum.%
Nitrite	0.128	-0.12	0.603	0.6	25.32	25.32
Nitrate	0.144	-0.29	0.46	0.59	19.33	44.65
Silicate	-0.00275	-0.508	0.406	0.99	17.04	61.69
Orthophosphate	-0.144	0.0806	0.353	0.59	14.84	76.53
TSS	0.0091	-0.0337	0.338	0.61	14.2	90.74
Total Phosphorus	-0.103	-0.134	0.221	0.77	9.26	100

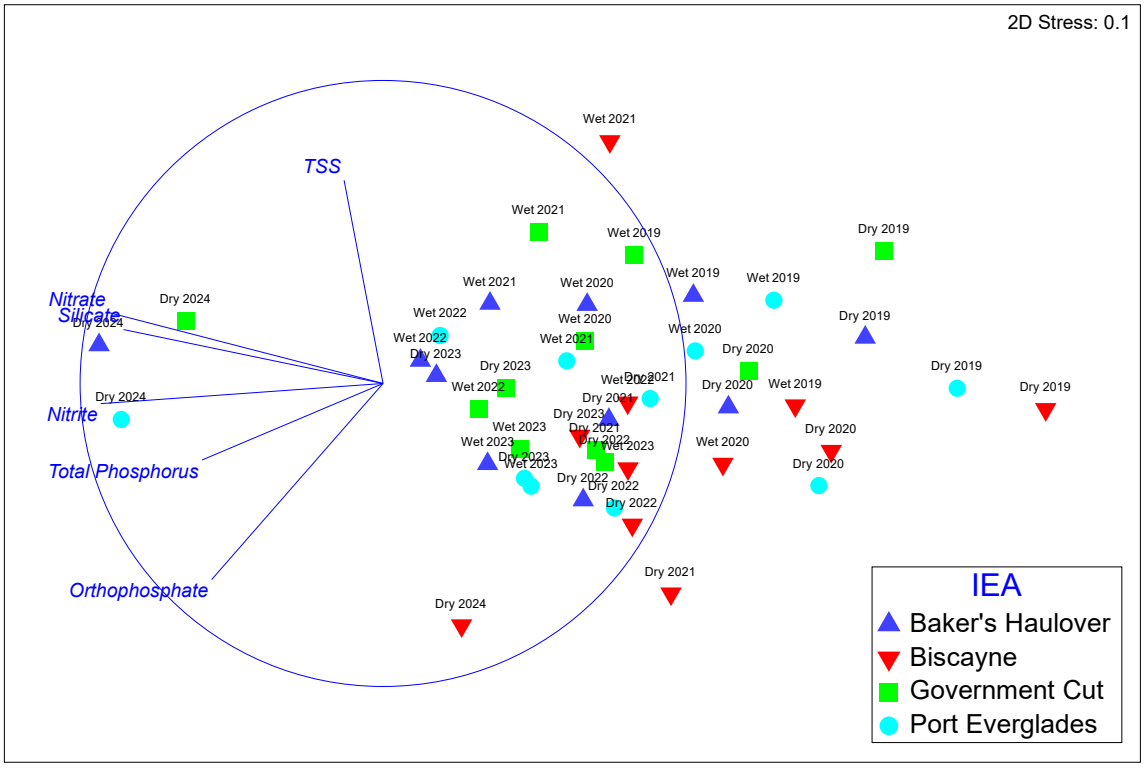

Figure 24. MDS plot of IEA seasonal similarity percentages of each analyte showing the similarity between IEAs over time. Blue lines indicate the analytes driving the similarities. Note the Biscayne is mostly on the right side indicating it had lower nutrients as compared to those further left. In Dry 2024 and 2021, Biscayne had higher orthophosphates than other IEAs and higher TSS in Wet 2021.

3.4. Task 6: Build statistical models to investigate the possible links between water quality seascapes, SCTLD occurrence, and patterns of coral bleaching

3.4.1. Modeling spatial and temporal variations in in situ water quality

There was considerable variation among analytes in their concentrations across the KJCAP, as well as within any given analyte across space and time (Figure 25). Our statistical models explained between 42% and 79% of this variation (i.e., using the training data), and 22% to 64% of the variation when predicting to data the models had not seen before (i.e., using the test data) (Table 5). These patterns of model performance also remained largely unchanged when the models were trained on a lower portion of the training data (0.5 bag fraction results in Table 5).

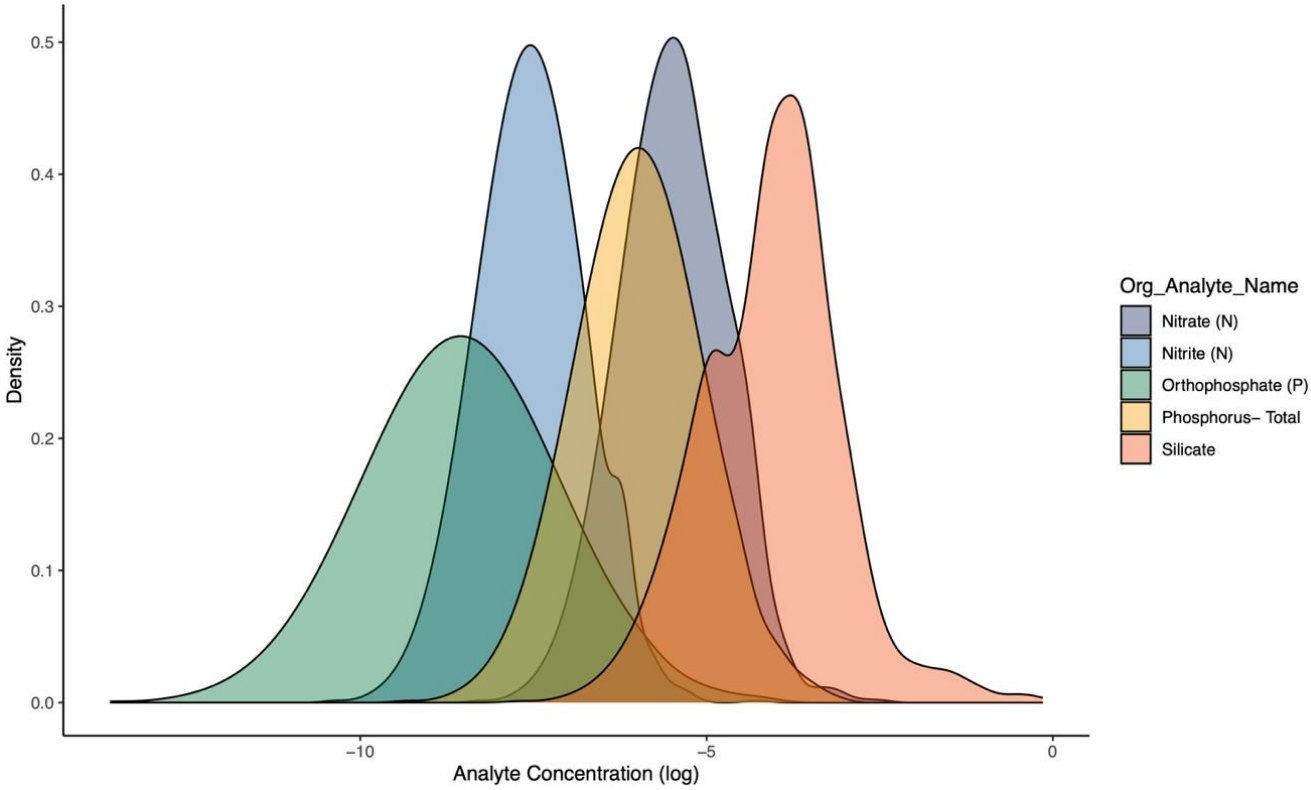

Figure 25. Variations in the MDL-adjusted log concentration of five of the six measured on-reef water quality analytes from Jan 2019 to Dec 2023 (total suspended solids not shown due to differences in scale) (n=1658 for each analyte).

Table 5. Boosted regression tree model performance statistics from predicting the on-reef variation in the concentration of six water quality analytes from Jan 2019 to Dec 2023 across the KJCAP. cv, cross-validated; cvPercentage explained (cross-validated percentage deviance explained) is used to assess model performance.

	Nitrate	Nitrite	Orthophosphate	Phosphorus	Silicate	TSS
Model Parameters						
Number observations	1658	1658	1658	1658	1658	1658
Tree complexity	4	5	5	4	4	4
Learning rate	0.001	0.001	0.001	0.001	0.001	0.001
Bag fraction	0.5	0.7	0.7	0.7	0.7	0.8
Number of trees	25550	19950	12500	14100	15800	13300
Model Performance						
Percentage explained (%)	**71.2**	**78.9**	**70.0**	**48.3**	**67.1**	**41.5**
cvPercentage explained (%)	**54.4**	**63.9**	**54.9**	**28.9**	**52.6**	**21.8**
Model Performance - 0.5 bag fraction						
Percentage explained (%)	71.2	78.2	69.6	47.9	66.5	40.2
cvPercentage explained (%)	54.4	63.6	54.5	28.6	52.2	21.1

Across the six analytes, the predictor variables responsible for explaining their patterns of underlying variation differed (Table 6). Variations in **nitrate** were predominantly explained by variations in inlet exposure area (IEA) outflow, high wind events, survey year, and rainfall. Overall, nitrate concentrations were higher when inlet outflow was higher, when there were more seaward and landward high wind events, in later years (particularly 2021-2023), and when there was more rainfall (Figure 26). Variations in **nitrite** were predominantly explained by survey year, IEA outflow, and rainfall. Overall, nitrite concentrations were higher in later years (particularly 2022-2023), when inlet outflow was higher, and when there was more rainfall (Figure 27). Variations in **orthophosphate** were predominantly explained by variations in survey year, as well as some variation explained by depth, and high wind events. Overall, orthophosphate concentrations were higher in later years (particularly 2021-2023), at shallower depths (particularly shallower than 5 m), and some (weaker) evidence of being higher when the number of both seaward and landward high wind events increased (Figure 28). Variations in **phosphorus** were also predominantly explained by variations in survey year, as well as some variation explained by rainfall, and high wind events. Overall, phosphorus concentrations were higher in later years and showed more nuanced relationships with rainfall and seaward high wind events (Figure 29). Variations in **silicate** were predominantly explained by variations in depth, survey year, and IEA outflow. Overall, silicate concentrations were higher at shallower depths (particularly shallower than 5 m), in later years, and when there was higher IEA outflow (Figure 30). Variations in **total suspended solids (TSS)** were predominantly explained by variations in IEA outflow, survey year, rainfall, and high wind events. Overall, TSS concentrations were higher when there was higher IEA outflow, in 2021-2022 compared to 2019-2020, and especially when compared to 2023, and when there were more landward high wind events (Figure 31). The relationship between TSS and rainfall was harder to decipher, but TSS concentrations appeared to decrease with increasing rainfall.

Table 6. Relative (Rel) influence of predictor variables in predicting the on-reef variation in the concentration of six water quality analytes from Jan 2019 to Dec 2023 across the KJCAP. The top four predictors are shown in each case, or when their cumulative (Cumul) relative influence was less than 40%, six are shown.

Analyte	Predictor	Rel Influence (%)	Cumul Influence (%)
Nitrate	Flow (7 days prior)	10.4	10.4
	Seaward wind (7 days prior)	10.1	20.5
	Landward wind (30 days prior)	8.6	29.1
	Flow (30 days prior)	8.1	37.2
	Year	8.1	45.3
	Rain (3 days prior)	7.9	53.2
Nitrite	Year	27.3	27.3
	Flow (7 days prior)	15.8	43.1
	Rain (30 days prior)	14.5	57.6
	Seaward wind (30 days prior)	5.4	63.0
Orthophosphate	Year	37.0	37.0
	Depth	7.6	44.6
	Seaward wind (3 days prior)	7.3	51.9
	Landward wind (30 days prior)	5.8	57.7
Phosphorus	Year	20.0	20.0
	Rain (30 days prior)	8.6	28.6
	Seaward wind (7 days prior)	8.2	36.8
	Rain (7 days prior)	7.4	44.2
Silicate	Depth	23.0	23.0
	Year	13.6	36.6
	Flow (30 days prior)	12.7	49.3
	Flow (7 days prior)	9.9	59.2
TSS	Flow (prior 30 days)	10.6	10.6
	Year	10.5	21.1
	Rain (7 days prior)	10.4	31.5
	Landward wind (7 days prior)	9.1	40.6

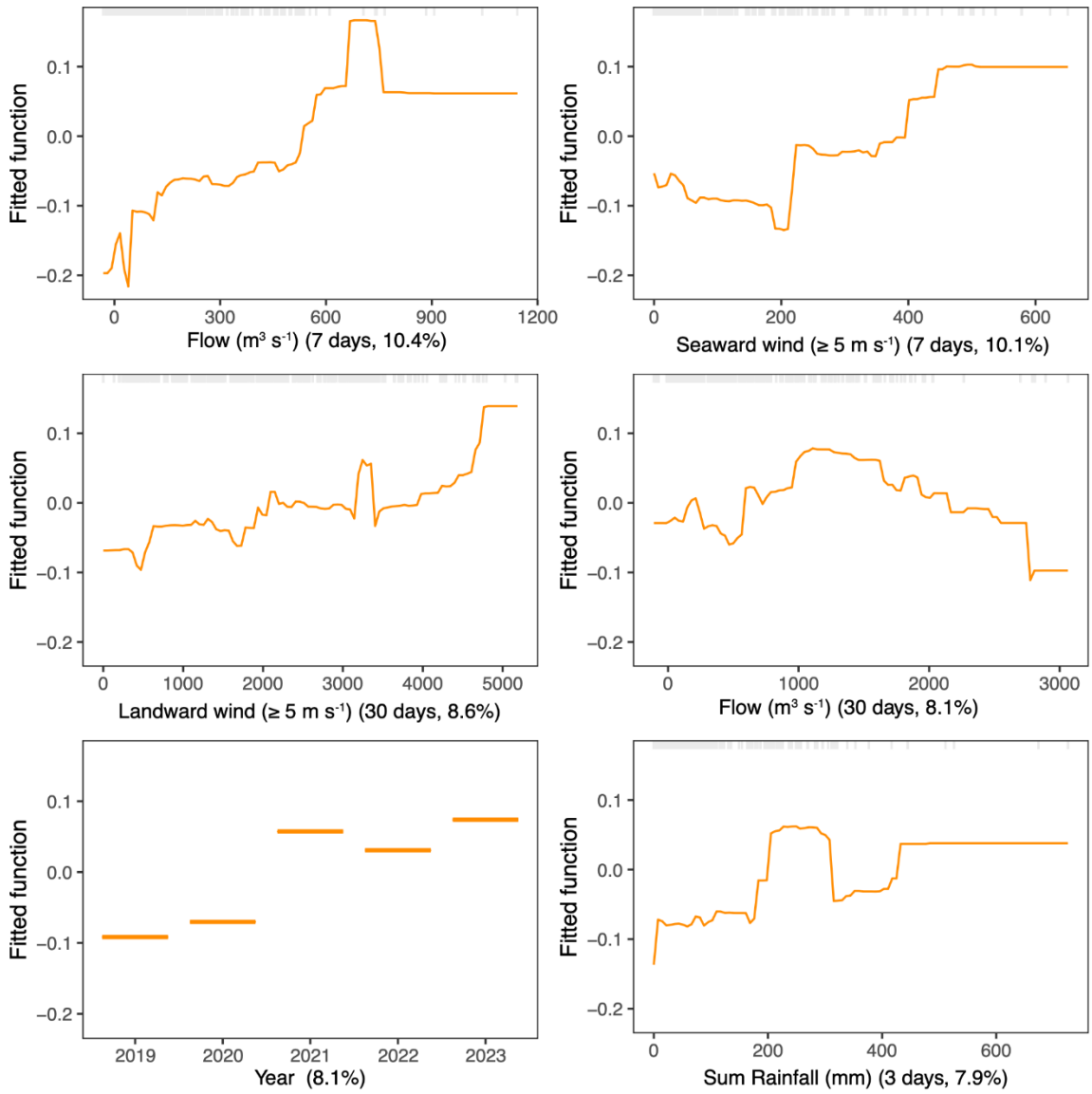

Figure 26. Partial dependency response plots from boosted regression tree (BRT) model relating changes in **nitrate** concentration (log) to gradients in inlet outflow, wind, and rainfall over various temporal windows, and a series of space/time categorical predictors. The orange lines depict the modeled relationship in each case (the relationship between nitrate and the predictor in question, while holding all other predictors in the model at their mean). For the categorical 'year' predictor, the fitted function median is shown. The thin grey lines along the top of each plot indicate replication along the predictor variable x-axis in each case. The relative influence of each predictor on overall model performance is shown in brackets.

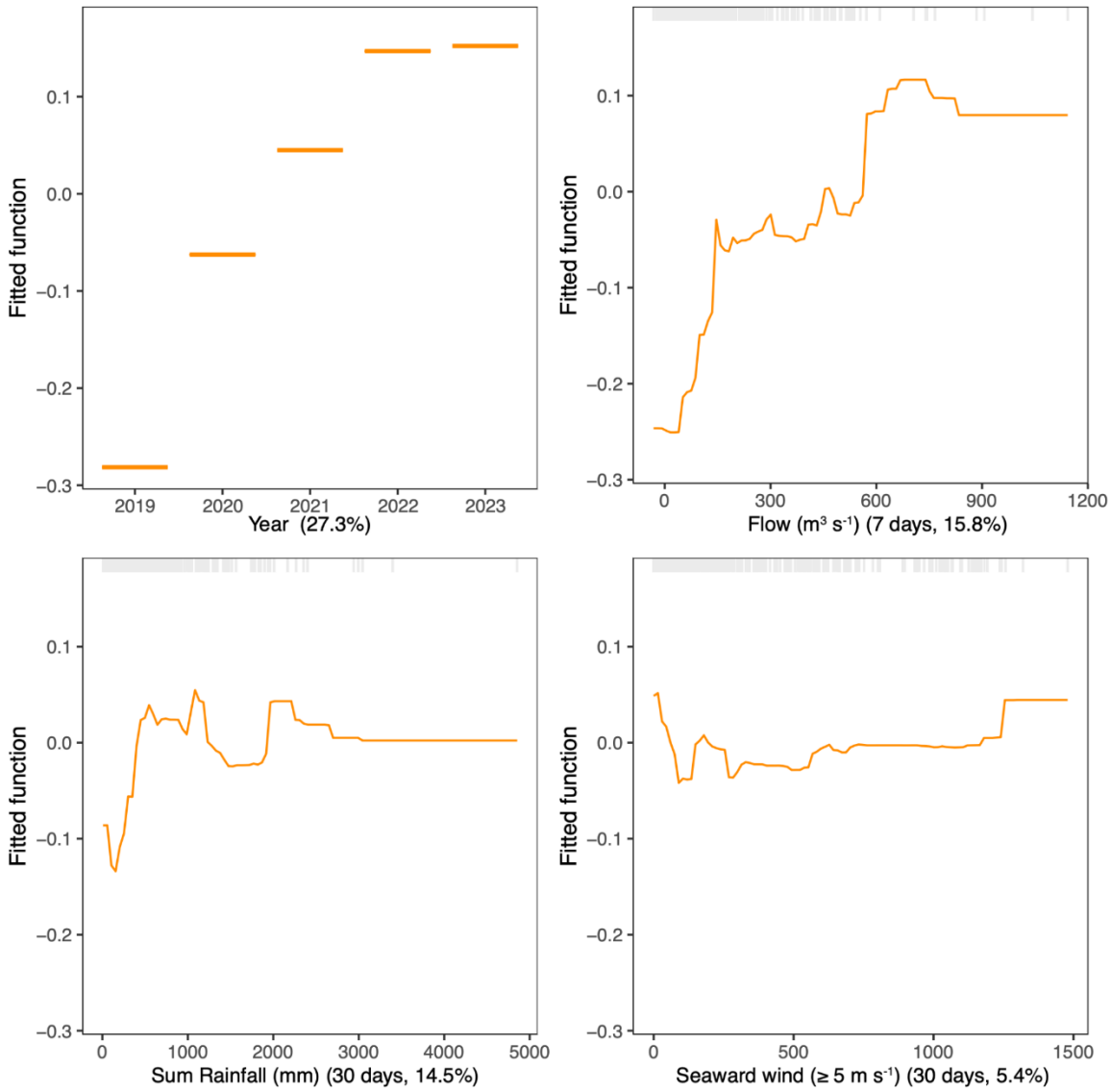

Figure 27. Partial dependency response plots from boosted regression tree (BRT) model relating changes in **nitrite** concentration (log) to gradients in inlet outflow, wind, and rainfall over various temporal windows, and a series of space/time categorical predictors. The orange lines depict the modeled relationship in each case (the relationship between nitrite and the predictor in question, while holding all other predictors in the model at their mean). For the categorical 'year' predictor, the fitted function median is shown. The thin grey lines along the top of each plot indicate replication along the predictor variable x-axis in each case. The relative influence of each predictor on overall model performance is shown in brackets.

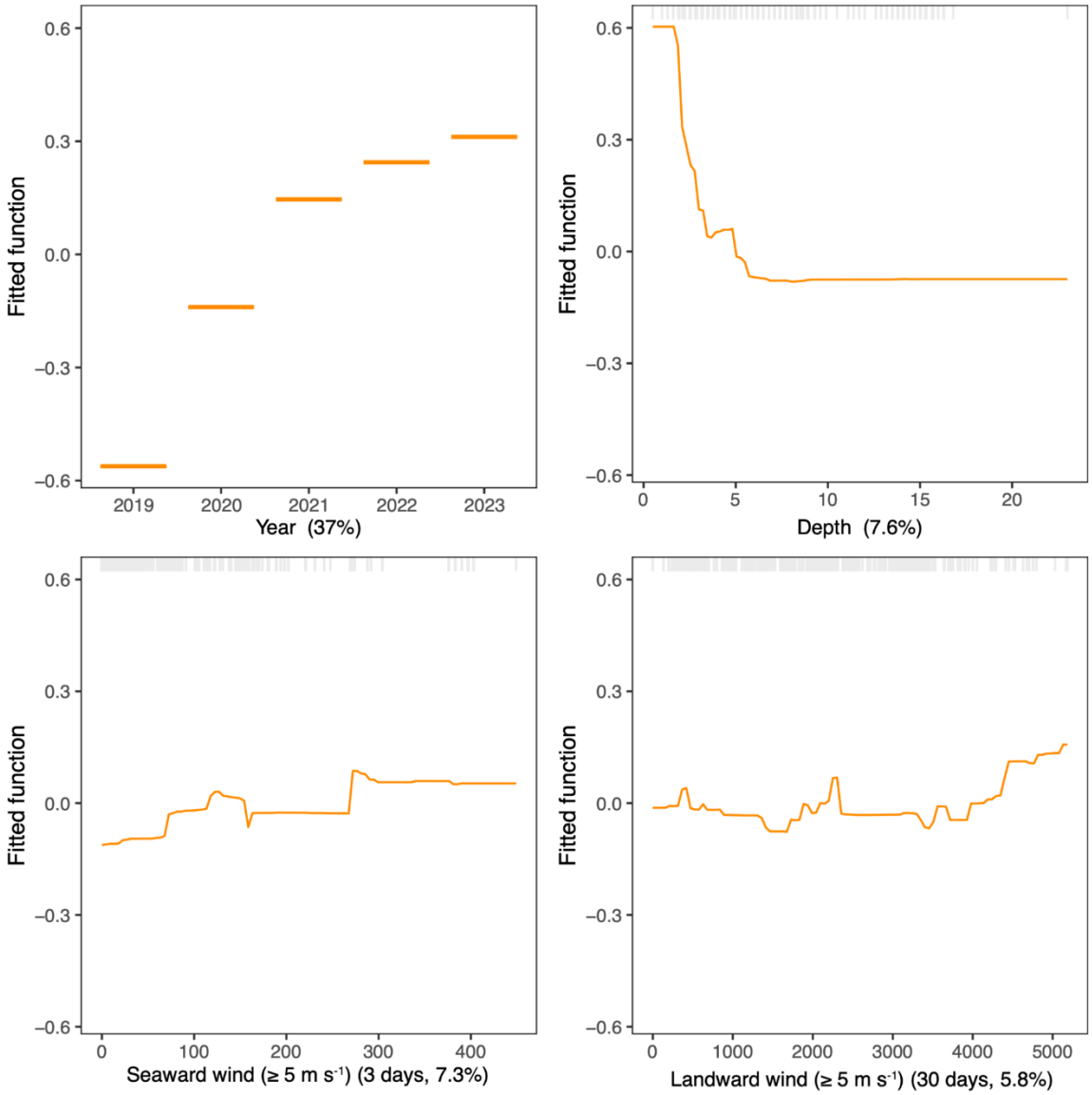

Figure 28. Partial dependency response plots from boosted regression tree (BRT) model relating changes in **orthophosphate** concentration (log) to gradients in inlet outflow, wind, and rainfall over various temporal windows, and a series of space/time categorical predictors. The orange lines depict the modeled relationship in each case (the relationship between orthophosphate and the predictor in question, while holding all other predictors in the model at their mean). For the categorical 'year' predictor, the fitted function median is shown. The thin grey lines along the top of each plot indicate replication along the predictor variable x-axis in each case. The relative influence of each predictor on overall model performance is shown in brackets.

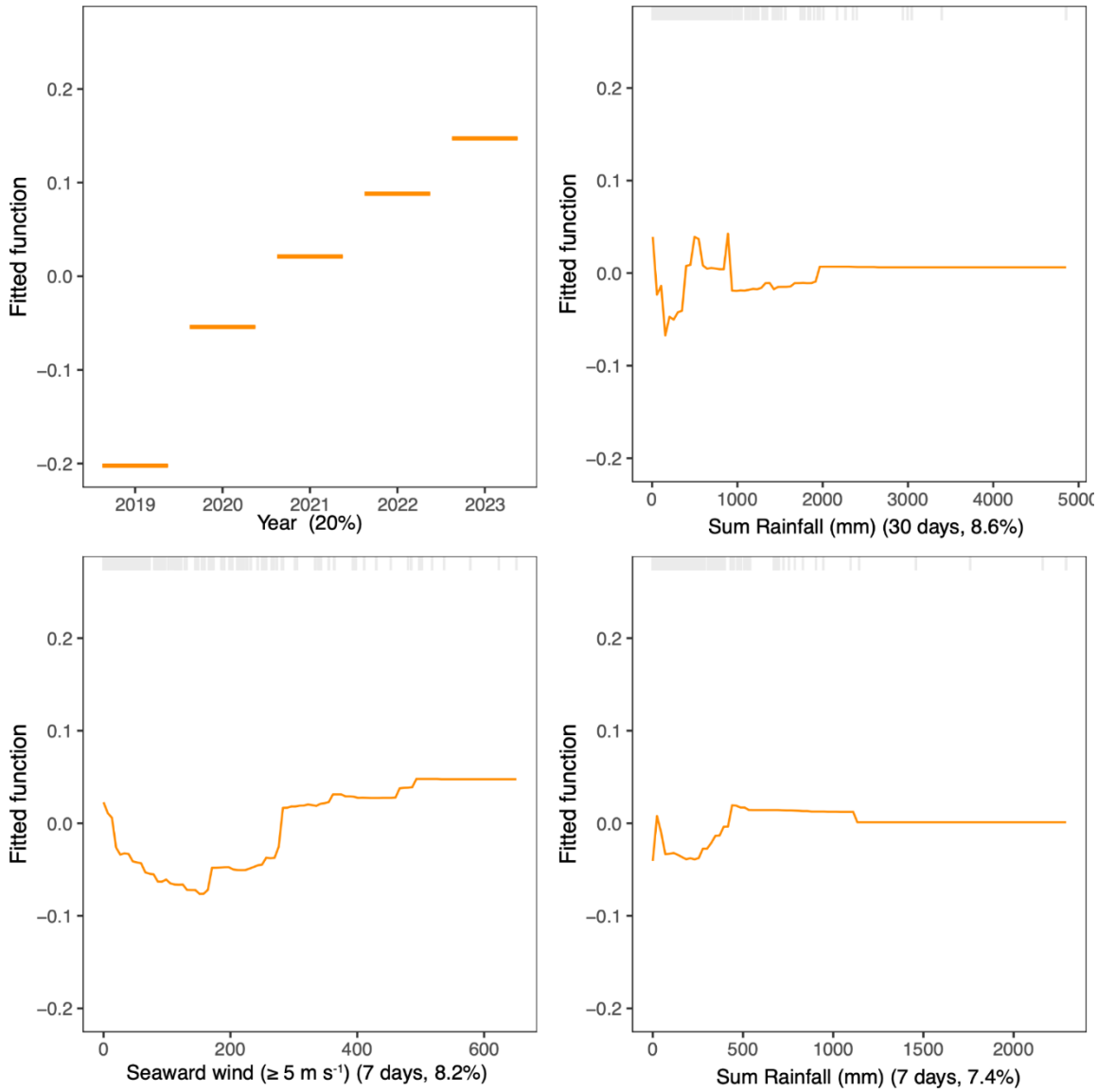

Figure 29. Partial dependency response plots from boosted regression tree (BRT) model relating changes in **phosphorus** concentration (log) to gradients in inlet outflow, wind, and rainfall over various temporal windows, and a series of space/time categorical predictors. The orange lines depict the modeled relationship in each case (the relationship between phosphorus and the predictor in question, while holding all other predictors in the model at their mean). For the categorical 'year' predictor, the fitted function median is shown. The thin grey lines along the top of each plot indicate replication along the predictor variable x-axis in each case. The relative influence of each predictor on overall model performance is shown in brackets.

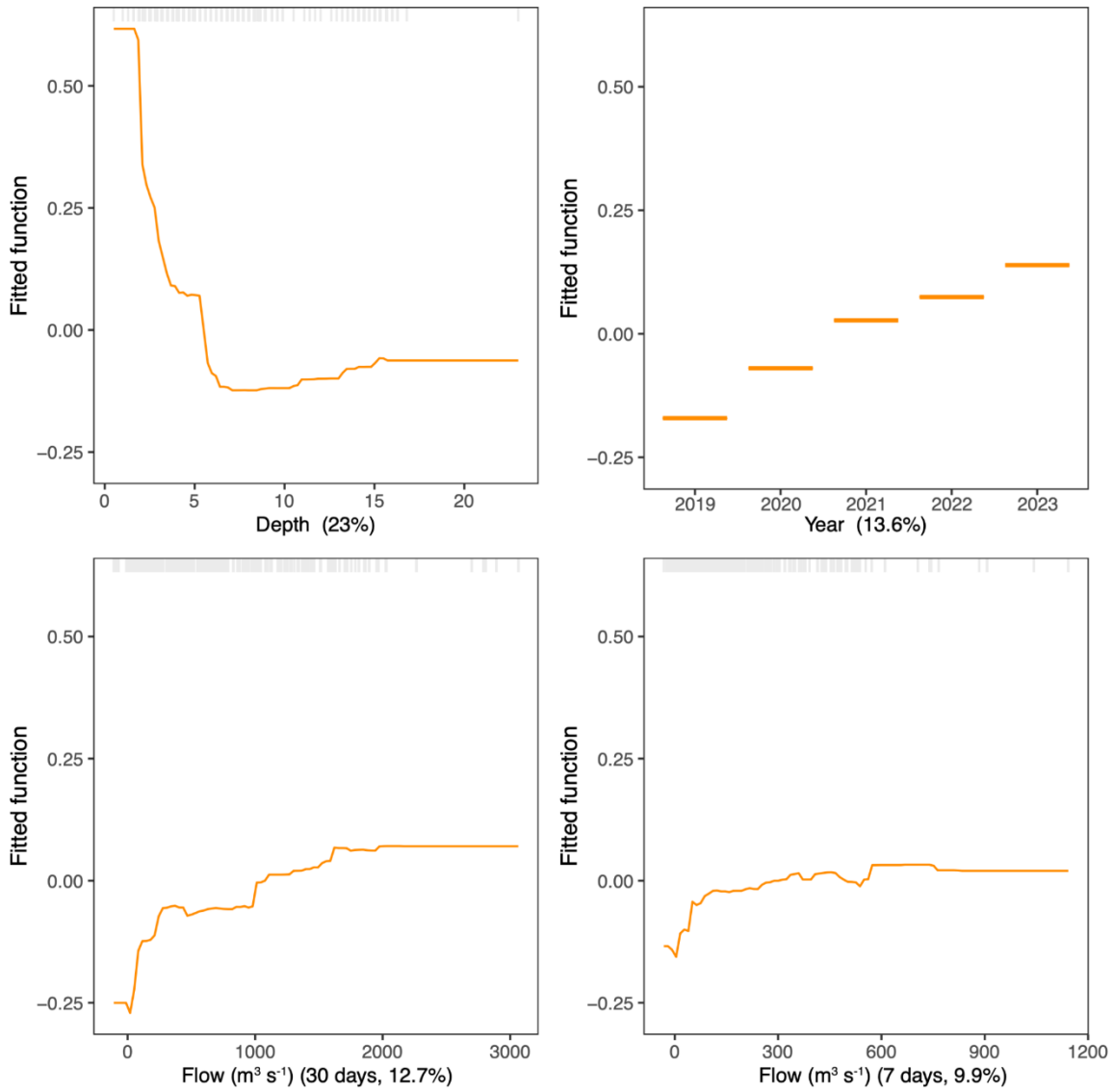

Figure 30. Partial dependency response plots from boosted regression tree (BRT) model relating changes in **silicate** concentration (log) to gradients in inlet outflow, wind, and rainfall over various temporal windows, and a series of space/time categorical predictors. The orange lines depict the modeled relationship in each case (the relationship between silicate and the predictor in question, while holding all other predictors in the model at their mean). For the categorical 'year' predictor, the fitted function median is shown. The thin grey lines along the top of each plot indicate replication along the predictor variable x-axis in each case. The relative influence of each predictor on overall model performance is shown in brackets.

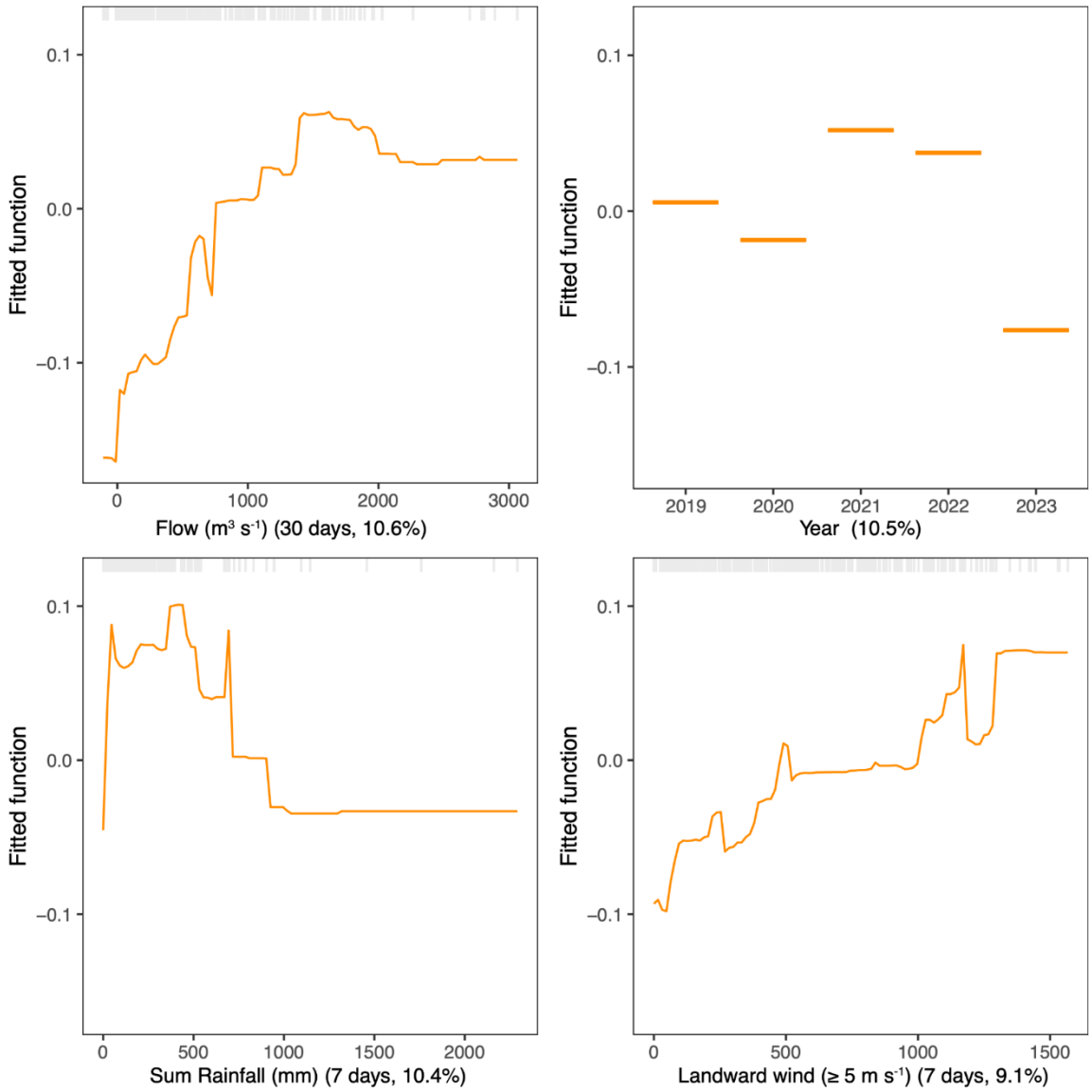

Figure 31. Partial dependency response plots from boosted regression tree (BRT) model relating changes in **total suspended solids (TSS)** concentration (log) to gradients in inlet outflow, wind, and rainfall over various temporal windows, and a series of space/time categorical predictors. The orange lines depict the modeled relationship in each case (the relationship between TSS and the predictor in question, while holding all other predictors in the model at their mean). For the categorical 'year' predictor, the fitted function median is shown. The thin grey lines along the top of each plot indicate replication along the predictor variable x-axis in each case. The relative influence of each predictor on overall model performance is shown in brackets.

3.4.2. Modeling spatial and temporal patterns of coral bleaching

Our statistical models explained between 92% and 93% of the variation in **coral bleaching** (i.e., using the training data), and 62% to 63% of the variation when predicting to data the

models had not seen before (i.e., using the test data) (Table 6). These patterns of model performance also remained largely unchanged when the models were trained on a lower portion of the training data (0.5 bag fraction results in Table 6). This variation was largely explained by coral colony identity and high wind events, as well as mean temperature and survey year (Table 4). Bleaching was more apparent in a subset of colonies (Figure 32) that did not appear to be strictly related to their north-south position along the coastline (Figure 20). Landward high wind events appeared to reduce the likelihood of coral bleaching overall, while higher mean temperature exacerbated bleaching, specifically above 30°C (Figure 32). There was a weak effect of survey year (independent of changes in temperature and wind), with higher bleaching in 2023 compared to all other years (Figure 32).

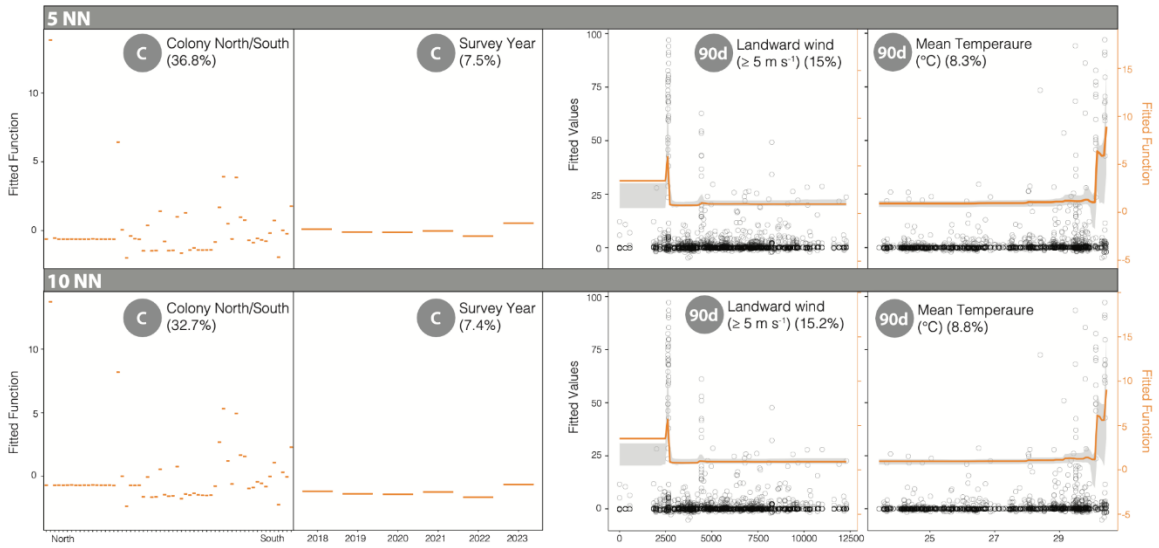

Figure 32. Partial dependency response plots from boosted regression tree (BRT) analyses relating changes in coral bleaching to gradients in inlet outflow, temperature, wind, and rainfall over various temporal windows (shown in circles as number of days prior to coral colony survey; C, categorical predictor variable), and a series of space/time categorical predictors. Solid orange lines represent the BRT fitted function with 95% confidence intervals (i.e., model uncertainty) shown in gray (corresponding to right-hand axes); for categorical predictors the median is shown. Open circles in plots represent the underlying raw data (corresponding to left-hand axes). The top and bottom set of plots show results with bleaching values less than 5% and 10% removed, respectively. NN, no nutrients - modeled nutrient loadings were not included in this analysis.

3.4.3. Modeling spatial and temporal patterns of SCTLD

Our statistical models explained between 43% and 58% of the variation in the number of new **SCTLD treatments and lesions** (i.e., using the training data), and 29% to 35% of the variation when predicting to data the models had not seen before (i.e., using the test data) (Table 7). These patterns of model performance also remained largely unchanged when the models were trained on a lower portion of the training data (0.5 bag fraction results in

Table 7). This variation was largely explained by coral colony identity, regardless of whether we modeled the entire geography (‘NN’ in

Table 8), or removed the southern Biscayne corals (‘NB’ in

Table 8), and whether the response was SCTLD treatments or number of lesions. Like coral bleaching, this colony effect did not appear to be strictly related to their north-south position along the coastline (Figure 33), but more a subset of colonies showing a higher propensity to develop SCTLD (Figure 20).

When the geography was restricted, and the Biscayne corals removed, both SCTLD treatments and lesions were also predicted by changes in silicate concentrations and exposure to Hot Snap thermal stress events (

Table 8). SCTLD treatments and lesions were both higher when silicate loadings were higher and when there were more Hot Snap events over the prior 7 days (Figure 33). When the entire geography was modeled, and the nutrient loading predictors removed from the model-fitting process, mean temperature over the prior 7 days replaced silicate as one of the top three predictors for both SCTLD treatments and lesions (

Table 8), with SCTLD becoming suddenly higher at the extreme upper end of the mean temperature range captured (above 30-31°C) (Figure 33). Finally, SCTLD lesions were also predicted by 'year' when the entire geography was modeled, with slightly fewer lesions occurring through time, however this effect was not particularly strong (lower relative influence) and should be interpreted with caution.

Table 7. Boosted regression tree model performance statistics from predicting the variation in coral bleaching and SCTLD across the KJCAP. cv, cross-validated; cvPercentage explained (cross-validated percentage deviance explained) is used to assess model performance. Bleaching_5, bleaching with all bleaching values less than 5% removed. Bleaching_10, bleaching with all bleaching values less than 10% removed.

	Bleaching_5 (no nutrients)	**Bleaching_10 (no nutrients)**	**SCTLD Treatments (no Biscyane)**	**SCTLD Lesions (no Biscyane)**	**SCTLD Treatments (no nutrients)**	**SCTLD Lesions (no nutrients)**
Model Parameters						
Number of observations	3486	3486	2533	2533	3486	3486
Tree complexity	5	5	1	1	3	3
Learning rate	0.001	0.001	0.001	0.001	0.001	0.001
Bag fraction	0.8	0.8	0.7	0.7	0.8	0.8
Number of trees	18250	16250	17450	18400	14450	16050
Model Performance						
Percentage explained (%)	**93.1**	**92.3**	**43.3**	**46.1**	**56.1**	**58.4**
cvPercentage explained (%)	**63.1**	**62.0**	**29.3**	**32.1**	**30.0**	**35.0**
Model Performance - 0.5 bag fraction						
Percentage explained (%)	87.9	86.1	40.7	43.5	46.9	57.7
cvPercentage explained (%)	56.4	54	28.5	30.6	25.5	31.5

Table 8. Relative (Rel) influence of predictor variables in predicting variations in coral bleaching and SCTLD across the KJCAP. The top four predictors are shown in each case, or the top three when this exceeded the cumulative (Cumul) relative influence of 70%. NN, no modeled nutrient predictors included in the model fitting process. NB, no Biscayne corals included as part of the response variable. Treat, treatments.

Response	Predictor	Rel Influence (%)	Cumul Influence (%)
Bleaching 5_NN	Colony	36.8	36.8
	Wind Landward (90day)	15.0	51.8
	Mean Temperature (90 day)	8.3	60.1
	Survey Year	7.5	67.6
Bleaching 10_NN	Colony	36.1	36.1
	Wind Landward (90day)	15.2	51.3
	Mean Temperature (90 day)	8.8	60.1
	Survey Year	7.4	67.5
SCTLD Treat_NB	Colony	51.9	51.9
	Silicate (7day)	20.8	72.7
	HotSnap (7 day)	3.8	76.5
SCTLD Lesions_NB	Colony	48.3	48.3
	Silicate (7day)	22.2	70.5
	HotSnap (7 day)	5.1	75.6
SCTLD Treat_NN	Colony	45.7	45.7
	Mean Temperature (7 day)	18.6	64.3
	HotSnap (7 day)	10.0	74.3
SCTLD Lesions_NN	Colony	38.1	38.1
	Mean Temperature (7 day)	15.6	53.7
	HotSnap (7 day)	8.4	62.1
	Survey Year	7.0	69.1

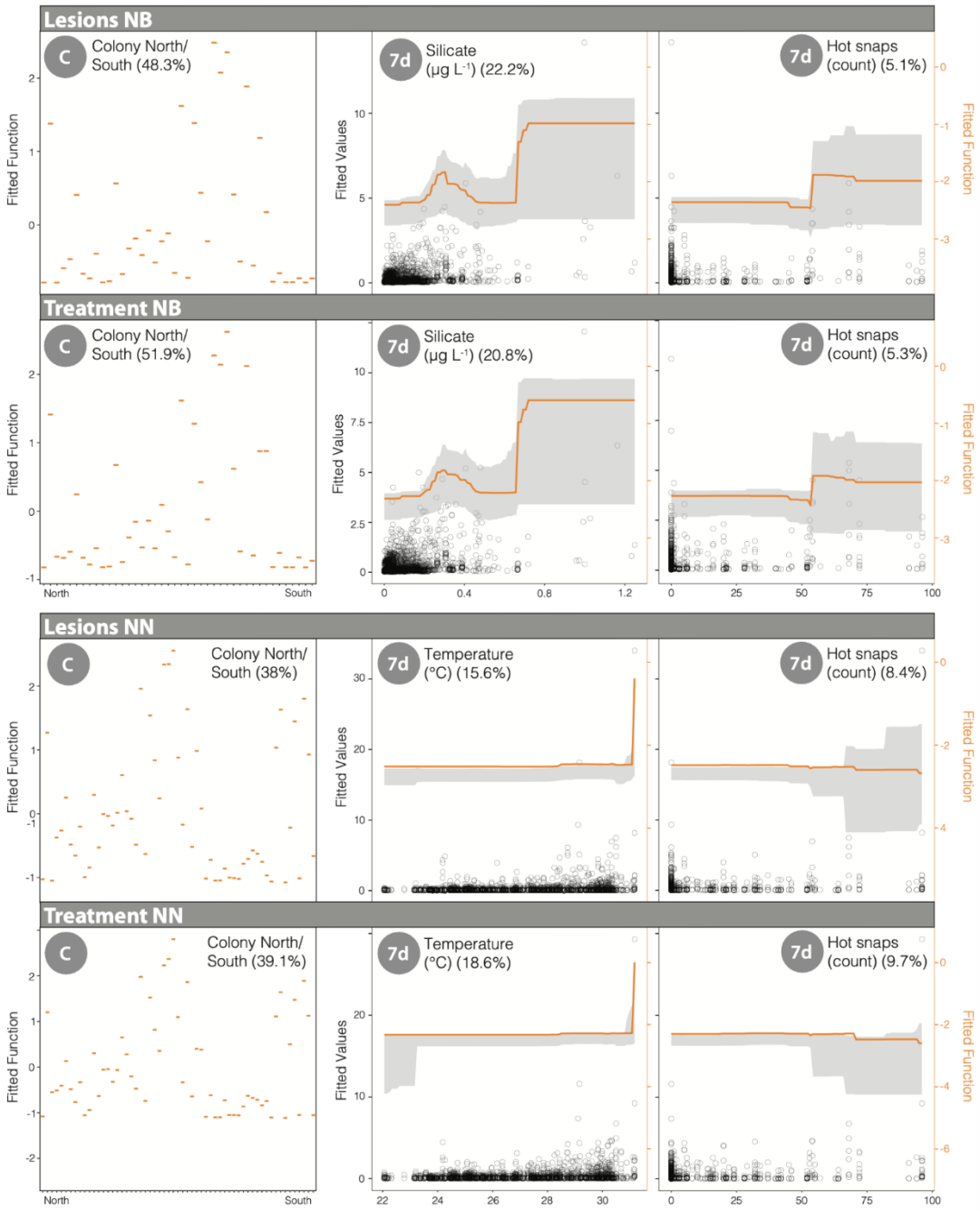

Figure 33. Partial dependency response plots from boosted regression tree (BRT) analyses relating changes in SCTLD (lesions and treatments) to gradients in inlet outflow, temperature, wind, and rainfall over various temporal windows (shown in circles as number of days prior to coral colony survey; C, categorical predictor variable), and a series of space/time categorical predictors. Solid orange lines represent the BRT fitted function with 95% confidence intervals (i.e., model uncertainty) shown in gray (corresponding to right-hand axes); for categorical predictors the median is shown. Open circles in plots represent the underlying raw data (corresponding to left-hand axes). NN, no nutrients - modeled nutrient loadings were not included in the analysis. NB, no Biscayne - all corals south of Government Cut were removed in this analysis.

3.5. Task 7: Integrate the inlet exposures into the RRC data analyses

We continued to engage with researchers from the RRC throughout the project period (via email and online meetings) to advise on the use and integration of various statistical analyses into their workflow to test their questions and hypotheses (see Table of specific meetings and their purpose under Task 1). This helped to ensure continuity in data analysis approaches across the RRC and ensure statistical rigor in terms of interpretation.

4. DISCUSSION

Reduced water quality on Florida's Coral Reef (FCR) from anthropogenic sources has long been implicated in the decline of the reef system. Over a century of replumbing the Everglades and coastal development has altered the historic water flows, leading to large scale ecosystem changes in south Florida. Residing downstream of the hydrographic flow, the FCR has experienced significant declines in the last 50 years, including the loss of over 25% live coral cover. Most of the coral losses were attributed to various extreme temperate and disease events beginning in the late 1970's and becoming more frequent over time, including stony coral tissue loss disease, which continues to decimate populations.

In dynamic ecosystems like coral reefs, pulse events of decline are easier to attribute to losses than slower incremental changes in water quality, which are much harder to detect. Analyses of *in situ* water quality data are confounded by many factors that affect analyte concentrations at specific times and locations. These factors must be accounted for before trends in the data can emerge. By accounting for these factors in the model, this study revealed annual increases in analyte concentrations that were previously obscured by the variability of water quality sampling and by changing environmental conditions – such as wind and rainfall – that influence offshore concentrations.

Our previous DEP and EPA funded projects found that inlet flow, rainfall, and wind predictors explained 79% and 55% of the overall variation in orthophosphate and nitrate concentrations at the KJCAP reef water quality sites from 2018 – 2021 (Whitall et al, *In revision*). Our machine-learning models on the larger dataset (2018-2024) in this study explained 41.5 – 78.9% of the variation in the water quality concentrations (training data) and 21.8 – 63.9% of the variation within data the model had not previously seen (test data). Many factors contributed to the changes in various analytes including inlet outflow, rainfall, and high winds, however year had a high influence in almost every test (8.1% for nitrate – 37% for orthophosphate). In almost every case, while holding all other predictors in the model (inlet outflow, wind, and rainfall over various temporal windows and a series of space/time categorical predictors) at their mean, the modeled relationship of each analyte showed increases by year, supporting previous studies in Biscayne Bay (Millette et al 2019). This suggests that some other factor not accounted for in the models was affecting yearly increases in reef analyte concentrations. One factor not in the models that might account for this effect is population growth. Miami-Dade and Broward are Florida's most populous counties totaling 4.88 million. From 2022 and 2024, there was a combined net increase of 270,353 new residents. Increases of this magnitude on already stressed

infrastructure could account for temporal decreases in water quality. Recognizing that excess nutrients cause a variety of environmental problems, Florida enacted county-level bans on nitrogen and phosphorus containing fertilizers in 2021. These restrict fertilizer application during the rainy season (May to October; Miami-Dade County 2021a) in the hope of improving water quality on nearshore coral reefs. Our models showed that the year effect in orthophosphate was lessened after 2021, indicating that implemented policies may be having a measurable, positive effect. Although on the right track, orthophosphates are still increasing on the reefs annually from our inland waterways and bays, so this action may not be enough to elicit system wide improvements.

Our hydrographic modeling of inlet water spanning from 2018 to 2024 supported findings of the previous models spanning from 2018 to 2021 (DEP C1FC2C), showing that the reefs northward of their adjacent inlet are most exposed to the water from that inlet and from inlets further south (Dobbelaere et al. 2024). While the analyte plumes extend mostly north of each of the source inlets, they also have a non-negligible southern footprint that extends over tens of kilometers. This is particularly the case for Government Cut and Baker's Haulover inlets whose inland water plumes clearly intrude into Biscayne Bay. Government Cut and Baker's Haulover also discharge the largest amounts of pollutants leading to inland water plumes with a higher analyte concentration. As these two inlets are the southernmost, they have the largest effect on the marine environment far beyond their immediate locales. When comparing wet and dry seasons, the model showed that inland water plumes generally had a larger analyte concentration during the wet season. However, higher analyte concentrations were observed south of the inlet during the dry season, especially for Government Cut and Baker's Haulover. Government Cut being the inlet with the southernmost position and the largest discharge, it had a significant impact on all considered reef sites. On average, 71.7% of the silicate reaching the reef sites originated from Government Cut. However, this fraction tended to be lower during the wet season, as the analyte load coming from the other sites became larger. Nonetheless, this suggests that reducing pollutant loads at Government Cut would significantly reduce the pollution over coral reefs in the KJCAP.

The effects of these water quality analytes on reef systems deserve significant research attention. The effect of nutrients on coral health can be driven by the levels of nutrient pollution and the stoichiometric ratios of C: N: P: Fe (Zhao et al 2021) and a specific coral host phosphate to nitrogen ratio to maintain stable photosymbiosis (Ezzat et al 2016). Tropical corals typically thrive in nutrient-poor environments through symbiosis (Stambler 1999; LaJeunesse et al 2018). High nutrient concentrations have been linked to increased coral bleaching and disease prevalence of white tissue loss diseases (Bruno et al 2007; Zhao et al 2021; Redding et al 2013) making it an important consideration for SCTLD. Nitrogen and phosphorous enrichment are linked to coral diseases in a variety of pathways (Zhao et al 2021). Increased nitrogen availability facilitates coral bleaching and disease (Redding et al 2013; Lapointe et al 2019; Wiedenmann et al 2013), likely by compromising the host-symbiont relationship, which is perhaps more specifically linked to anthropogenic nitrogen sources like nitrate (Zhao et al 2021; Donovan et al 2020; Burkepile et al 2020). Nitrate assimilation impairs the host-symbiont relationship by increasing oxidative stress, promoting phototrophic symbionts growth, and inducing phosphate starvation in the

symbionts (Zhao et al 2021). Anthropogenic nitrogen may also increase viral production in corals to the detriment of the host causing a virus-mediated vortex of coral reef decline (Vega Thurber et al 2008).

The bleaching models from 2018-2024 explained 93% of the variation of partial bleaching of 5% or greater. The strong effect of colony identity on coral bleaching (36.8%) reflected inter-colony differences in bleaching susceptibility. This was mostly driven by a few colonies that had a high partial bleaching prevalence (Figure 20). The reasons for their high prevalence of bleaching are unknown, however these colonies also had a high SCTLD prevalence. Colony-specific bleaching and SCTLD differences could be driven by various factors such as symbiont communities, genetic susceptibilities, or some other aspect of the coral holobiont or localized environment that differs at inter-colony scales (Edmunds 1994; Berkelmans and van Oppen 2006; Sampayo et al. 2008; Álvarez-Noriega et al. 2025; Ward 2007). These are being investigated as part of the SCTLD Resistance Research Consortium (Walker et al 2025).

Interestingly, the models found more coral bleaching when there were fewer high wind events. Higher winds can reduce thermal stress by mixing surface waters, disrupting water stratification, and reducing temperatures (Smith 2001). Landward high wind events were associated with raised TSS levels across the KJCAP (Figure 31) supporting prior work showing increased turbidity can decrease UV stress to corals and ameliorate coral bleaching (Sully and van Woesik 2020), particularly during extreme wind events (Lucas et al. 2023). This might explain why low wind conditions can favor localized heating, lower TSS and therefore greater penetration of solar radiation that can exacerbate coral bleaching (Hendee et al. 2001).

The tendency for bleaching to occur above a specific thermal threshold that we observed in the KJCAP corroborates numerous other studies from other geographies both in the Atlantic, Caribbean and Indo-Pacific (Fitt et al. 2001; Berkelmans 2002; Williams et al. 2010; Mollica et al. 2019). The positive relationship between thermal stress and disease, whether mean temperature or Hot Snap exposure, is also well established in the literature (Bruno et al. 2007; Maynard et al. 2015), including our own prior work on SCTLD in the KJCAP (Walker et al. 2022). Corals south of Government Cut were visibly bleaching after four weeks of mostly consistent temperatures ≥30.5°C, whereas areas further north had much more inconsistent temperatures with several drops below 30.5°C for periods of time. Extreme temperatures can compromise coral host resistance and increase pathogen virulence, both of which can then increase the likelihood of disease occurrence (Maynard et al. 2015), however the relationship with thermal stress and SCTLD is more complicated.

Several studies support evidence that SCTLD epidemiology is related to temperature, at least in intermediately susceptible species (e.g. *Orbicella faveolata*, *Montastraea cavernosa*) (Jones et al 2021; Walker et al 2021; Carreiro 2022). At the initial onset of SCTLD, pillar corals infected with a white syndrome were seen in February of 2014 (Jones et al 2021) before SCTLD was reported in the late summer of 2014 after significant temperatures stress (Precht et al 2016; Manzello 2015). Additionally, thermal stress and bleaching can slow and stop SCTLD lesions entirely (Meiling et al 2020; Neely et al 2025)

and daily infection rates of *Montastraea cavernosa* were significantly lower in times of lower heat stress (Walker et al 2021). Although persistent year-round in Florida, SCTLD incidence and prevalence was at least double in the wet summer seasons in the KJCAP (Walker et al, In prep; Toth et al 2024).

In July 2023, the highest SCTLD prevalence on the monitored *O. faveolata* colonies was recorded in the five-year dataset. In August, the colonies south of Government Cut had the highest recorded bleaching, which took about five months to recover (no mortality from bleaching was observed), whereas no colonies further north visibly bleached. Unbleached colonies continued to acquire SCTLD lesions in the north, whilst SCLTD quiesced on bleached colonies. Thus, it appears that high temperatures in early and mid-summer exacerbated SCTLD, but the higher temperatures south of Government Cut caused those corals to bleach, which quiesced SCTLD in those colonies.

Nutrient variability north and south of Government Cut may have also played a role in the SCTLD and bleaching observations. The NB SCTLD model including the modeled nutrient data explained 46% of the variation in lesions driven by colony, modeled silicate, and hot snaps. Silicates can be used as a proxy for terrestrial water sources, suggesting that increased exposure to terrestrial waters increases SCTLD lesions. Further, the seasonal analysis of the water quality sites indicated that the waters south of Government Cut were distinctly different most of the time. In 2023, the water quality monitoring sites between Government Cut and Baker's Haulover had much higher total phosphorus, nitrate, silicate, and nitrite than those south of Government Cut. Government Cut has been identified as a major transition between ecoregions in SE FL where significant *Thalassia* seagrass beds exist in the oceanside nearshore habitats further south, but none further north (Walker 2012; Walker and Gilliam 2013). Sea grasses uptake more nutrients in warmer temperatures (Lee et al 2007) and phosphorus is a key element needed for seagrass growth (Fourqurean et al 1992; Gras et al 2003). The stoichiometric ratios of C: N: P: Fe availabilities determine the ultimate effect of nutrients on coral health (Zhao et al 2021). Zhou et al (2025) explains that nitrate enrichment exacerbates bleaching under thermal stress (Burkepile et al 2020) and Symbiodiniaceae may provide less photosynthetically fixed carbon to the host (Ezzat et al 2016), while the lack of phosphorus inhibits Symbiodiniaceae cell division and metabolism weakening the corals resistance to stress (Rosset et al 2017). In the 2023 wet season, the average values of total phosphorus in Biscayne were 4.7 times lower than normal and nitrate was 1.6 times lower. Might the presence of the extensive seagrass beds in the southern Biscayne region have caused an imbalance in the available nutrients for corals and their symbionts lowering their bleaching threshold? More research is needed to investigate this possibility.

5. REFERENCES

Aeby, G., et al. (2021). "Changing Stony Coral Tissue Loss Disease Dynamics Through Time in Montastraea cavernosa." Frontiers in Marine Science **8**(1343).

Álvarez-Noriega M, Aston EA, Becker M, Fabricius KE, Figueira WF, Gordon SE, Krensel R, Lechene MAA, Remmers T, Toor M, Ferrari R. 2025. Challenging Paradigms Around the Role of Colony Size, Taxa, and Environment on Bleaching Susceptibility. Global Change Biol 31:e70090

Berkelmans R. 2002. Time-integrated thermal bleaching thresholds of reefs and their variation on the Great Barrier Reef. Mar Ecol Prog Ser 229:73-82

Berkelmans R, van Oppen MJH. 2006. The role of zooxanthellae in the thermal tolerance of corals: a 'nugget of hope' for coral reefs in an era of climate change. Proceedings of the Royal Society B-Biological Sciences 273:2305-2312

Breiman L, Friedman JH, Olshen RA, Stone CJ. 1984. Classification and Regression Trees. Wadsworth International Group, California

Bruno JF, Selig ER, Casey KS, Page CA, Willis BL, Harvell CD, Sweatman H, Melendy AM. 2007. Thermal stress and coral cover as drivers of coral disease outbreaks. PLoS Biol 5:1220-1227

Burkepile DE, Shantz AA, Adam TC, Munsterman KS, Speare KE, Ladd MC, et al. Nitrogen Identity Drives Differential Impacts of Nutrients on Coral Bleaching and Mortality. Ecosystems. 2020;23(4):798-811.

Dobbelaere T, Hanert E, Williams GJ, Whitall D, Aeby GS, Maynard JA, Walker BK (2024) Hydrographic connections of inland water to diseased corals and water quality sites in SE FL. Final Report Florida DEP Miami, FL, 26 p

Dobbelaere, T., Muller, E. M., Gramer, L. J., Holstein, D. M., & Hanert, E. (2020). Coupled epidemio-hydrodynamic modeling to understand the spread of a deadly coral disease in Florida. *Frontiers in Marine Science*, 7, 1016.

Dobbelaere T., Holstein DM, Muller E, Gramer LJ, McEachron L, Williams SD, Hanert E (2022) Connecting the Dots: Transmission of Stony Coral Tissue Loss Disease from the Marquesas to the Dry Tortugas. *Frontiers in Marine Science*, 9, 778938.

Donovan MK, Adam TC, Shantz AA, Speare KE, Munsterman KS, Rice MM, et al. Nitrogen pollution interacts with heat stress to increase coral bleaching across the seascape. Proceedings of the National Academy of Sciences. 2020;117(10):5351-7.

Edmunds PJ (1994) Evidence that reef-wide patterns of coral bleaching may be the result of the distribution of bleaching susceptible clones. Mar Biol 121:137-142

Elith J, Leathwick JR, Hastie T (2008) A working guide to boosted regression trees. J Anim Ecol 77:802-813

Ezzat L, Maguer J-F, Grover R, Ferrier-Pagès C. Limited phosphorus availability is the Achilles heel of tropical reef corals in a warming ocean. Scientific Reports. 2016;6(1):31768

Fitt WK, Brown BE, Warner ME, Dunne RP (2001) Coral bleaching: interpretation of thermal tolerance limits and thermal thresholds in tropical corals. Coral Reefs 20:51-65

Flynn MR (2010) Analysis of censored exposure data by constrained maximization of the Shapiro-Wilk W statistic. Ann Occup Hyg 54:263-271

Fourqurean, J. W., et al. (1992). "Phosphorus limitation of primary production in Florida Bay: Evidence from C:N:P ratios of the dominant seagrass *Thalassia testudinum*." Limnology and Oceanography **37**(1): 162-171.

Friedman JH, Meulman JJ (2003) Multiple additive regression trees with application in epidemiology. Stat Med 22:1365-1381

Frys, C., Saint-Amand, A., Le Hénaff, M., Figueiredo, J., Kuba, A., Walker, B., Lambrechts, J., Vallaeys, V., Vincent, D., & Hanert, E. (2020). Fine-Scale coral connectivity pathways in the Florida Reef Tract: Implications for conservation and restoration. *Frontiers in Marine Science*, *7, 312*.

FWC-FWRI (2017). Unified Reef Map v2. 0. Tallahassee, FL: Florida Fish and Wildlife Conservation Commission-Fish and Wildlife Research Institute.

Geuzaine, C., & Remacle, J. (2009). Gmsh: A 3-D finite element mesh generator with built-in pre- and post-processing facilities. *International Journal for Numerical Methods in Engineering*, *79*(11), 1309–1331.

Gras, A. F., et al. (2003). "Phosphorus uptake kinetics of a dominant tropical seagrass *Thalassia testudinum*." Aquatic Botany **76**(4): 299-315.

Hendee JC, Mueller E, Humphrey C, Moore T (2001) A data-driven expert system for producing coral bleaching alerts at Sombrero Reef, Florida Keys, USA. Bull Mar Sci 69:139-147

Heron SF, Willis BL, Skirving WJ, Eakin CM, Page CA, Miller IR (2010) Summer Hot Snaps and Winter Conditions: Modelling White Syndrome Outbreaks on Great Barrier Reef Corals. PloS One 5:e12210

Hijmans RJ, Phillips S, Leathwick J, Elith J (2017) dismo: species distribution modeling. R package version 1.1–4. See https://CRAN.R-project.org/package=dismo.

Jouffray J, Wedding LM, Norström AV, Donovan MK, Williams GJ, Crowder LB, Erickson AL, Friedlander AM, Graham NAJ, Gove JM, Kappel CV, Kittinger JN, Lecky J, Oleson KLL, Selkoe KA, White C, Williams ID, Nyström M (2019) Parsing human and biophysical drivers of coral reef regimes. Proceedings of the Royal Society B: Biological Sciences 286:20182544

LaJeunesse TC, Parkinson JE, Gabrielson PW, Jeong HJ, Reimer JD, Voolstra CR, et al. Systematic Revision of Symbiodiniaceae Highlights the Antiquity and Diversity of Coral Endosymbionts. Curr Biol. 2018;28(16):2570-80.e6.

Lapointe BE, Brewton RA, Herren LW, Porter JW, Hu C. Nitrogen enrichment, altered stoichiometry, and coral reef decline at Looe Key, Florida Keys, USA: a 3-decade study. Mar Biol. 2019;166(8):108.

Lee, K.-S., et al. (2007). "Effects of irradiance, temperature, and nutrients on growth dynamics of seagrasses: A review." Journal of Experimental Marine Biology and Ecology **350**(1): 144-175.

Lucas CC, Lima IC, Garcia TM, Tavares TCL, Carneiro PBM, Teixeira CEP, Bejarano S, Rossi S, Soares MO (2023) Turbidity buffers coral bleaching under extreme wind and rainfall conditions. Mar Environ Res 192:106215

Maynard J, van Hooidonk R, Eakin CM, Puotinen M, Garren M, Williams G, Heron SF, Lamb J, Weil E, Willis B, Harvell CD (2015) Projections of climate conditions that increase coral disease susceptibility and pathogen abundance and virulence. Nature Climate Change 5:688-694

Meiling, S., et al. 2020. 3D Photogrammetry Reveals Dynamics of Stony Coral Tissue Loss Disease (SCTLD) Lesion Progression Across a Thermal Stress Event. Frontiers in Marine Science 7(1128).

Miami-Dade County. 2021a. Ordinance relating to regulation of fertilizer. 644 https://www.miamidade.gov/govaction/legistarfiles/MinMatters/Y2021/210882min.pdf

Millette, N. C., et al. (2019). "Using Spatial Variability in the Rate of Change of Chlorophyll a to Improve Water Quality Management in a Subtropical Oligotrophic Estuary." Estuaries and Coasts **42**(7): 1792-1803.

Mollica N, Cohen AL, Alpert AE, Barkley HC, Brainard RE, Carilli JE, DeCarlo TM, Drenkard EJ, Lohmann P, Mangubhai S, Pietro KR, Rivera HE, Rotjan RD, Scott-Buechler C, Solow AR, Young CW (2019) Skeletal records of bleaching reveal different thermal thresholds of Pacific coral reef assemblages. Coral Reefs 38:743-757

Muller EM, van Woesik R (2014) Genetic Susceptibility, Colony Size, and Water Temperature Drive White-Pox Disease on the Coral *Acropora palmata*. PLoS ONE 9:e110759

Neely, K. L., et al. (2024). "Too hot to handle? The impact of the 2023 marine heatwave on Florida Keys coral." Frontiers in Marine Science Volume 11 - 2024.

Pollock FJ, Lamb JB, Field SN, Heron SF, Schaffelke B, Shedrawi G, Bourne DG, Willis BL (2014) Sediment and turbidity associated with offshore dredging increase coral disease prevalence on nearby reefs. PloS one 9:e102498

Priestas AM (2022) Turbidity analysis data report Port Everglades, Florida. Prepared for Jacksonville District, US Army Corps of Engineers:54 pp

Redding JE, Myers-Miller RL, Baker DM, Fogel M, Raymundo LJ, Kim K. Link between sewage-derived nitrogen pollution and coral disease severity in Guam. Mar Pollut Bull. 2013;73(1):57-63.

Richards BL, Williams ID, Vetter OJ, Williams GJ (2012) Environmental factors affecting large-bodied coral reef fish assemblages in the Mariana Archipelago. PLoS One 7:e31374

Sampayo EM, Ridgway T, Bongaerts P, Hoegh-Guldberg O (2008) Bleaching susceptibility and mortality of corals are determined by fine-scale differences in symbiont type. Proceedings of the National Academy of Sciences of the United States of America 105:10444-10449

Smith NP (2001) Weather and hydrographic conditions associated with coral bleaching: Lee Stocking Island, Bahamas. Coral Reefs 20:415-422

Stambler N. Coral reefs and eutrophication. 1999.

Sully S, van Woesik R (2020) Turbid reefs moderate coral bleaching under climate-related temperature stress. Global Change Biol 26:1367-1373

Vega Thurber R, Payet JP, Thurber AR, Correa AMS. Virus–host interactions and their roles in coral reef health and disease. Nature Reviews Microbiology. 2017;15(4):205-16.

Walker BK, Aeby GS, Baker AC, Buckley S, Garg N, Maynard J, Meyer J, Neely K, Paul VJ, Traylor-Knowles N, Voss J, Whitall DR, Williams GJ, Woodley CM, Andrade N, Becker CC, Buckley S, Cauvin AR, Dennison CE, Houk J, Mazurek H, Noren H, Parry A, Saunders J, and Sharkey R. 2025. SCTLD resistance research consortium (RRC) *Orbicella faveolata* bioinformatics and data analyses synthesis. Final Summary Report. Florida DEP. Miami, FL, 124p.

Walker B.K., Noren H., Sharkey R., Buckley S., Wheeler S., Wagner A., Spekis R., and T. Buckell. 2025. 2024-2025 SE FL KJCAP Reef-building-coral Disease Intervention and Preparation for Restoration Final Report. Florida DEP. Miami, FL. 30p.

Walker B.K., Noren H., Sharkey R., Buckley S. and A. Zummo. 2024. 2023-2024 SE FL ECA Reef-building-coral Disease Intervention and Preparation for Restoration Final Report. Florida DEP. Miami, FL. 1-26p.

Walker BK, Williams GJ, Aeby GS, Maynard JA and Whitall D. 2022. Environmental and human drivers of stony coral tissue loss disease (SCTLD) incidence within the Southeast Florida Coral Reef Ecosystem Conservation Area, 2021-22. Final Report. Florida DEP. Miami, FL., 36 p.

Ward JR (2007) Within-colony variation in inducibility of coral disease resistance. J Exp Mar Biol Ecol 352:371-377

Whitall, D., S. Bricker, D. Cox, J. Baez, J. Stamates, K. Gregg, F. Pagan. 2019. Southeast Florida Reef Tract Water Quality Assessment. NOAA Technical Memoradum NOS NCCOS 271. Silver Spring. 116 pages

Whitall, D, S Bricker. 2021. Examining Ambient Turbidity and Total Suspended Solids Data in South Florida Towards Development of Coral Specific Water Quality Criteria. NOAA Technical Memorandum NOS NCCOS 297. Silver Spring. 23 pages.

Wiedenmann J, D'Angelo C, Smith EG, Hunt AN, Legiret F-E, Postle AD, et al. Nutrient enrichment can increase the susceptibility of reef corals to bleaching. Nature Climate Change. 2013;3(2):160-4.

Williams, G. J., Aeby, G. S., Cowie, R. O. M. & Davy, S. K. 2010. Predictive Modeling of Coral Disease Distribution within a Reef System. *PLoS One* 5, e9264.

Williams GJ, Knapp IS, Maragos JE, Davy SK. 2010. Modeling patterns of coral bleaching at a remote Central Pacific atoll. Mar Pollut Bull 60:1467-1476

Zhao H, Yuan M, Strokal M, Wu HC, Liu X, Murk A, et al. Impacts of nitrogen pollution on corals in the context of global climate change and potential strategies to conserve coral reefs. Sci Total Environ. 2021;774:145017

4. APPENDIX

4.1. Plume arrival time to the reefs

For each inlet, we estimated the time needed for inland water plumes to reach the reefs. Overall, that duration was always smaller than the 25-day backtracking simulation duration, hence justifying the choice for that duration. As an illustration, it did not exceed 13 days in September 2020 for all four inlets (Fig. A1).

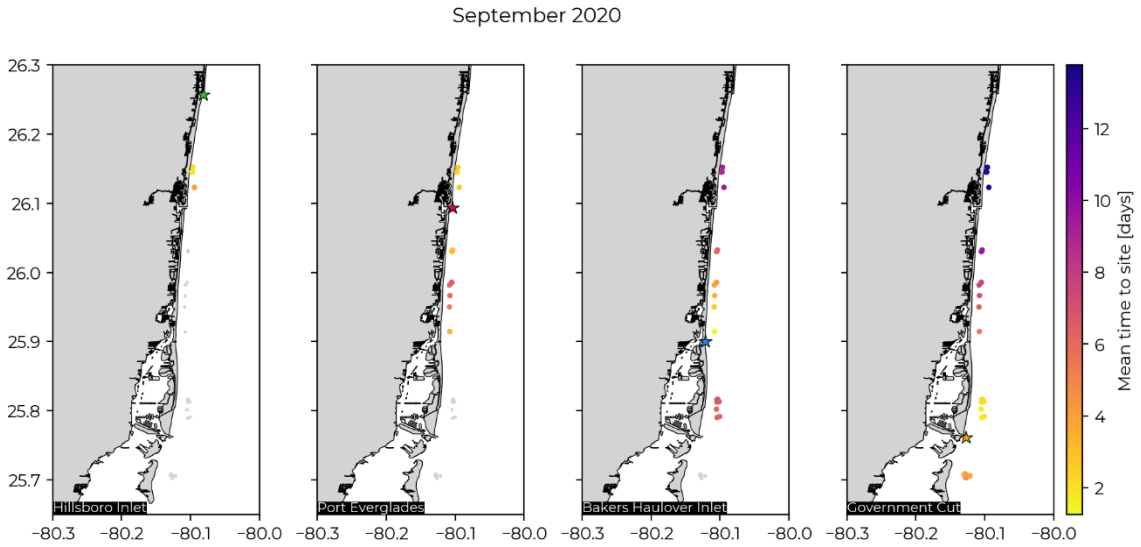

Figure A1: Monthly-averaged time needed for an inland water plume originating from each of the four inlets to reach the surrounding reefs.

4.2. Mean analyte concentrations

Here we provide the mean analyte concentration for both the wet (May to October) and dry (November to April) seasons, and the difference between them, over the 3-year simulated period for nitrate (Fig. A2), nitrite (Fig. A3), orthophosphate (Fig. A4), phosphorus (Fig. A5), silicate (Fig. A6) and TSS (Fig. A7).

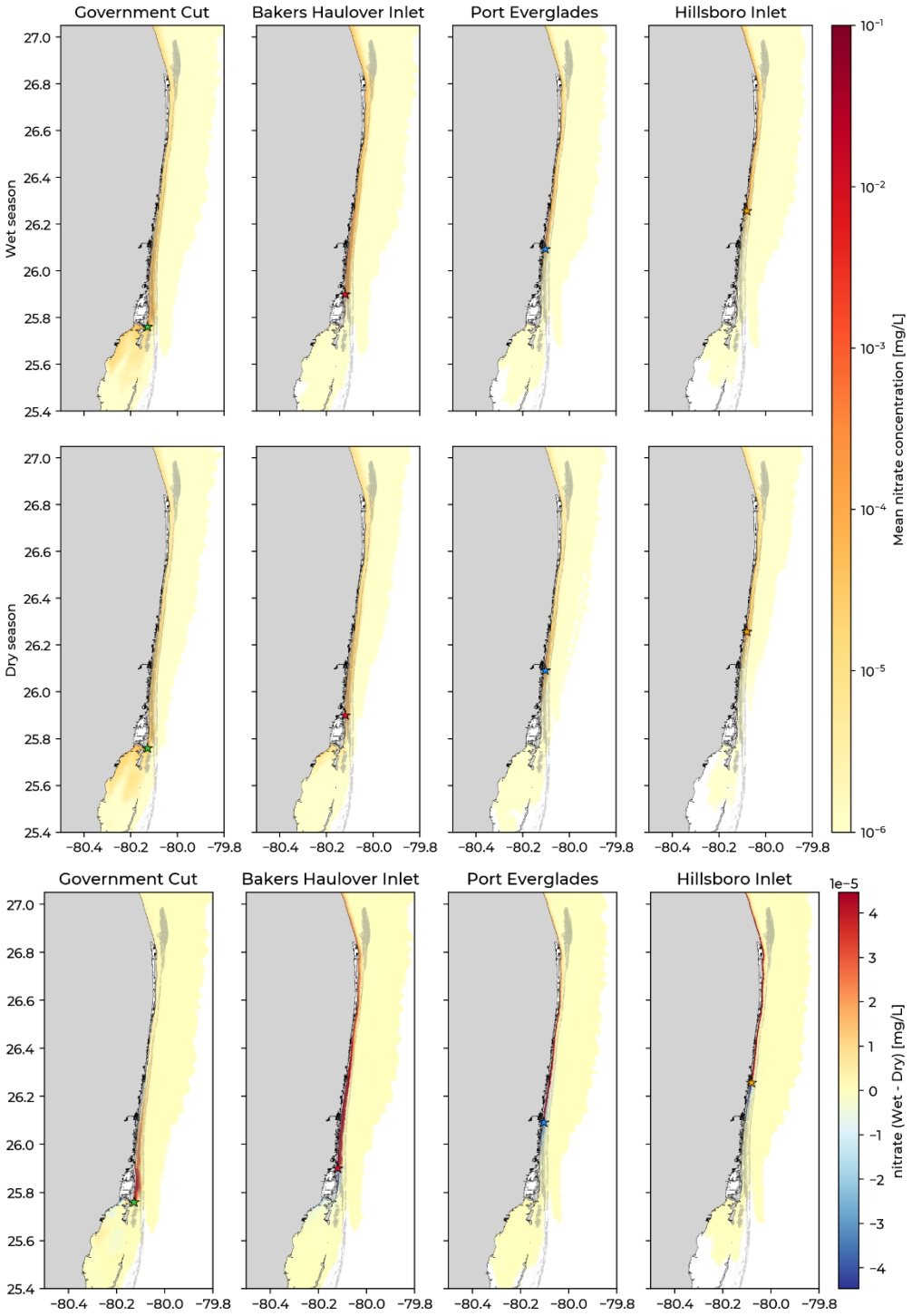

Figure A2: Seasonal mean concentration of nitrate coming from the different inlets for the wet (top panels) and dry seasons (bottom panels). The difference in concentration between wet and dry seasons is shown in the bottom panel.

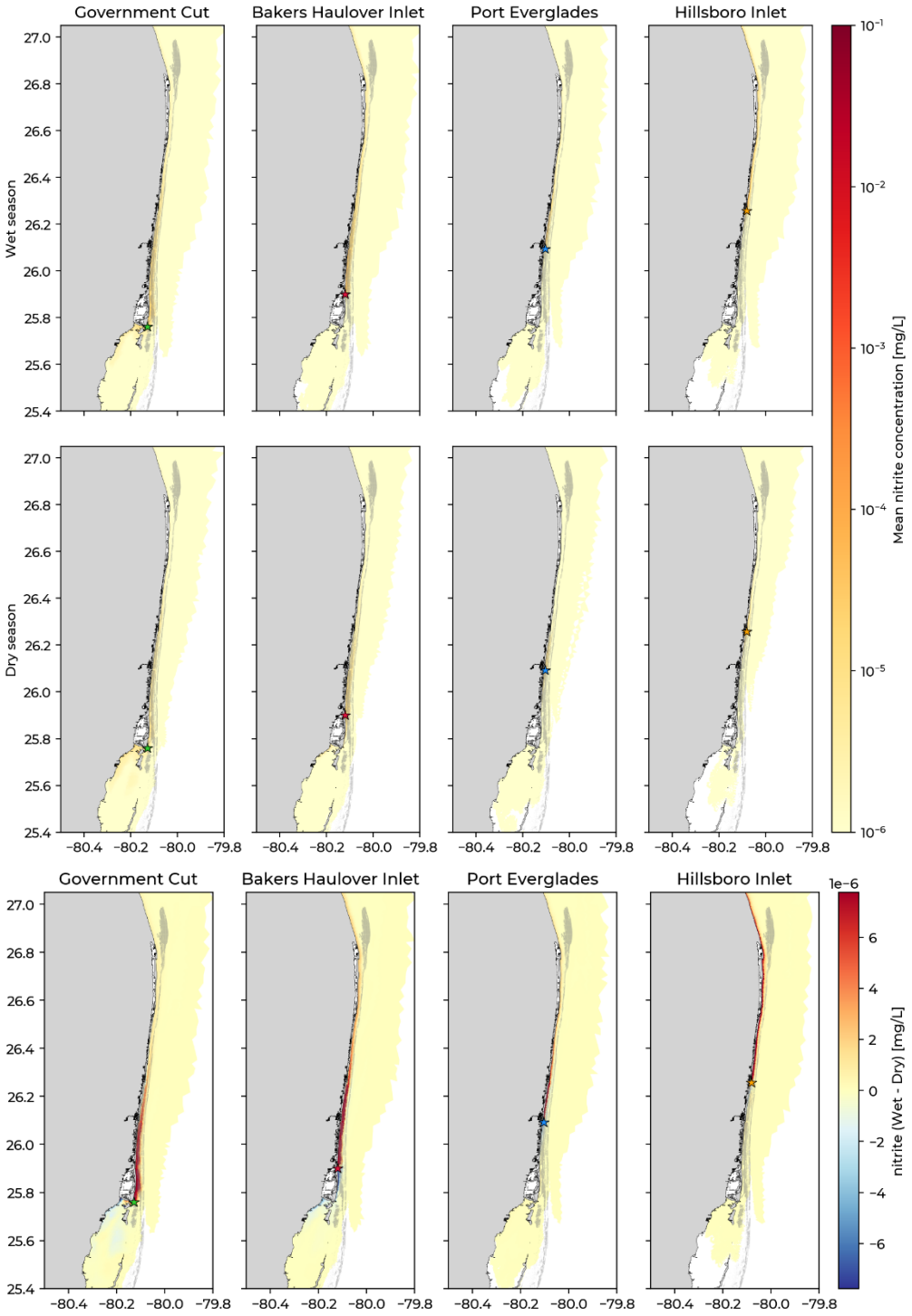

Figure A3: Seasonal mean concentration of nitrite coming from the different inlets for the wet (top panels) and dry seasons (bottom panels). The difference in concentration between wet and dry seasons is shown in the bottom panel.

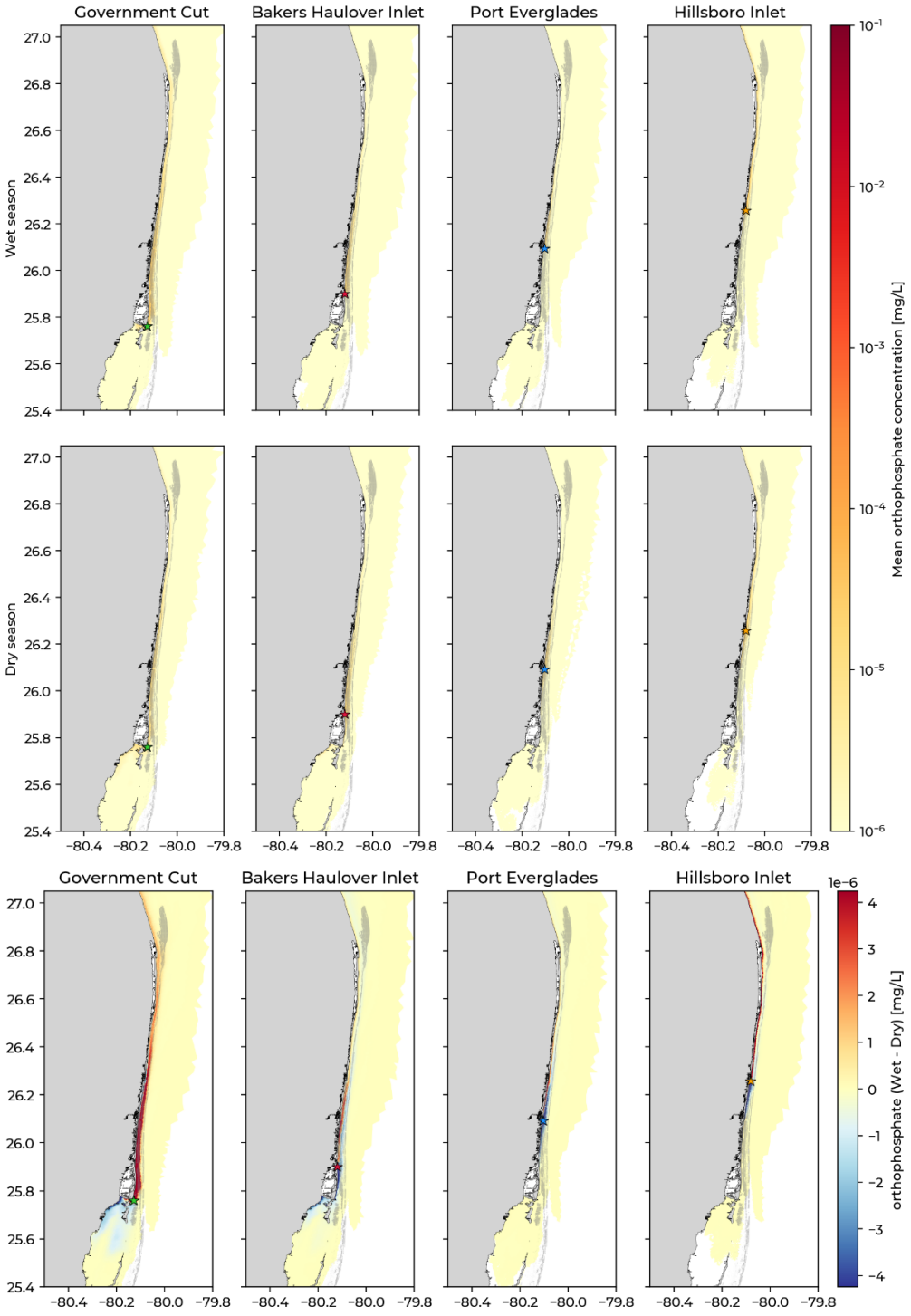

Figure A4: Seasonal mean concentration of orthophosphate coming from the different inlets for the wet (top panels) and dry seasons (bottom panels). The difference in concentration between wet and dry seasons is shown in the bottom panel.

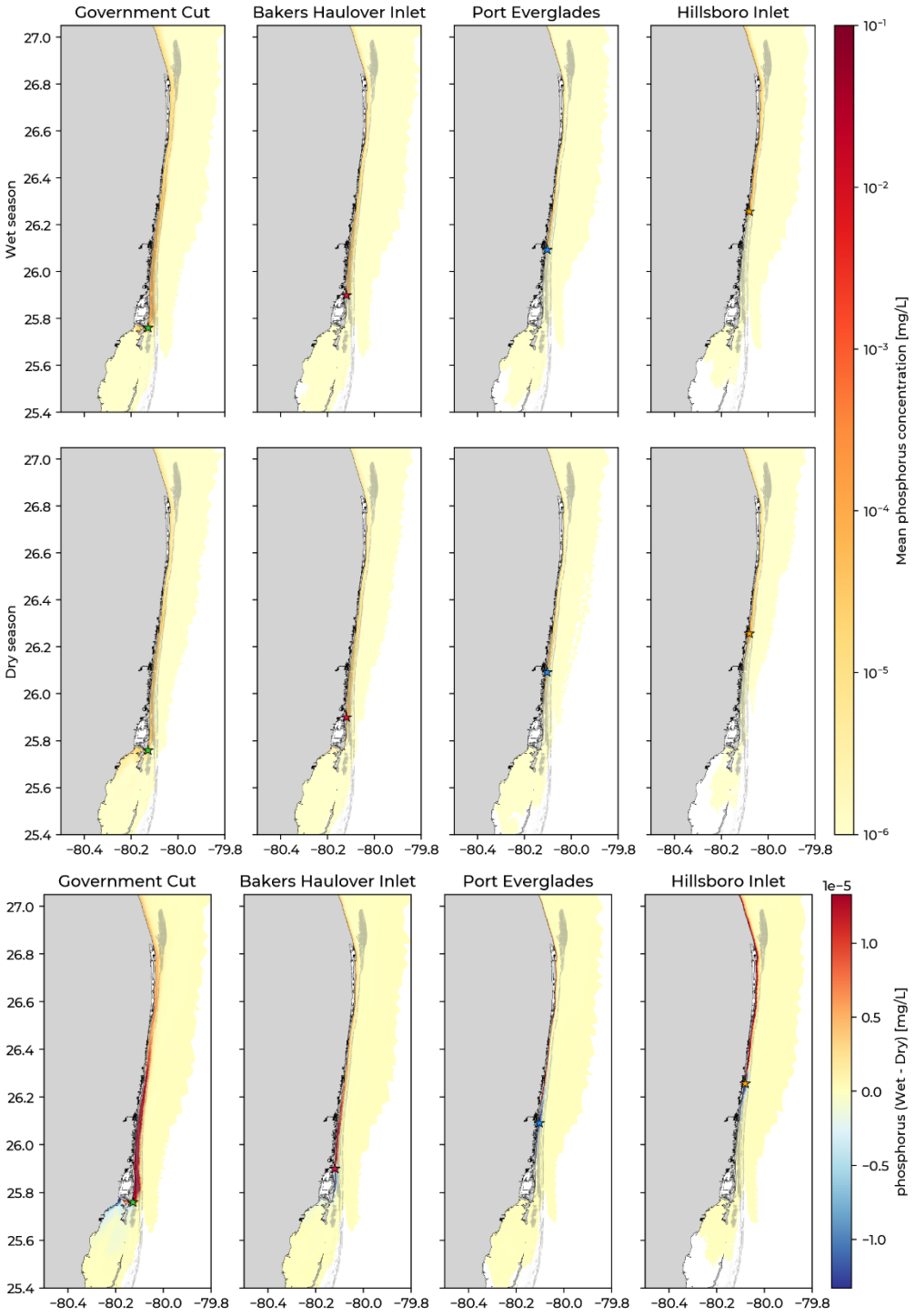

Figure A5: Seasonal mean concentration of total phosphorus coming from the different inlets for the wet (top panels) and dry seasons (bottom panels). The difference in concentration between wet and dry seasons is shown in the bottom panel.

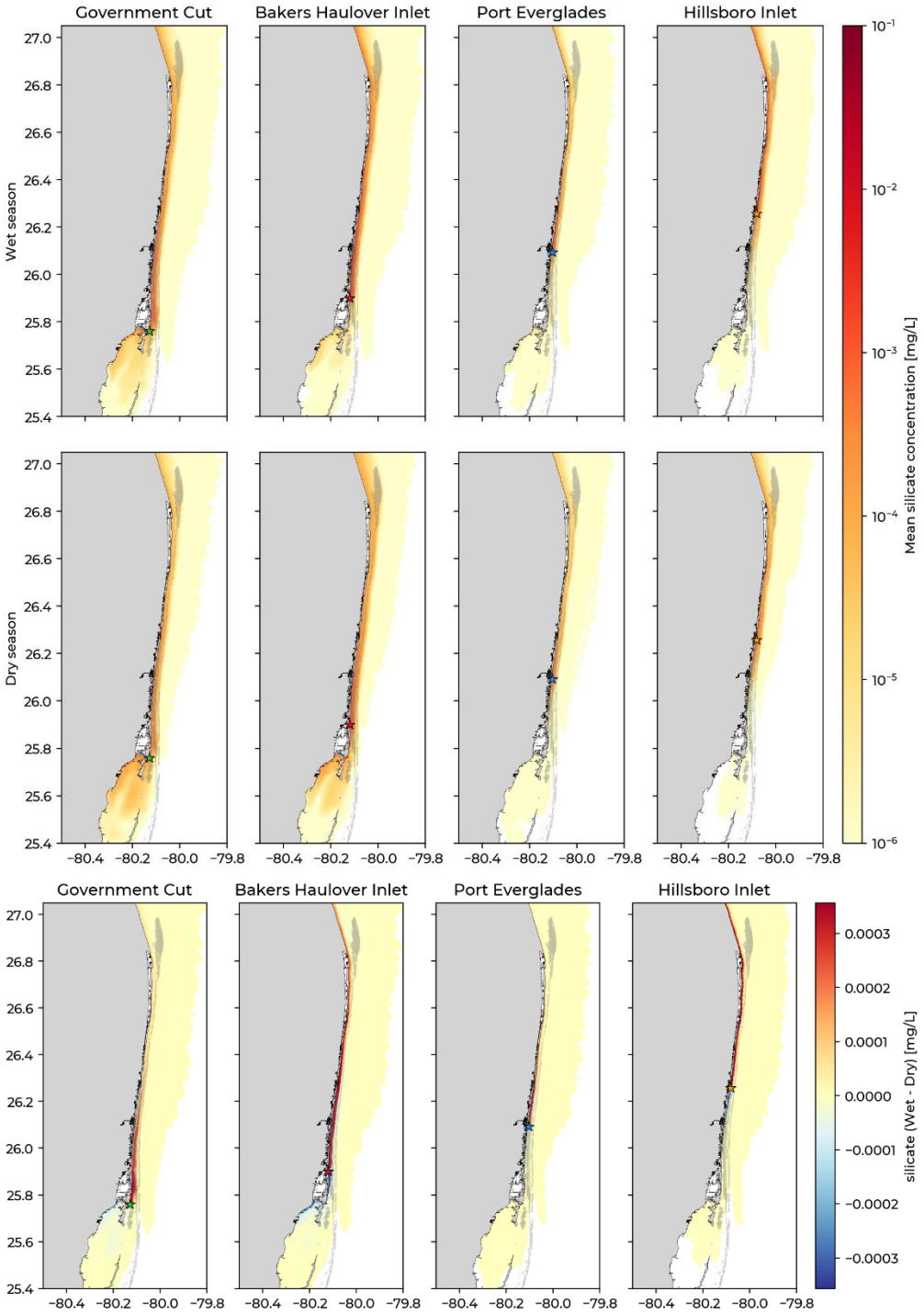

Figure A6: Seasonal mean concentration silicate coming from the different inlets for the wet (top panels) and dry seasons (bottom panels). The difference in concentration between wet and dry seasons is shown in the bottom panel.

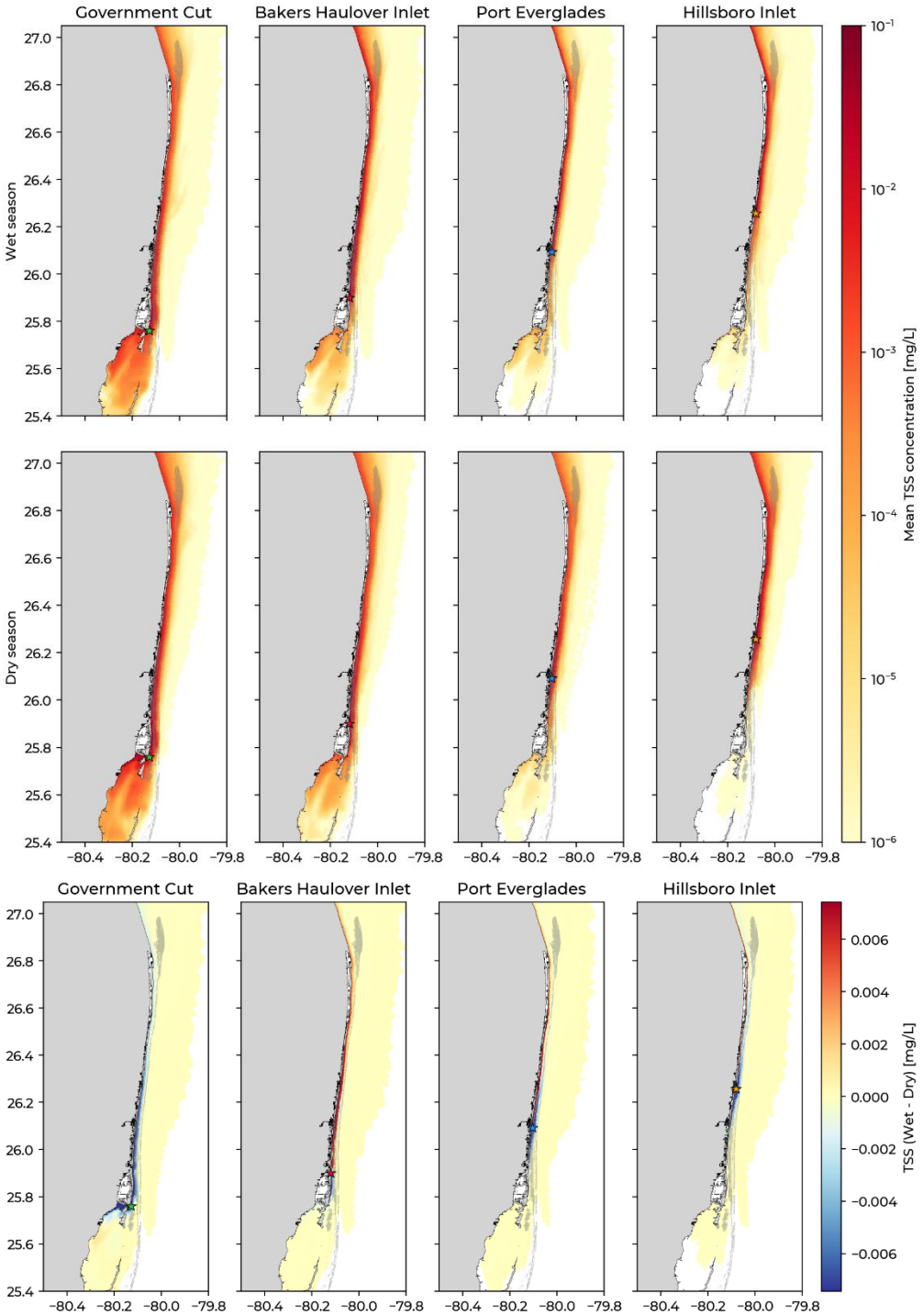

Figure A7: Seasonal mean concentration of total suspended solids (TSS) coming from the different inlets for the wet (top panels) and dry seasons (bottom panels). The difference in concentration between wet and dry seasons is shown in the bottom panel.